

Analysis and Redesign of an Elbow Exoskeleton Joint to Improve Human-Exoskeleton Interaction

Department of Materials and Production



Anne Grøn
Harun Leto



Design of Mechanical Systems
Master Thesis

Dette projekt omhandler analyse og redesign af et eksoskelet og dets interaktion med brugeren. Projektet er udarbejdet i samarbejde med Wolturnus. Projektet tager udgangspunkt i et allerede eksisterende eksoskelet med hovedformål at assistere kørestolsbrugere i flytningen til og fra kørestole. Eksoskelettet er transportabelt, og det er ønsket af forfatterne, at den funktion skal kunne udvides til at omfatte hverdagsaktiviteter.

Det åbenlyse ønske til forbedring af eksoskelettet var at gøre det lettere og stivere end den forrige generation, og Wolturnus har et ønske om at anvende letvægtsmaterialer som eksempelvis kulfiber. Kroppens øvre lemmer er undersøgt med det formål at udvikle et eksoskelet, der tilgodeser kroppens kinematik ift. frihedsgrader og ergonomi.

Lastscenarier, som skal repræsentere de ønskede funktioner, er opstillet og undersøgt både gennem tankeeksperimenter, analyser og tests. Analyserne præsenterer, at forholdsvis små momenter opstår i armen under hverdagsaktiviteter, og at de største laster i eksoskelettet derved forekommer ved assistance til løft af kørestolsbrugere.

De fysiske tests, der er udført i forbindelse med projektet, har alle indikeret, at implementeringen af fleksibilitet vil øge brugeroplevelsen. Resultaterne af testene giver også anledning til at foreslå en mekanisme der passivt kan forlænges og forkortes idet armen bøjer om albueledet. Med udgangspunkt i at skulle fremstille et fysisk produkt inden for den nærmeste fremtid (juni 2018), undersøges det hvilke materialer og fremstillingsmuligheder, der er tilgængelige.

På baggrund af alle de indledende undersøgelser er det besluttet at fokusere på komfort og på at tilgode alle kroppens kinematiske egenskaber. Det på trods af, at der er risiko for at pålægge ekstra vægt til den eksisterende løsning ved implementering af den forømtalte mekanisme. Fokuspunktet er desuden valgt med den konsekvens, at nogle designparametre og krav til dets funktion er svært målbare.

Målbarehed af komfort er søgt gennem prototyper, som kan være gavnlige i evalueringen deraf, og projektet er på baggrund af det især præget af praktiske overvejelser om fremstilling og test af koncepter.

En model, der som prototype kan teste designkoncepterne om rotationsfleksibilitet og forlængelse af underarmen, er udviklet. Modellen sammenkobler en aluminiumsdel, der giver mulighed for begrænset glidning langs armens akse, med en kompositdel af kulfiber, der giver mulighed for at tilføre fleksibilitet i den ønskede retning. På baggrund af modellerne er det bekræftet, at de foreslåede designforslag kan modstå de belastninger, der opstår under brug af eksoskelettet.

Test af prototypen er klargjort, men den er ved færdiggørelse af dette projekt ikke testet.



Fibigerstræde 16, 9220 Aalborg East

Project title: Analysis and Redesign of an Elbow Exoskeleton Joint to Improve Human-Exoskeleton Interaction
Project theme: Engineering Design of Mechanical Systems
Writing period: From 01-02-2018 to 01-06-2018

Project group:

Fib 14/23A

Members of group:

Harun Leto
Anne Grøn

Supervisors:

Shaoping Bai
Jørgen Asbøll Kepler

No. of pages: 105
End of project: 01-06-2018

Synopsis

This project investigates how to improve the human-exoskeleton interaction. It was initially believed that the interaction would be improved by creating a light and stiff redesign of the exoskeleton using composite materials. It was discovered during strain gauge measurements on the previous design generation that the rigidity instead caused discomfort. A new design accommodating the natural movements of the forearm was instead sought. Further experiments verified that an increase in compliance also increased the comfort felt by test subjects. The improved ergonomics were achieved by creating a new design which incorporated an aluminium sliding mechanism with a carbon fibre support structure. The final design can elongate a total of 30 mm along the length of the forearm. The new design maintained relatively low weight - approximately 44 gram heavier, while enabling enhanced user interaction through compliance. The new design was created in a manner such that it could be attached directly onto the previous design generation.

Preface

This report is a master thesis written by two students enrolled in 'Design of Mechanical Systems' at Aalborg University.

Reading and Formalities

It is recommended to print in colors, to fully interpret some illustrations.

Overall report structure consists of chapters, that are subdivided into sections and subsections. Appendices are located in the back of the report and appendix pages are numerated as page A1, A2 etc.

References are notated based on the Harvard method and a detailed bibliography list is present after the last chapter. By use of the Harvard method, a reference is displayed as: [Surname of author(s), year of publication].

References to specific statements, or knowledge based on a specific source, is displayed immediately after the sentence. A reference will be present at the top of a section or chapter, if content is based on the referenced source.

Equations, figures and tables are numerated according to chapters and sections, i.e. a reference to the first figure in chapter one is displayed as 1.1, the second 1.2 etc. Equations are furthermore displayed with surrounding brackets, for example equation (1.1). For numbered equations, the number is displayed in the right margin of the page, next to the respective equations. Figure- and table numbers are displayed underneath the corresponding figure and table, along with a brief description of what is illustrated or listed.

Notation and Mathematics

System of notation is European, with positional notation using period as decimal marker and comma for thousandth marker, e.g. 7,234.12

Contents

Abstract	iii
1 Introduction	1
2 Project Scope	3
2.1 Previous Design Generation and Component Restriction	3
2.2 Function of the Exoskeleton	4
2.3 Design Process	5
3 Motion of Human Upper Limbs	7
3.1 Mechanical System	7
3.2 Muscle Interactions	9
3.3 Ergonomics	10
4 Loading Scenerios	15
4.1 Preliminary Load Considerations	15
4.2 Test of Loading Scenerios	18
4.3 Procedure	23
4.4 Processing of Test Data	24
4.5 Results	25
5 Estimation of Load-Sharing Factor	29
5.1 Analytical Evaluation of Upper Limb System	29
6 Materials & Manufacturing	35
6.1 Available Materials and Key Concepts	35
6.2 Manufacturing Method for Composites	37
7 Evaluation of Comfort, Weight and Manufacturing	41
7.1 Design of Initial Prototypes	41
7.2 Manufacturing of Prototypes	44
7.3 Evaluation of Manufacturing	44
7.4 Test of Prototypes	45
7.5 Evaluation of Prototypes	47
8 Additional Design Considerations	49
9 Requirement Specification	53
9.1 Design Circumscription	53
9.2 Requirement Specification	55
10 Design of the Elbow Joint Forearm	57
10.1 Conceptual Design	57
10.2 Design and Simulation Approach	58

10.3 Design Results	64
11 Discussion and Conclusion	71
11.1 Discussion	71
11.2 Conclusion	72
11.3 Future work	73
Bibliography	75
A Questionnaire for Concept Test	A79
B Datasheets	A84
C Component Overview	A94
D Mould & Template	A96

The use of exoskeletons is seen in various applications, both in nature, and in commercial use. The principle of the exoskeleton is essentially to provide with an external stabilizing framework or structure, opposed to an endoskeleton (internal supported framework or structure). Commonly used examples are the hard protective shell surrounding a lobster's soft internal organs, and lower body exoskeletons, which are used in rehabilitation programs to aid in the recovery, and training, of patients with limited mobility. In this project the term *exoskeleton* covers an assistive elbow joint.

This thesis is a part of an ongoing research- and development project of upper body assistive exoskeletons, done in collaboration with Wolturnus. Wolturnus is a Danish company that develops and manufactures various types of wheelchairs. Their target group is currently wheelchair users, as they experience high stress within their shoulder, elbow and wrist during the transferring movement on and off wheelchairs. Several studies suggest that this repetitive movement over time causes upper body pain and injury over time [Kankipati, 2012], [Erhan et al., 2013]. Another study has found the flexor and extensor strength of the elbow to play an important part in the upper body pain, mobility performance, experienced by paraplegic persons [Mulroy et al., 2015].

To meet the need for assistance for wheelchair users, Aalborg University and Wolturnus agreed to collaborate in the development of an upper body exoskeleton to aid in the movement of the arm by actuating the elbow joint. The initial motivation behind this thesis is therefore to improve the independence, daily activity and life quality of wheelchair users, with the aid of an exoskeleton elbow joint. However, Wolturnus also has a strong wish to create a more versatile design, which in general may help users in the aid of daily activities as well. Currently, two design generations have been developed, in which the main focus was actuation and development of the control system.

From the previous design generations, possible needs for the elbow joint exoskeleton have been assessed. These needs are mostly related to comfort and ergonomics. The use of the exoskeleton requires lengthy wear, and to avoid conflicts/to improve comfort, the interaction between the human and the exoskeleton should be as frictionless as possible, literally and metaphorically. The investigations to test this interaction are widespread, as the findings of one investigation lead to the motivation of another investigation. This implies that the establishment of a defined problem requires a comprehensive analysis of the problem.

The human-exoskeleton interaction, i.e. comfort, is a very topical issue within exoskeletons. For lower body exoskeletons, the comfort can be related to shock absorption and low weight to limit the metabolic burden, e.g. [Sugar et al., 2017]. For the upper body, compliant actuators are developed with the function of releasing and storing energy and ability to absorb shocks [Simona et al., 2017]. Misalignment of the exoskeleton's joints and the joints of the wearer can result in hyperstaticity, which is the application of unintended and uncontrolled interaction forces. [Masia et al., 2017] A recent strategy to accommodate this problem is with the use of exosuits, that has intrinsic compliance and close to no joint misalignment.

The long term effects of wearing exoskeletons is not documented [Bastide et al., 2017], but it has been found, that the immediate effect on the upper limb movement, i.e. muscle activity and angular velocity are influenced, suggesting that natural movements are difficult to perform when wearing exoskeletons. [Bastide et al., 2017]



Figure 1.1: *Exoskeletons [Hoffman] [TED]*

This thesis carries the work done in previous projects further, with the usage of composite materials to improve the ergonomics of the earlier generations of the elbow joint. The aim of the next design generation, proposed in this thesis, is to create a lightweight elbow joint, which focuses on comfort and ergonomics. This should be developed while still maintaining sufficient structural strength and stiffness, to accommodate in the aid of the transferring movement for wheelchair users, and in everyday the daily activities of people with limited muscular strength. As this is a further development of earlier designs, the new design must be compatible with electrical components used in previous design generations, but also accommodate new requirements specified by the company.

With the user experience as a prioritized objective, fabrication of prototypes is important for this project, and it is important to have a reference for the performance metrics of the exoskeleton (i.e. a test person). The fabrication of prototypes is desired to take place at Aalborg University and it should be based on available materials. This objective affects the thesis, as the choices are characterised by the limitations set by the facilities.

Project Scope 2

As described in the introduction, the project takes departure in an ongoing project and therefore already existing elbow joint exoskeleton. This chapter presents the previous design generation and outlines the process of improving it.

2.1 Previous Design Generation and Component Restriction

The current design, that is to be improved, consists of three major components: an upper arm structure, a forearm structure piece, and a worm gear drive, illustrated in figure 2.1. These three components together, form the basis of the structural support.

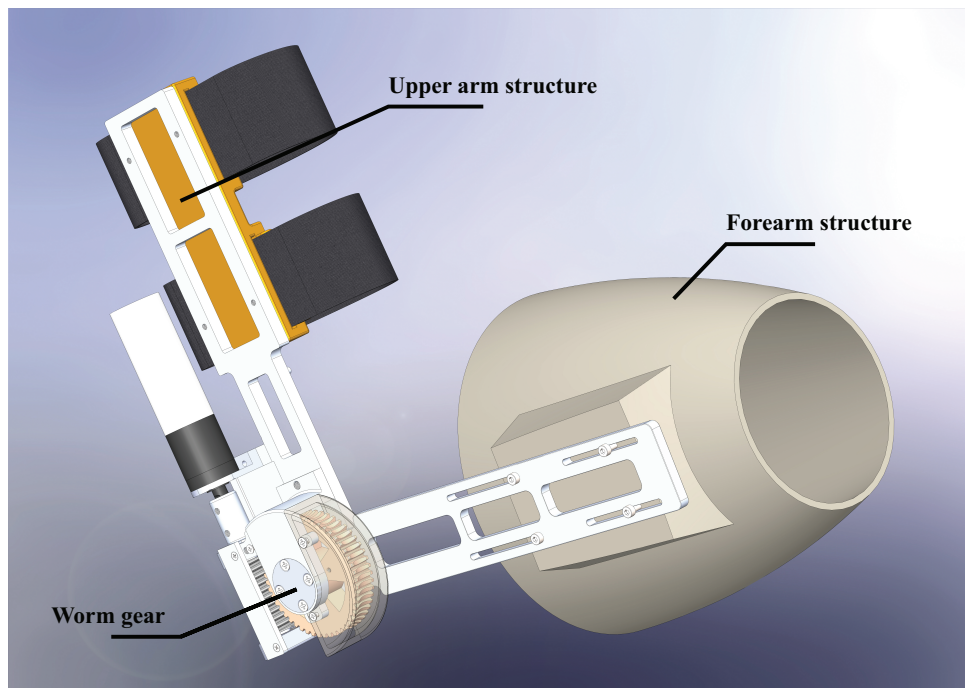


Figure 2.1: *Previous design.*

The concept behind the current design is to attach the upper arm structure of the exoskeleton on the outside of the biceps, away from the body. The forearm structure is either attached to, or supported by lower arm, depending on the design of the actual support interface between the lower limb and the arm. A support like structure was proposed by the designers of the previous design generation. The lower frame support can be micro adjusted to fit clients, which is done by the slider mechanism seen in figure 2.1. Lastly, a worm gear drive is attached to the upper limb of the exoskeleton, which allows a small DC-motor to rotate the lower limb through a worm gear.

The actuation of the lower frame is driven by a 90W EC-4pole 22 brushless DC-motor. The current gear ratio between the DC-motor and the frame is 1:270. This ratio occurs from 1:5.4 between the motor and the worm shaft, and 1:50 between the worm shaft and the frame. The current weight of the design, without the motor, is 450 grams, and with the motor 640 grams.

The motor is capable of providing 43.9 mNm for continuous use at 1.58 A [Maxon Motor, 2018]. For use in the exoskeleton elbow joint, the electric current is allowed to reach 4.0 A during short time operations, as the demand for such high torques are intermittent. With a torque constant of 28.1 mNm/A, the maximum available torque is 112.4 mNm. For the applied gear ratio (1:270), the motor configuration is capable of exerting a maximum of torque 30.35 Nm and 11.9 Nm during continuous use at the elbow joint. The motor of the previous design generation is rated to carry a maximum payload of 5kg.

The exoskeleton needs external devices to operate, more specifically sensors to recognize the movement, the arm is trying to perform, and determine how much aid should be contributed. The current sensors in use is a "Force Sensitive Resistor". 3-5 sensors are attached to a strap which is attached around the biceps. The sensor measures differences in surface pressure, or in the case of flexion movement of the biceps, the volumetric change within the band.

For the new design, Wolturnus has a desire to attach the exoskeleton to a newly developed shoulder harness. The shoulder harness is shown in figure 2.2. The purpose of the shoulder harness is to stabilize the shoulder, during operation of the elbow exoskeleton.

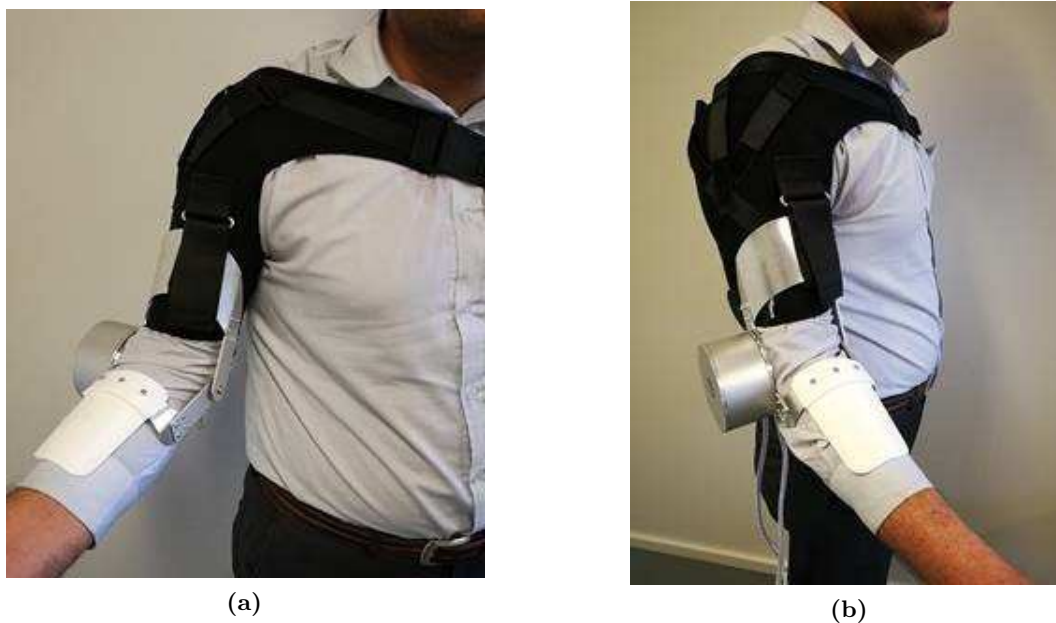


Figure 2.2: *Shoulder harness attached to another concept. (a) Front view, (b) Side view.*

2.2 Function of the Exoskeleton

The function of the exoskeleton must be outlined. The previous design is considered when setting up desired functions of the desired exoskeleton, as it contains some obvious elements and qualities to improve section 2.1. Some issues have been identified with existing design. The shape is not appealing and seems very inorganic compared to its function of assisting the body. The weight of the exoskeleton is sought reduced to improve the overall experience of the exoskeleton. The current support is adjustable in the circumference, but the adjustability is mainly limited to be constant around the arm and not to vary along the axis of the arm, which results in a gap where the arm narrows down in area. The control of the motor is based on the biceps sensor, but with the current attachment, it has been difficult to fit the biceps sensor in a place where it is not squeezed behind the support of the upper arm. Another issue related to the support of the arm occurs due to the slight extension of the arm as it flexes around the elbow, and the

support aims to slide along the arm and cause irritation. As a starting point, the weight and stiffness is desired improved.

2.3 Design Process

The general design process for the entire project can be outlined to contain the points listed in figure 2.3 [Shefelbine et al., 2002].

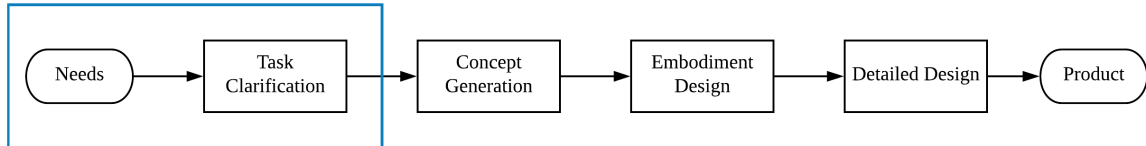


Figure 2.3: Replication of designproces from Shefelbine et al. [2002].

During the *Task Clarification*, the problem is defined, the needs are identified and the requirements are established. From here on, the *Concept Generation* implies identification and evaluation of possible solutions. With one or more selected solutions, determination of the layout and structure helps elaborate the solutions as a part of the *Embodiment Design*. *Detailed Design* finalises the details (i.e. final dimensions and materials).

For this project, both the *Needs* and the *Task Clarification* is a very comprehensive part, as a lot of investigations are made in order to obtain a defined Requirement Specification.

Steinfeld et al. [2006] presents a list of performance metrics within navigation, perception, management of tasks and manipulation. Furthermore, Bostelman and Hong [2018] presents additional factors, such as duration of wear, speed and acceleration, ease of use and ergonomics.

Testing an exoskeleton for all these performance metrics is very time consuming and requires a comprehensive study. In order to be able to evaluate the performance metrics in depth, it is chosen to circumscribe the problem through research before starting to solve a problem. .

The study and findings necessary for this is presented within chapter 2 to chapter 9.

The process of the project is illustrated in figure 2.4, which illustrates the interdependency and iterations.

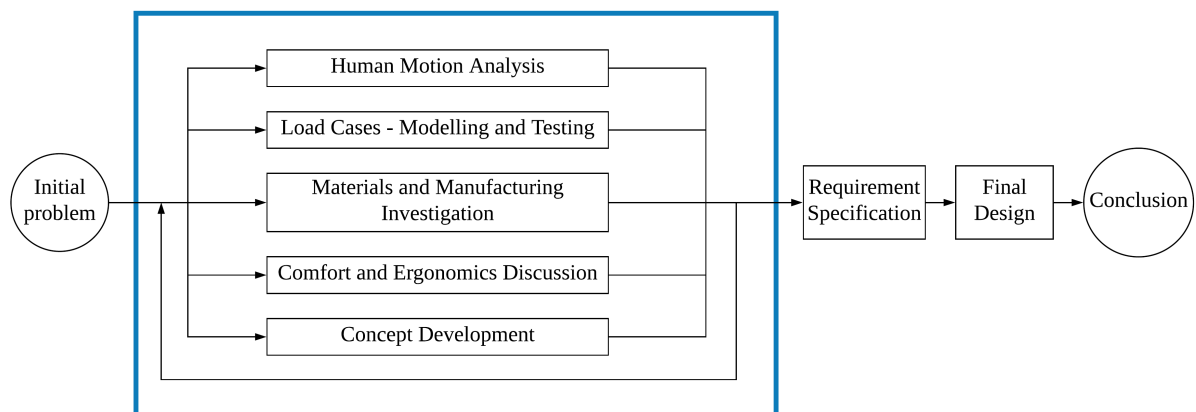


Figure 2.4: Process of the project. The blue box indicates the Needs and Task Clarification (figure 2.3), and it contains the interdependent investigations and the iterations prior to the Requirement Specification.

Due to this described structure of the project, and the interdependency of the chapters, the report is characterized by a lot of cross references within the investigations.

Motion of Human Upper Limbs 3

In order to understand the function of the exoskeleton, the behaviour of the structure it exists to support must first be understood. The human factors such as the mechanical system and muscle interactions are presented, and the ergonomics are discussed in relation to an exoskeleton

3.1 Mechanical System

The body can be considered as a mechanical system, whose degree of freedom (DOF) defines the independent parameters that determines the motion or configuration for the mechanical system. The exoskeleton functions next to the human body, and it must therefore possess the same manoeuvrability as the body in terms of DOF. The number of DOF is arguable up to nine DOF: In the shoulder exists three rotational DOF and two translational DOF, in the elbow is one rotational DOF and in the wrist are three rotational DOF. [Xie, 2016]

The 1 DOF within the elbow joint is based on two articular circular surfaces, that are placed concentrically. This gives a defined axis of rotation which means that a prosthesis or an external supporting skeleton can also exist with only one rotation axis.



Figure 3.1: *Rotation mechanism in the elbow. [ROC, 2016]*

The axis of rotation (flexion-tension axis, FT-axis) is 6-7 degrees from transverse to the centerline of the upper arm (figure 3.2). This gives a *carrying angle* when the arm in is full extension of 12-14 degrees. [Amis, 2002][Felstead and Ricketts, 2017]

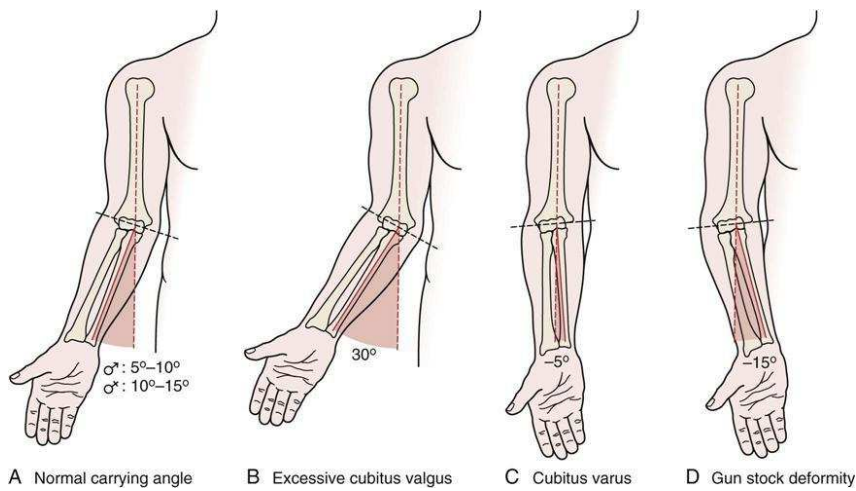


Figure 3.2: Carrying angle of arm based on rotated FT-axis. [Best Performance Group]

The range of motion around the FT-axis is between 0 and 145 degrees for most people, where 0 degrees is fully extended (figure 3.3). Around the axis of the lower arm, rotation is allowed, as supination can occur for 90 degrees and pronation can occur for 80 degrees. [Amis, 2002]

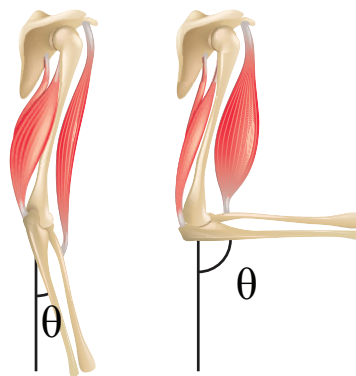


Figure 3.3: Flexion-extension angle. $\theta=0$ indicates full extension.

The FT-axis can work as z-axis in the global coordinate system for the upper limb.

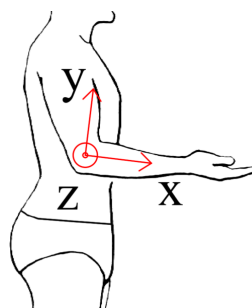


Figure 3.4: Local coordinate system. FT-axis is coincident with the z-axis, and the x-axis is always following the axis of the underarm.

3.2 Muscle Interactions

The movement of the body is controlled by muscles, and these need to be taken into account when designing the exoskeleton. This has two main reasons: the sensors for the actuator use muscle contractions as input (refer to the current design chapter), and the support points of exoskeleton should be placed away from large deformations to provide attachment as comfortable as possible.

The muscle interactions are most prominent in the upper arm as flexion and extension of the elbow joint is controlled by the muscles in the upper arm. On the anterior side (front) are three main muscles that in contraction are used for flexion of the elbow. The muscles applying the main moment around the FT-axis to bend the arm are the biceps brachii and the brachialis (figure 3.5). A stabilizing muscle for this movement is the brahioradial placed on the lower arm. On the posterior side (back) is the triceps (figure 3.6). When the triceps contracts, it is used for extension of the arm. The change change in transverse area of the anterior muscles is more prominent than for the posterior muscles. [Hale et al., 2010] [Pigeon et al., 1996]

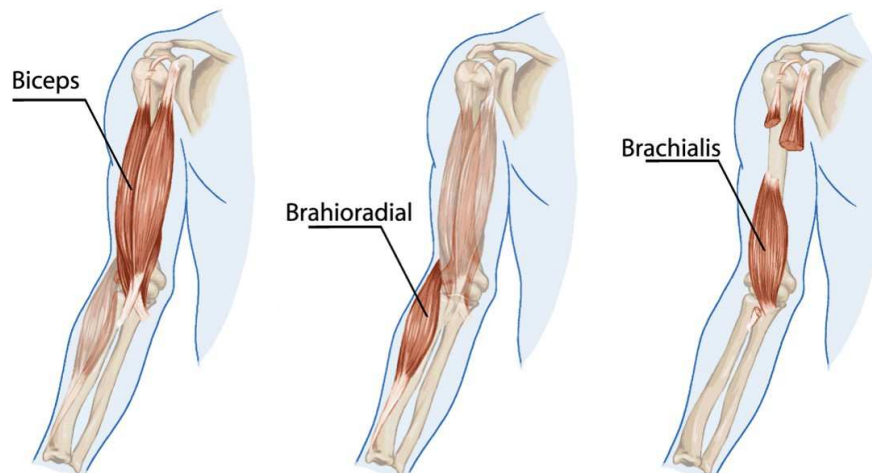


Figure 3.5: Arm bending muscles. [Wilfredofitness, 2018]

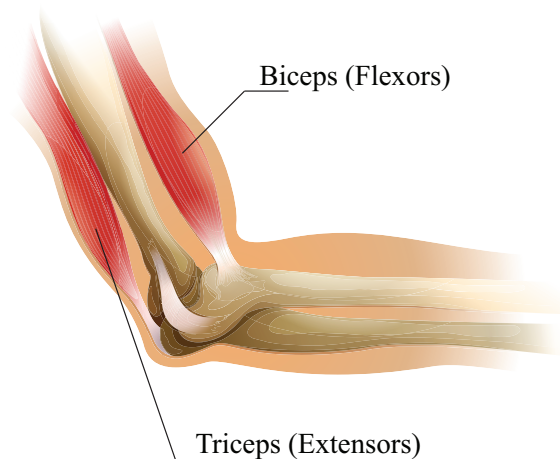


Figure 3.6: Flexion- and extension muscles in the upper arm.

3.2.1 Muscle Action in Relation to Movement

The muscles contract to counteract the payload, eg. the biceps contracts for a positive movement against gravitational load (by means of definition cf. figure 3.7). If the arm is yielding from the applied force towards extension (negative movement, gravitational force), the arm bending muscles (biceps etc.) will bear the weight, as the arm extends while the muscles release. In line with this principle, when an arm bending moment is applied to an extended arm, a controlled motion can only be ensured by slow release of the triceps contraction.

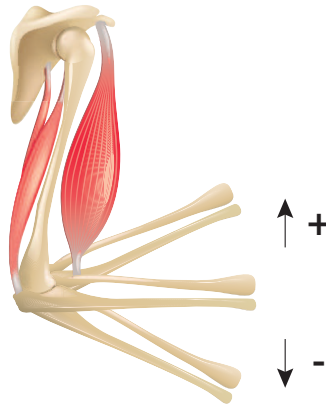


Figure 3.7: *Definition of positive and negative movement, respectively flexion and extension.*

	Biceps (Anterior group)	Triceps (Posterior group)
Contraction	Flexion	Extension
Release	Extension	Flexion

Table 3.1: *Movement based on the action in the muscle group*

3.3 Ergonomics

Ergonomics is an important aspect whenever designing something in conjunction with the human body. Ergonomics, in this thesis, is defined as a parameter, from which comfort and the compatibility with the human body, can be assessed. The following considerations are divided into four categories - kinematical constraints, support placement and geometry, weight and compliance. These considerations are factors that contribute to the ergonomics of the new design. One large challenge is that these considerations are interdependent e.g, removing kinematical constraints requires implementation of more advanced mechanism, which comes with a weight penalty. Furthermore, another challenge is that the ergonomics of a design is a subjective evaluation. It cannot necessarily be measured, or assessed, through simulations as other typical design tasks with defines performance metrics. Prototyping and testing is therefore needed to evaluate if the selected design changes are the most influential. The following considerations are discussed in summary at the end of this part, from which new design changes are selected.

3.3.1 Upper Limb Kinematical Constraints

The new exoskeleton should feel comfortable during all operations of use. This implies that the exoskeleton should follow the natural movement of the arm. It is thought that the best possible design should feel like an extension of the upper limb itself, but the current design imposes several design issues, from a structural point of view, that hinders and limits the comfort during operations. The current design possesses one DOF of freedom in the elbow

joint, while constraining the rotational DOF of the forearm - the supination and pronation movement. However, another constraint is felt during operation of the exoskeleton. The axis of rotation of the exoskeleton is not aligned with the axis of rotation of the elbow. This causes the user of the exoskeleton to feel that the forearm support wants to slide back and forth along the forearm during operation. This adds another constraint to the current design, since the exoskeleton is strapped onto the forearm. In summary, the current exoskeleton design adds two constraints the movement of the upper limb (from the elbow to the wrist). Removing these constraints in the new design will improve the ergonomics of the design. In fact, it is measured that the forearm structure would slide up to 20 mm from the configuration shown in figure 3.8a to the configuration shown in figure 3.8b.

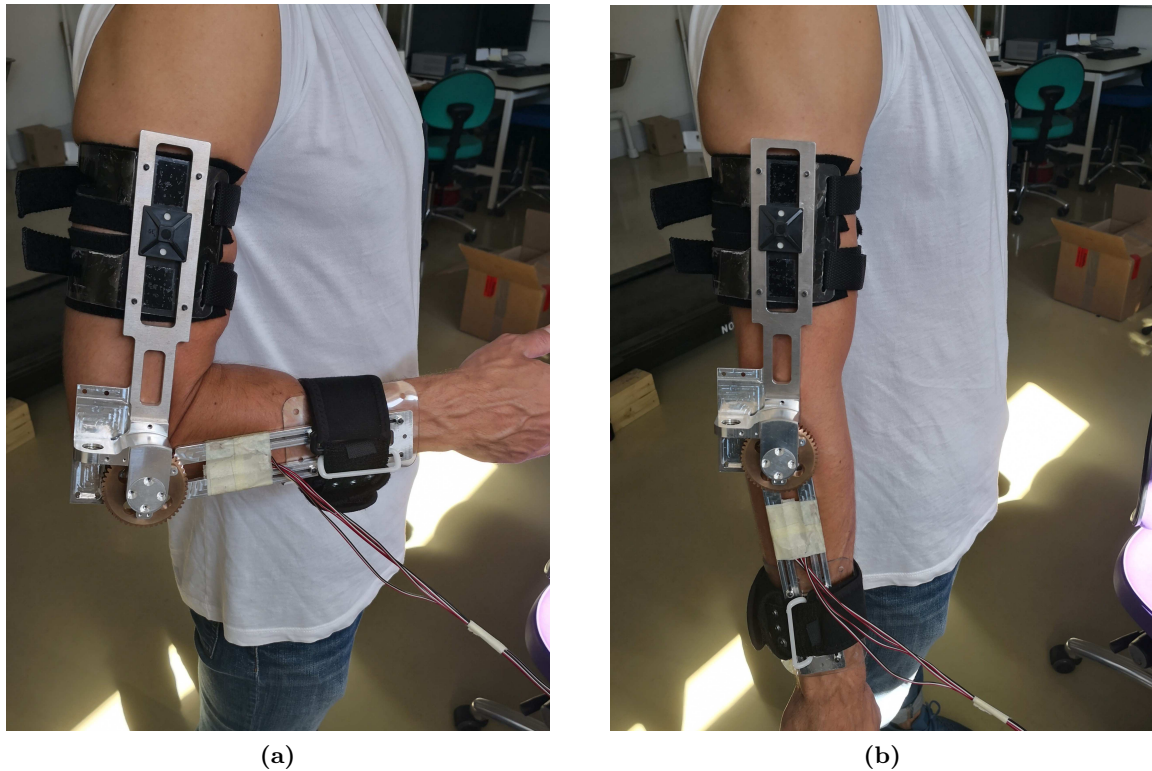


Figure 3.8: (a): Exoskeleton attached on a bended arm, (b): Exoskeleton attached on a stretched arm.

3.3.2 Support Placement and Geometry

The support of the exoskeleton is an expression for the contact points between the exoskeleton and the arm.

Overall, two factors determine the pressure exerted on the arm from the support. One factor is the distance from the elbow, in which the moment is occurring, as an increase in distance yields a decrease in the reaction force. The pressure experienced at the support is dependent on the area of the support. The area has to be a certain size to lower the pressure, but it cannot be too big, as movements of the arm makes the surface of the skin move relative to itself.

The shape of the forearm cross section is assumed elliptical. This means, that its shape can be determined by a width and a height (height > width).

The distance must favour the individual user, which is why this study has taken departure in a test person, and dimensions of this persons upper limb (table 3.2).

Dimension	Size [mm]
FT axis to wrist	240
FT axis to load introduction in hand	300
FT axis to approximated shoulder rotation point	270
Width of lower arm, 210 mm from FT-axis	77
Height of lower arm, 210 mm from FT-axis	67.5

Table 3.2: *Measures of test person*

Further adaption to the user can be ensured by for instance thermo plast, that has the capability of being shaped after the body, and provide with strength without over stiffening the support and sacrificing comfort.

3.3.3 Weight

The human body uses energy whenever it preforms controlled movements. The energy exerted by the muscles within the body is commonly defined as work. During lifting and pushing operations much of the work is used to overcome gravitational force, i.e the work exerted is potential energy. Conservation of energy cannot be applied to the energy exerted by the muscles.

A common example is lifting your arm to a horizontal position as shown in figure 3.9 on the facing page. Moving the arm to a horizontal position requires energy. However, holding your arm in this position does not require energy, by means of typical energy considerations, from an mechanical engineering point of view, although one can agree that it certainly does not feel like no energy is used after holding your arm in this position for a couple of minutes. This sensation occurs as the muscles in the upper limb are working against the gravitational force and become fatigued as they prevent the arm from returning to its natural down right position [jing Wan et al., 2017]. This is just a very simple but extreme example, and it occurs due to the weight of the upper limb. The weight of the upper limb is for the test person estimated to 3 kg. (4.3% of bodyweight, [Tözeren, 2000]). Any weight of external devices (e.g. an exoskeleton) is added to the bodyweight, and must therefore be carried by the muscles as well.

In general the weight of the exoskeleton should be limited to avoid discomfort during longer periods of use, as some muscle groups such as deltoids have to compensate for extra weight of the elbow joint.

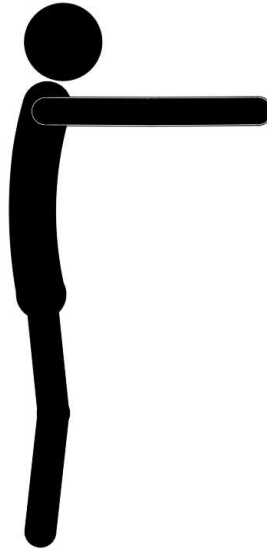


Figure 3.9: *Horizontal arm position*

3.3.4 Compliance

It was realised during the strain gauge measurements (section 4.2 on page 18) that the stiffness of the aluminium forearm caused discomfort during lifting operations. The high bending stiffness greatly limited the instinctive supination and pronation movement of the forearm and wrist during lifts. It is believed that the discomfort can be relieved by adding more compliance to the structure. The use of composite materials allows the designer control of the stiffness and hereby also the compliance of the structure. This is not a trivial task, as the fibre orientation is greatly correlated with the stiffness and strength of the overall laminate.

Loading Scenerios 4

4.1 Preliminary Load Considerations

Designing and working with orthotropic materials yields somewhat a greater challenge than when working with isotropic materials such as steel. The margin of error is lower, failure indications do not exist in the same manner as for most metals, i.e yield, and the designer must take the force flow, or loading directions and magnitudes, into account when designing components to successfully utilize the properties of orthotropic materials.

In the introduction it is mentioned that the new elbow design, should aid in the transferring movement between eg. wheelchairs and chairs for wheelchair users. A study conducted at the University of Aalborg was set to investigate the flexion moment at the elbow joint, during four common movements for wheelchair users. The movements investigated in the study are a push up maneuver, a weight relief maneuver, a forward movement out of the wheelchair lastly a backwards movement onto the wheelchair. Each of the movements initial and final positions can be seen in figure 4.1 on the following page.

These four movements form a foundation for what loading scenarios that can be expected during operation of the exoskeleton. From these four movements, the largest recorded flexion moment was found to be 85.17 Nm, achieved during the backwards movement onto the wheelchair [Sandal et al., 2018]. This moment will be used as a benchmark, when determining an appropriate payload for the new design. It should be noted that the load will be shared between the exoskeleton and the human arm, and not fully carried by the exoskeleton. This is discussed later on in chapter 5.

It is also expected that the exoskeleton can be operated and used for everyday activities. Defining a list, with all possible activities is too tedious, and so as an initial circumscription, it is decided to narrow down everyday activities to household tasks. A couple of common household tasks, in which the exoskeleton could be useful, are lifting grocery bags, doing laundry, or moving furniture during vacuum cleaning. In general it is assessed that that household tasks, in which the exoskeleton can be useful, can be divided into two groups, *lifting or carrying objects* and *moving or pushing objects*. A study investigating the end user needs for a upper body exoskeleton showed that the achievable movements for user to be push/pull, lift/drop, overhead lift, reach to the side, and carry objects in front with two arms [O’Sullivana et al., 2015]. These movements correspond well with the two movements mentioned previously.

Based upon these findings it is decided to check the structural integrity of the design for three different positions.

The first load scenario is arms fully stretched in a horizontal position, with a gravitational load, representing the carrying object task as shown in figure 4.2 on page 17. The horizontal position is chosen, as this is the position in which the flexion moment is most likely to be largest during a lifting or carrying operation. However, another moment should also be included as it was discovered in section 4.2 on page 18, that a secondary moment around the y-axis also occurs

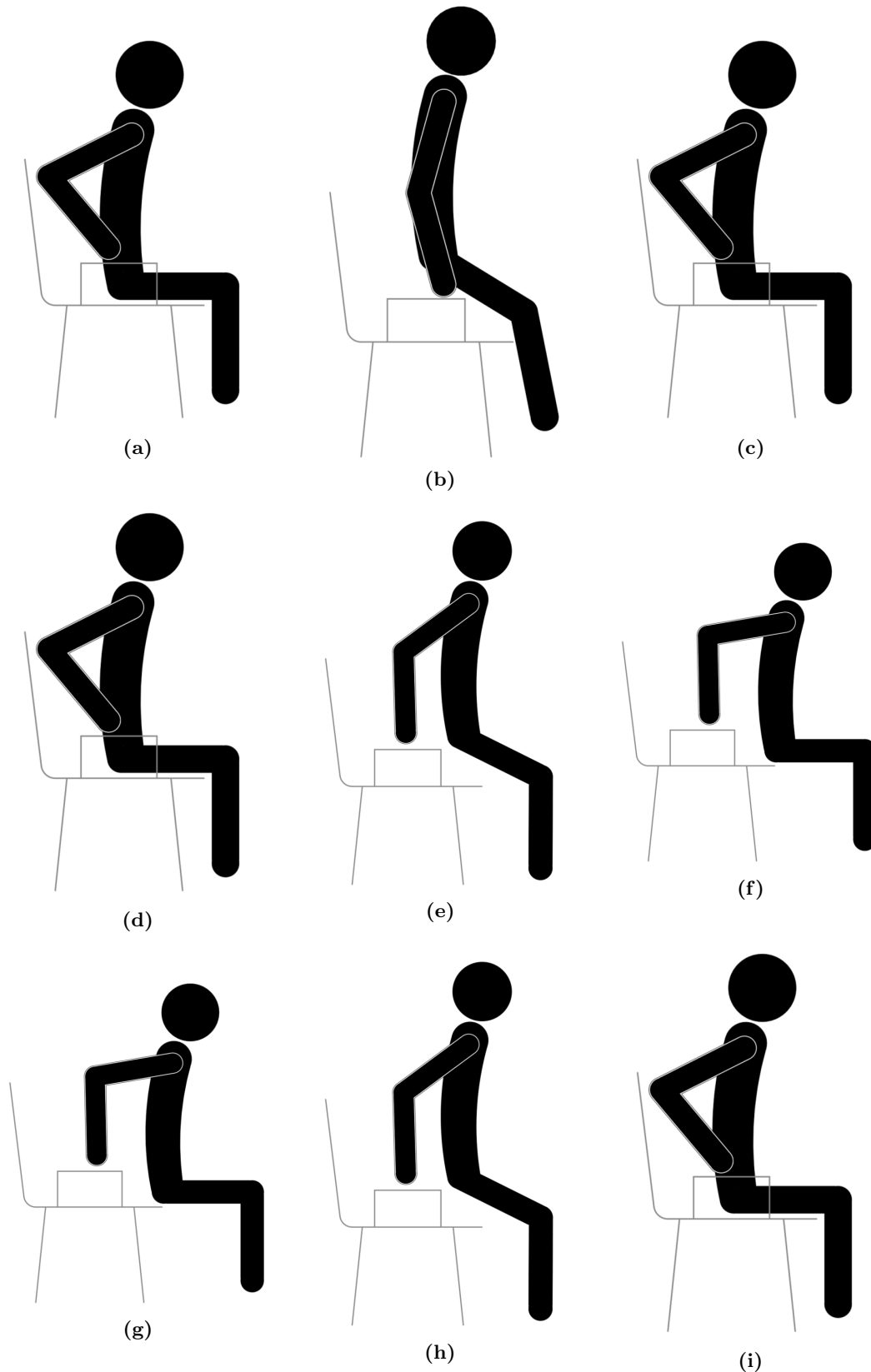


Figure 4.1: *Movements for measurement of the flexion moment in the elbow. Positions are connected horizontal from left to right.*

Pushup movement is illustrated by (a), (b) and (c).

Weight relief maneuver is illustrated by (a), (b) and (c), where position (b) is held for five seconds.

Forward movement is illustrated by (d), (e) and (f).

Backwards movement is illustrated by (g), (h) and (i).

simultaneously during regular lifting operations. This moment is assessed to have half of the magnitude of the moment around the z-axis.

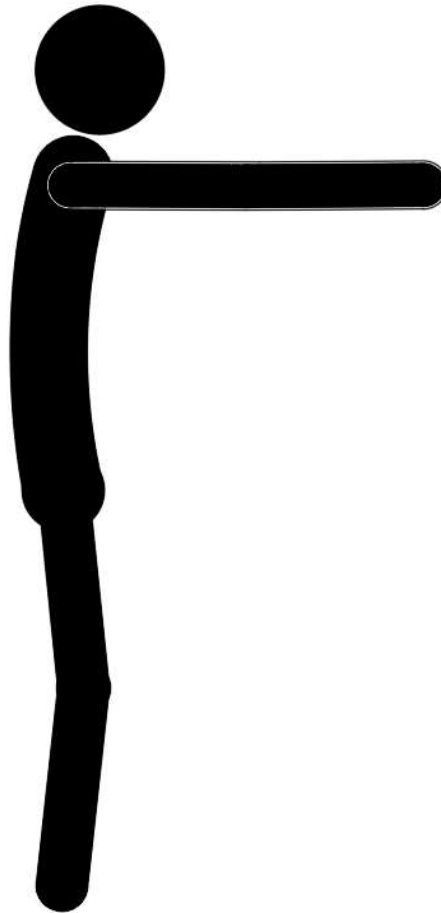


Figure 4.2: *Loadscenario when carrying a horizontal weight.*

The second load scenario is a position of the arm where a moment occur around the z-axis and around the y-axis (see figure 3.4 for axis). Tests have been carried out (chapter 4.2) to investigate the moments around the two axis. From this it is determined that two moments are present during the movement. However, the tests are ambiguous, and not entirely conclusive. It is therefore decided that two moments with the same magnitude are present for this load scenario, but with opposite sign convention. (Insert figure of movement)

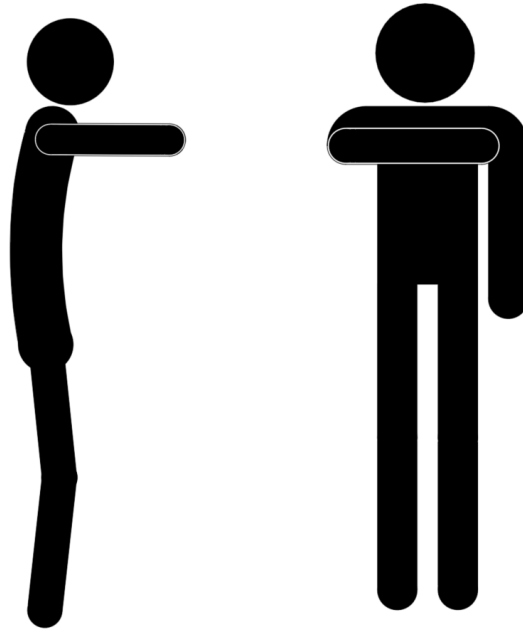


Figure 4.3: *Position of arm when testing the effect of excentric loads (push movement).*

The third load scenario is an investigation of the moments occurring during a push movement instead of carrying a weight (working against gravity). During the pushing operation, it was discovered that the moment around the y -axis was approximately one-third of the moment around the z -axis (figure 4.13 on page 26).

4.2 Test of Loading Scenarios

To validate the presumed loading scenarios and to gain a qualitative impression of the exoskeleton in use, physical tests are performed.

4.2.1 Concept

The forces acting in the exoskeleton during use are sought to determine if any excentricity (moment out of the xy -plane) occurs when the exoskeleton interacts with an arm. The internal forces of the greatest interest are the moment around the flexion axis of the exoskeleton (z -axis according to figure 3.4), and the moment transverse to the underarm around the y -axis (figure 3.4). Strain gauges are applied on the lower arm of the exoskeleton to measure the strains on the surfaces, and these strains are converted to internal forces (i.e. moment around z - and y -axis). The upper arm is not investigated by strain gauges.

The experiment consist of two main parts:

Calibration The exoskeleton is calibrated, relating the internal moment to the experimental strains. Finite Element Analysis of the exoskeleton is included for comparison of strains.

Exoskeleton on arm The exoskeleton is mounted on the arm with the purpose of testing the interaction of the arm on the exoskeleton. The arm performs defined movements. Some of the movements are actuated by the exoskeleton, and some are performed with a fixed elbow position.

The two parts include different set-ups and movements as listed in table 4.1 and table 4.2. The movements are included to obtain different loadcases on the lower arm of the exoskeleton.

Test #	Moment around axis i	No. of loadsteps	Reference figure
1	$i=y$	6	Figure 4.8a and figure 4.9a
2	$i=y$	6	Figure 4.8a and figure 4.9b
3	$i=z$	7	Figure 4.8b and figure 4.9a
4	$i=z$	7	Figure 4.8b and figure 4.9b

Table 4.1: Configurations included in the calibration test.

Test #	Movement and description	Exoskeleton configuration	Elbow position	Shoulder position	Duration of one cycle	Reference figure
1	Flexion of elbow, causing in-plane bending of lower arm. Carrying no weight.	Elbow actuated by exoskeleton	$\sim 39^\circ - \sim 104^\circ$	$\sim 0^\circ$	3 sec.	Figure 4.10a
2	Flexion of elbow, causing in-plane bending of lower arm. Carrying 1.3 kg.	Elbow actuated by exoskeleton	$\sim 39^\circ - \sim 104^\circ$	$\sim 0^\circ$	3 sec.	Figure 4.10a
3	Flexion of elbow, causing in-plane bending of lower arm. Carrying 2.9 kg.	Elbow actuated by exoskeleton	$\sim 39^\circ - \sim 104^\circ$	$\sim 0^\circ$	3 sec.	Figure 4.10a
4-6	Flexion of elbow, causing in-plane bending of lower arm. Carrying 4.0 kg.	Elbow actuated by exoskeleton	$\sim 39^\circ - \sim 104^\circ$	$\sim 0^\circ$	3 sec.	Figure 4.10a
7-9	Abduction of shoulder, causing bending out of plane. Carrying 4.0 kg. Shoulder actuated by testperson.	Elbow fixed by exoskeleton.	$\sim 90^\circ$	$\sim 0^\circ - \sim 90^\circ$	~ 5 sec.	Figure 4.10b
10-12	Pushing wall. Small variations within fixed elbow are actuated by testperson.	Elbow fixed by exoskeleton.	$\sim 100^\circ$	$\sim 40^\circ$	-	-

Table 4.2: Movements included in the Exoskeleton on arm-test. The indicated weights are carried by the hand.

The measurement of the two moments is done with four strain gauges (SG) placed strategically on the exoskeleton (figure 4.4). The four SG are numbered 1 to 4. They form two full bridges related to the moment-axis as table 4.3 describes.

Moment round axis i	SG-pairs forming full bridges
$i = y$	1 - 4 and 2 - 3
$i = z$	1 - 2 and 3 - 4

Table 4.3: Measurement of moment around axis i by the use of strain gauges # .

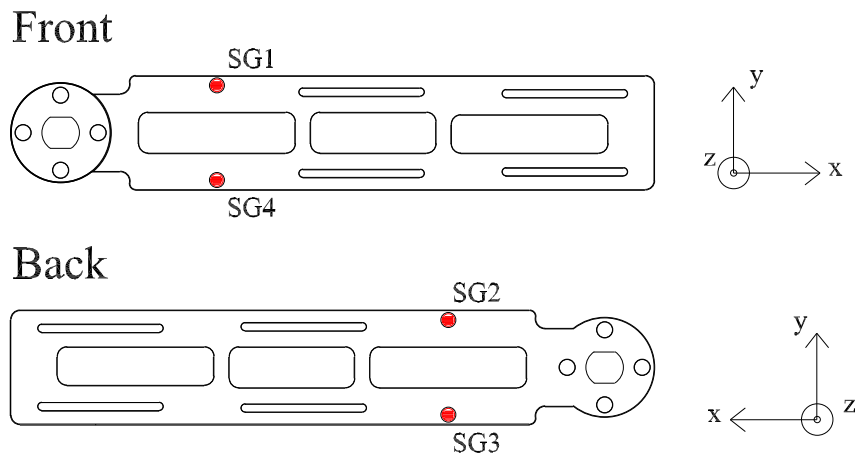


Figure 4.4: Placement of the strain gauges.

Materials for *Calibration*

- Strain gauges: 4 single gauges (MicroMeasurements, MMF003128, Linear Strain Gauge $\pm 3\%$ 0.100" (2.54mm))
- Computer connected to the strain gauges
- Exoskeleton elbow joint, generation 2, including actuator with programmed movement.
- Controller Arduino Mega micro controller together with a ESCON control board
- Volunteer testperson (Anne)
- Hooked weight: 1.3 kg, 2,9 kg and 4 kg

Materials for *Exoskeleton on arm*

- Strain gauges: 4 single gauges (MicroMeasurements, MMF003128, Linear Strain Gauge $\pm 3\%$ 0.100" (2.54mm))
- Computer connected to the strain gauges
- Exoskeleton elbow joint, Generation 2, lower part.
- Cylindrical dynanometer
- Weights: 50g, 100g, 200g
- Pulley system attached on plate (figure 4.8)

4.2.2 Strain Gauges

Four strain gauges are included to form two bridges around the two axes. All four strain gauges are attached as quarter bridges through a Wheatstone bridge. The quarter bridge modelling implies that measurement of strains are performed individually for each SG. The bridges are combined to what is equivalent to full bridges around the two axes after the test.

Wheatstone Bridge

The Wheatstone bridge is a set of four resistances (R_1 - R_4) connecting a voltage input, V_s , on point 2 and 4 to an output, V_o , on point 1 and 3 (figure 4.5). In an unaffected Wheatstone bridge, the voltage input is equal to the output. When replacing one or more of the resistive arms in the bridge with a strain gauges, it is possible to measure the change in resistance as the SG elongates. [Hoffmann, 1989]

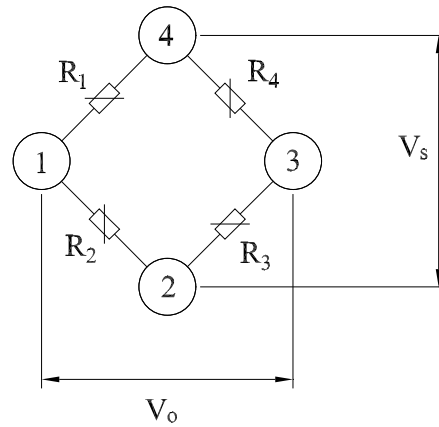


Figure 4.5: Wheatstone bridge. Inspiration from Hoffmann [1989]

The simplified relation between the Voltage input (V_s) and Voltage output (V_o) is

$$\frac{V_o}{V_s} = \frac{1}{4} \left(\frac{\Delta R_1}{R_1} - \frac{\Delta R_2}{R_2} + \frac{\Delta R_3}{R_3} - \frac{\Delta R_4}{R_4} \right) \quad (4.1)$$

in which the change in resistances are related to the strains through the gauge factor, k , by:

$$\frac{\Delta R}{R} = k \varepsilon \quad (4.2)$$

Different configurations can be set up from the Wheatstone bridge, depending on the number of active elements (i.e. SG) in the Wheatstone bridge.

The **quarter bridge** set up is made by replacing one of the four resistances in the Wheatstone bridge, and it has the capability to measure either axial or bending strain (figure 4.6a).

The **full bridge** is made by replacing all four resistances on the Wheatstone bridge. As the quarter bridge it is made for axial or bending strains, but it has either the potential to take Poisson effect into consideration or configure a high sensitivity to bending strain (figure 4.6b).

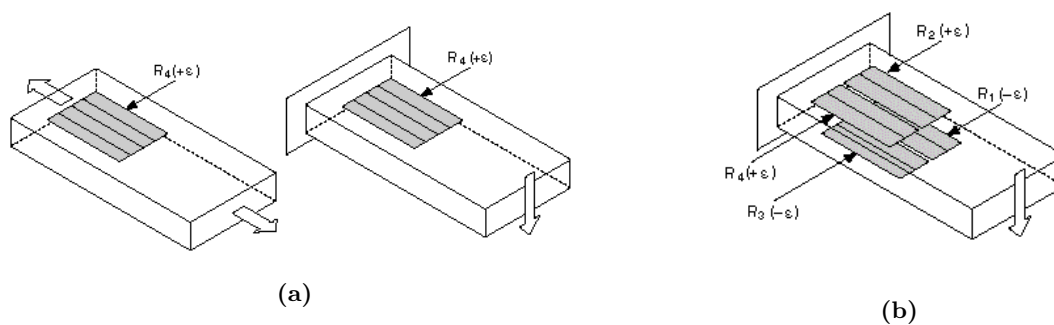


Figure 4.6: (a): Configuration of quarter bridge by the use of one SG. R_4 is varied by extension of the SG. (b): Configuration of full bridge by the use of four SG. All resistances (R_1, R_2, R_3, R_4) are changed in by extension/compression of the SG. [National Instruments, 2016]

Conversion from Strain to Moments

The strains measured from the strain gauges are for some of the results desired to evaluate as moments around the two axes. The full bridge configuration is used, as the strains from the four

quarter bridges are converted to a bending strain (figure 4.7).

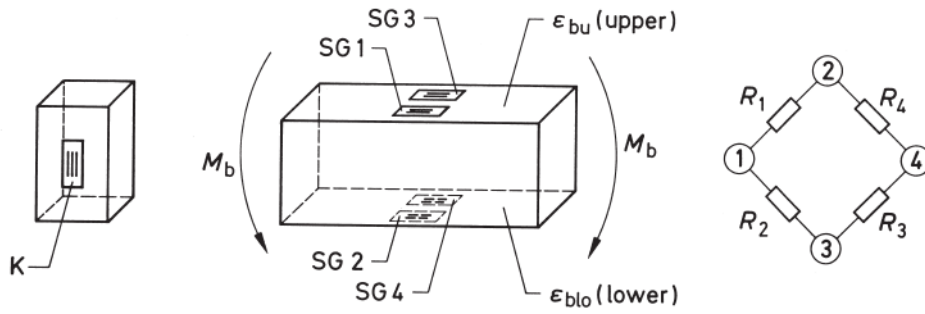


Figure 4.7: Use of SG in full bridge configuration for conversion to a bending moment. The number indicated on the strain gauges on this illustration are not related to figure 4.4, but they should at any time be related to the applied moment. [Hoffmann, 1989]

The bending strain is found as:

$$\varepsilon_b = \frac{\varepsilon_i}{4} = \frac{\varepsilon_1 - \varepsilon_2 + \varepsilon_3 - \varepsilon_4}{4} \quad (4.3)$$

where

ε_b	Bending strain
ε_i	Indicated strain value
ε_k	Strain from SG k

Through the constitutive relation of Hookes' law and the simple bending formula rewritten, the strains are converted to the moment by following relation:

$$M = \frac{E \varepsilon_b I}{y} \quad (4.4)$$

where

M	Moment in cross section
E	Young's Modulus, table 6.1
I	Moment of inertia around bending axis
y	Distance from center line to point in which σ is evaluated

Notes Regarding Strain to Moment-Conversion

This assumption required for the simple bending formula is violated for the bending around the Z-axis, as the height of the cross section is high, but it is chosen for simplification

4.2.3 Actuating the Exoskeleton

The actuation of the exoskeleton during the tests is done by trajectory-based control. When the exoskeleton is in use, the control will be interaction-based, but the sensors for measuring muscle activity has not been available.

The trajectory is adjusted through the current input of the motor, and it is defined to have a period of 3 seconds and a amplitude that results in a movement of ... °

4.3 Procedure

Calibration

Strain gauges were placed on the exoskeleton (figure 4.4), and they were connected to the computer.

The calibration was done by two generally different test setups to create the moment around the two axes, both including two setups with small variations ("flat" and "high", figure 4.9). During the tests, the prescribed load was applied, and meanwhile the strains were measured by the strain gauges as a function of time.

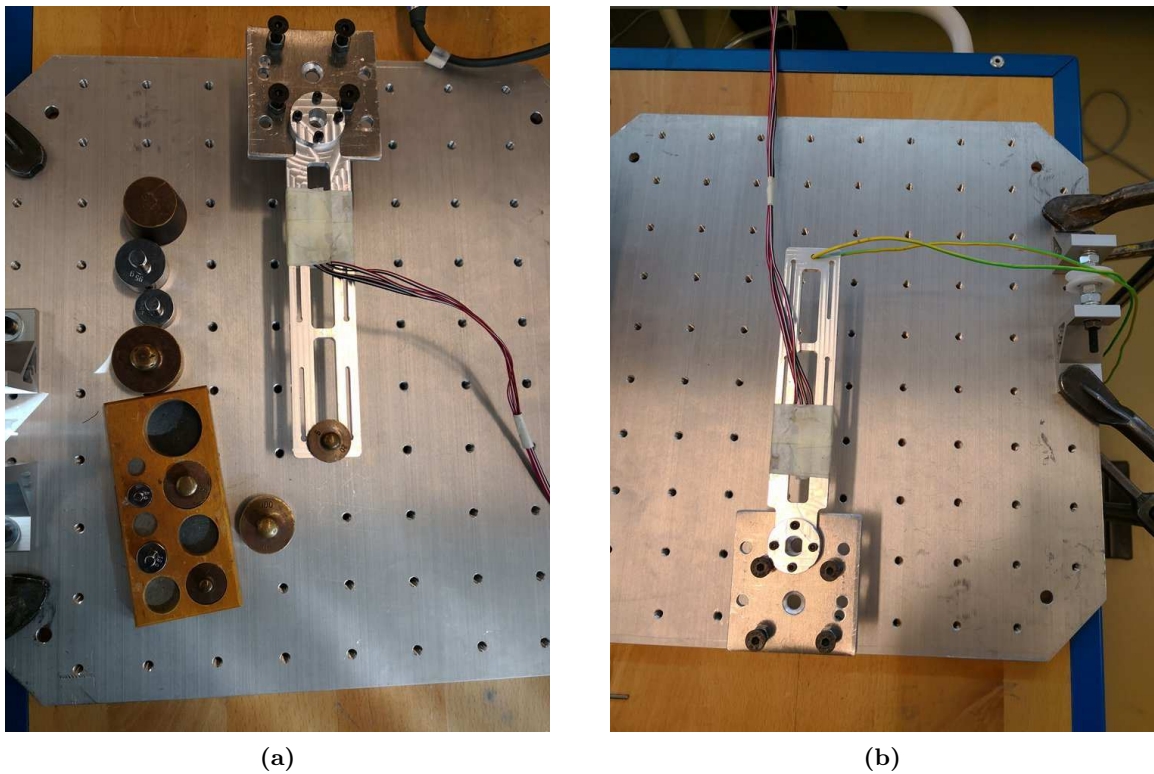


Figure 4.8: (a): Test setup for calibration around the y-axis with the use of weights. (b): Test setup for calibration around the z-axis with the use of a wire and a dynamometer.

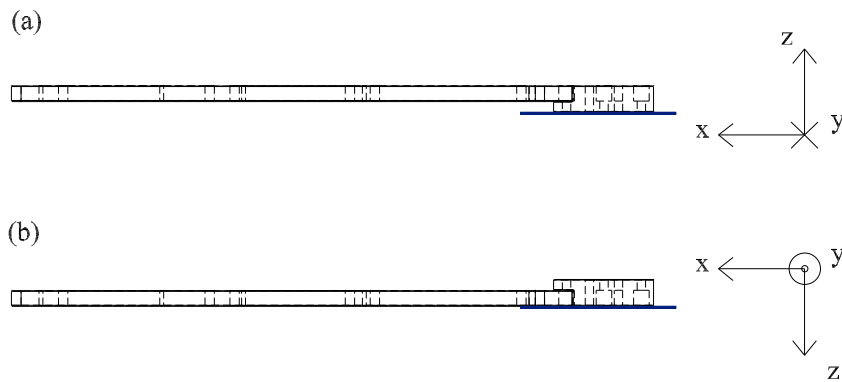


Figure 4.9: *Difference in setup at attachment point. The blue line indicates the plate on which the exoskeleton piece is attached. (a)="high". (b)="flat"*

Exoskeleton on Arm

The exoskeleton with attached strain gauges were placed on the test person. Motions were performed based on table 4.2. The motions were mainly controlled by the test person and approved by the observer. The motions were all executed thrice. During the movements, the strains were measured as a function of the time.

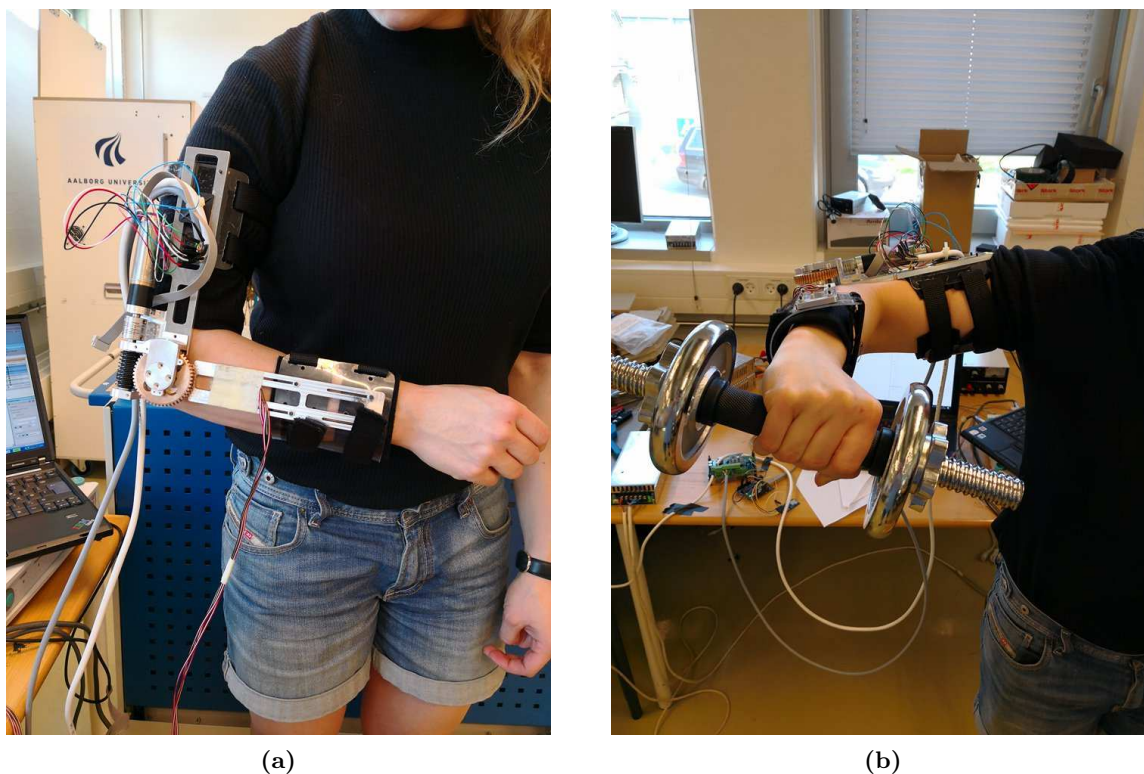


Figure 4.10: *(a): Test setup for flexion of elbow-movements. (b): Test setup for abduction of shoulder-movement.*

4.4 Processing of Test Data

The raw data from the tests were strains as a function of time. The processing of the data

Calibration

For the calibration test, the strains were plotted as a function of the physical moment applied to the exoskeleton (found from the applied force and the distance to the application point), as the purpose of these tests were to relate the strains to the moment.

Simulations representing the calibration setup has been set up, and the strains on the surface in the area where the strain gauges are mounted are extracted and plotted alongside the measured strains.

Exoskeleton on Arm

The strains are converted to a moment around both of the axes. This calculation are based on equation (4.4). The moment around the two axes are plotted as a function of time.

4.5 Results

Calibration

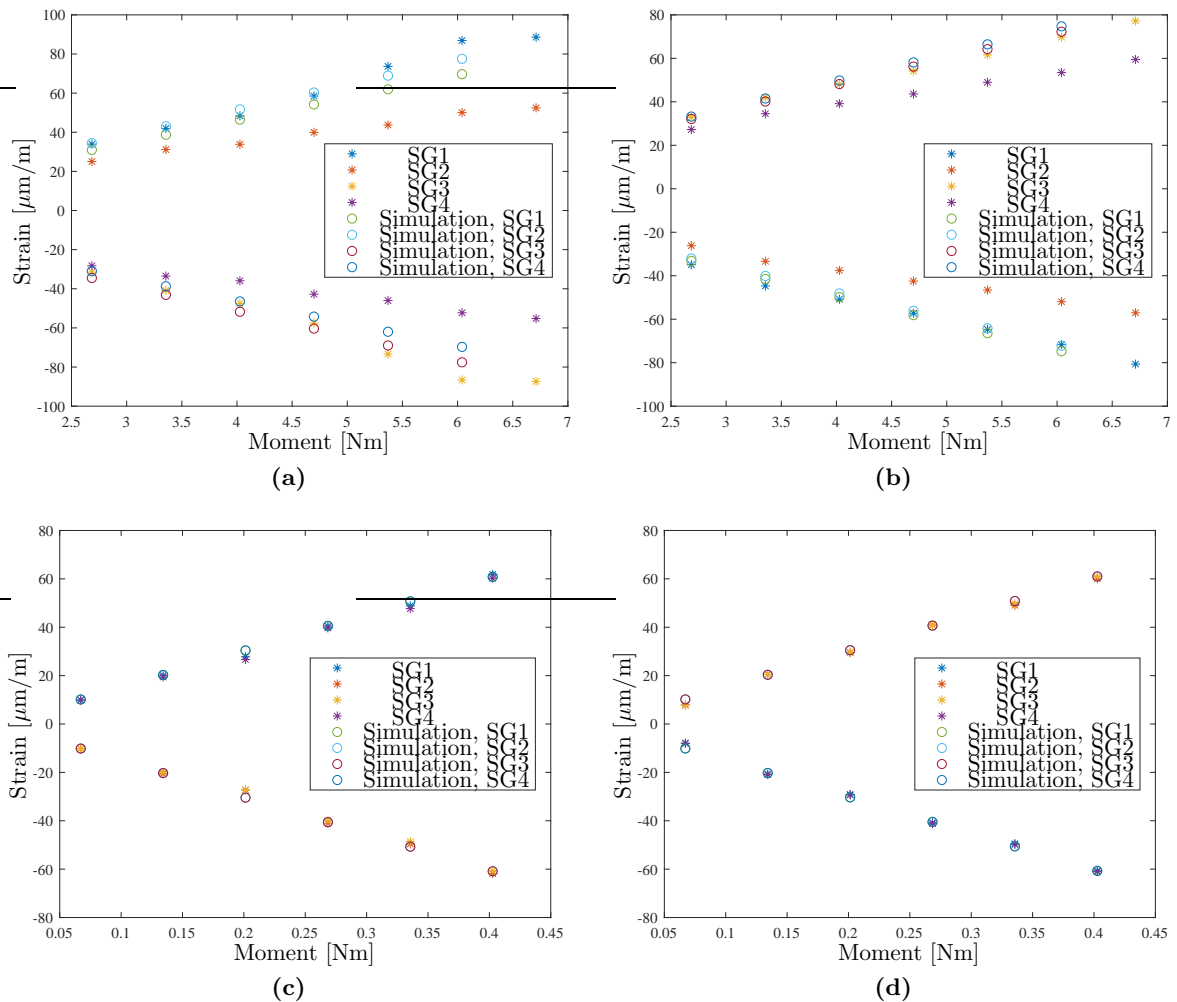


Figure 4.11: Plots from the calibration tests. (a) Moment around z-axis, "flat" configuration. (b) Moment around z-axis, "high" configuration. (c) Moment around y-axis, "flat" configuration. (d) Moment around y-axis, "high" configuration.

From the calibration plots (figure 4.11) it is seen, that when bending is applied around the strong axis (z -axis), the strains in the top (SG1 and GS2) vary in magnitude, which is also seen from the strain gauges in the bottom (SG3 and SG4). This indicates, that there has not been applied pure bending around the z -axis. The strains vary more in the physical test than in the simulation, which could indicate that it has been difficult to control the applied force during the test to same level as in the simulation.

For bending around the weak axis (z -axis), the strains vary very little within the measurements in top (SG1 and SG4) and bottom (SG2 and SG3), which could indicate a pure bending mode. The simulation results are close to the test results.

Based on the calibration tests around the strain gauges are estimated to have an adequate correlation between the occuring moment and the strains.

Exoskeleton on Arm

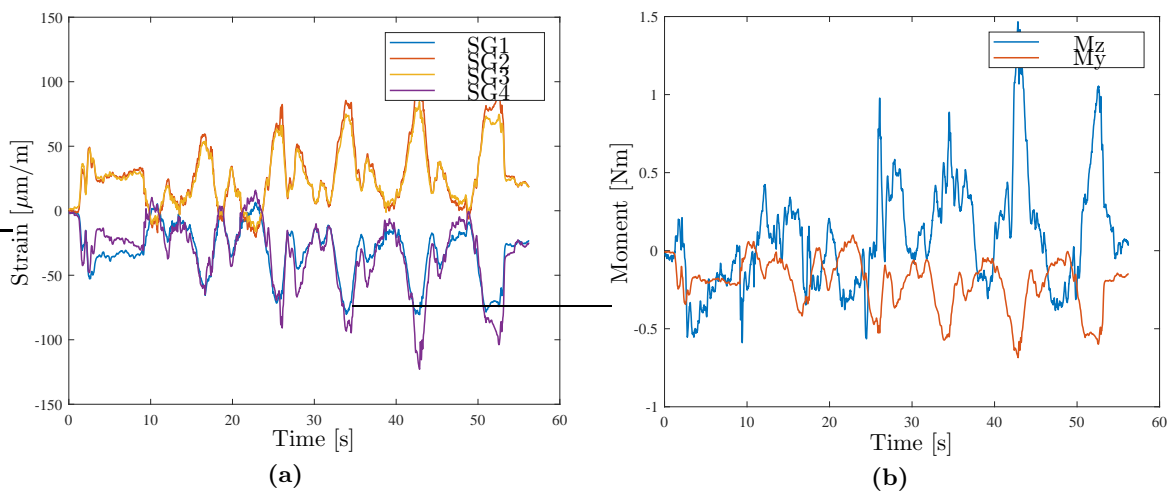


Figure 4.12: Results from flexion of elbow (4 kg). (a) Strains during the movements (b) Moment around z -axis (M_z) and y -axis (M_y) during the movement.

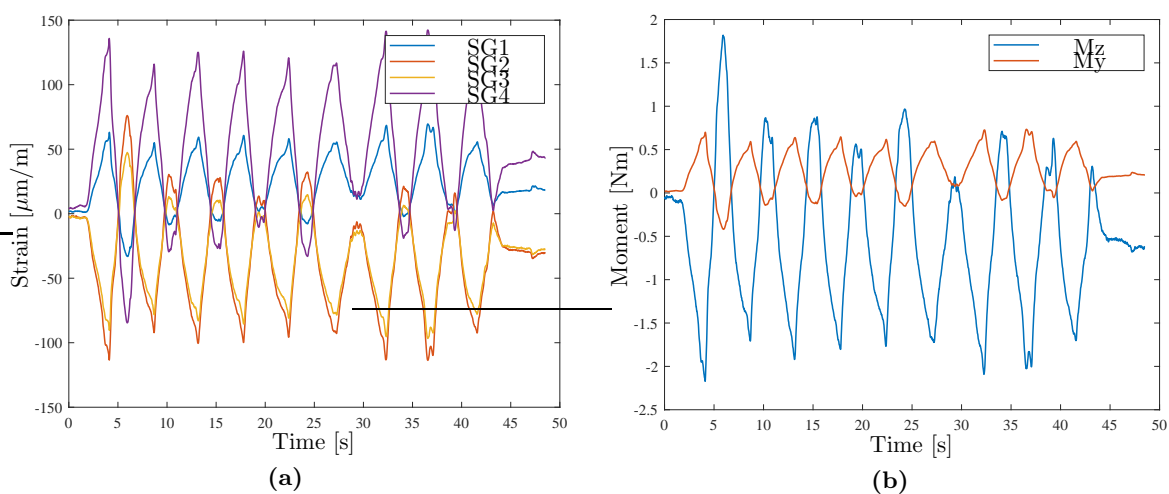


Figure 4.13: Results from push wall movement. (a) Strains during the movements (b) Moment around z -axis (M_z) and y -axis (M_y) during the movement. Representative plots.

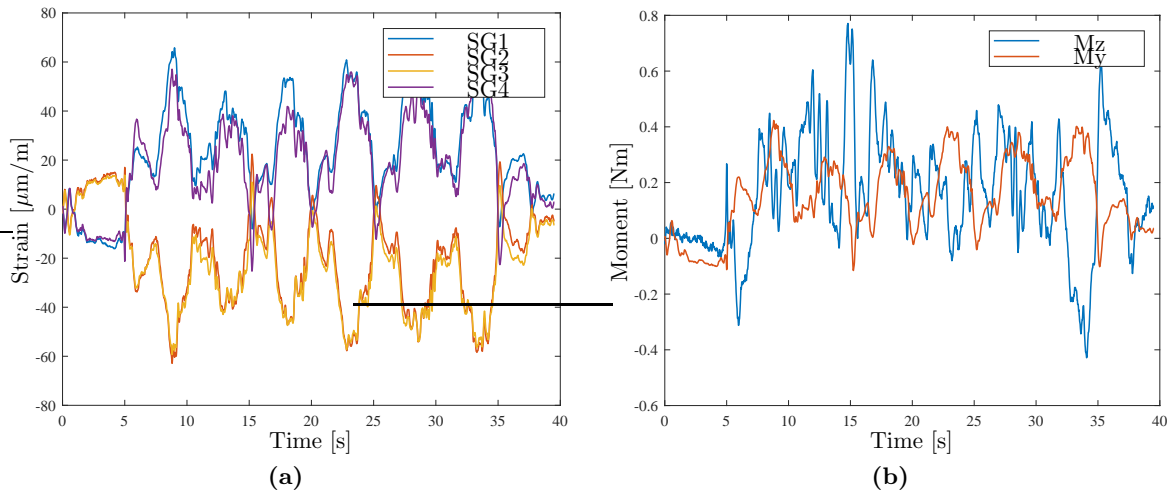


Figure 4.14: Results from shoulder abduction. (a) Strains during the movements (b) Moment around z -axis (M_z) and y -axis (M_y) during the movement. Representative plots

Test #	Maximum moment around z -axis [Nm]	Maximum moment around y -axis [Nm]	Ratio, $z:y$
1	0.8	0.5	1.6
2	0.8	0.5	1.6
3	0.8	0.2	4
4-6	2.4	0.8	3
7-9	1	0.6	1.7
10-12	3	1	3

Table 4.4: Summary of maximal moments around z and y (achieved amongst all the tests). The test number corresponds to table 4.2 on page 19. All the values are approximated to 1 decimal.

It appears from all the samples, that for most of the tests, there is a moment occurring around both the y -axis and the z -axis, with a magnitudinal relation of approximately 1:3, when the load reached an appreciable magnitude.

4.5.1 Update of Loading Scenarios

The indication of bending out of plane during the different movements suggests, that the test person has been counteracting the exoskeleton, as the positive moment around the y -axis occurs from pushing the arm outwards. This reaction to the exoskeleton could appear to avoid discomfort from the support.

From the test results it is decided to apply 1/3 of the moment around the z -axis as a moment occurring around the y -axis.

Estimation of Load-Sharing

Factor

5

The load-sharing factor is the load carried by the exoskeleton divided by the total load carried by the arm and exoskeleton combined. The upper limb is modelled with the desired payload (5 kg) and the moment occurring from that payload is compared to the capacity of the motor and the exoskeleton.

5.1 Analytical Evaluation of Upper Limb System

Considering the upper limb as a mechanical system, a free body diagram (FBD) can be constructed to determine the boundary conditions (BC). The BC of the upper limb considered valuable for determining the load-sharing factor is the (internal forces occurring in the attachment points between the exoskeleton and the arm, and the) torque in the elbow (figure 5.1).

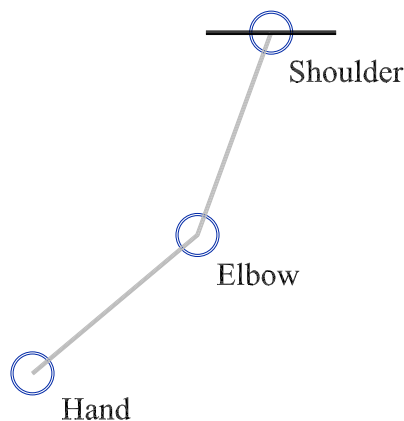


Figure 5.1: Configuration of the arm related to the upper limb. Center lines connecting hand, elbow and shoulder.

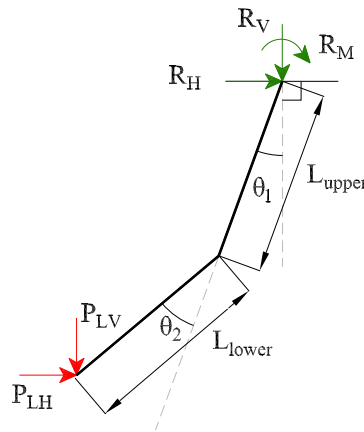


Figure 5.2: Configuration of static system. Parameters defined.

5.1.1 Assumptions

Following assumptions are made for the BC to be determined.

- The arm is fully clamped in the shoulder joint, representing the torque induced by the shoulder to resist movement. This is expected possible with the aid of the shoulder harness (section 2.1).
- The arm is sketched and calculated by the center line.
- The calculations are solely made based on the applied load. The weight of the arm is not considered, as the load-sharing factor is based on the share of the applied load. (Argument: we want to have the exoskeleton carrying a payload, not helping just moving the arm. The load sharing factor should therefore be based exclusively on the arm.) QUESTION: how does the exoskeleton distinguish: I suppose the assumption is, that the arm can carry itself, and we need to figure out what extra torque is induced by the applied load.

5.1.2 Procedure

The procedure of determination of boundary conditions followed a concept outlined by following steps:

1. Configuration of an arm attached to the shoulder, consisting of two links (FBD: Figure 5.2). The arm is sketched by the center line. Independent parameters of the system/mechanism are length of the upper- and lower arm, and angular position with rotation around the shoulder and elbow respectively (see table 5.1 for parameterdefinition). The system is modelled in 2D (XY-plane cf. figure 3.4).
2. Application of loads on the hand based on the loading scenarios.
3. Configuration of the arm based on the movement of the arm (adjustment of θ_1 and θ_2).
4. Calculation of internal loads through the arm, either in a static configuration or as a function of movements (variations of θ_1 and θ_2).

5.1.3 Independent Parameters

Parameters to define the upper limb system are presented in table 5.1 on the next page. *Fixed values* are based on test person for all tests of loading scenarios.

The payload is the load the exoskeleton is designed to carry during everyday use (section 2.1 on page 3).

Independent parameter	Fixed value
L_{lower}	0.30 m
L_{upper}	0.27 m
Payload, P_{LV}	5 kg
Payload 7, P_{LH}	0 kg m
	Range of value
θ_1	0° -90 °
θ_2	0° -90 °

Table 5.1: Independent parameters of upper limb. Lengths are measured based on load introductions.

5.1.4 Relations

Static equations of the system is set up.

Section 1

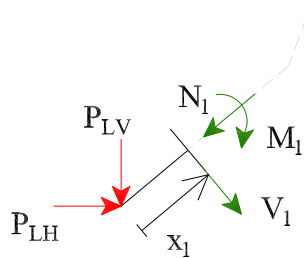


Figure 5.3: Section 1 of static system. The figure comprise the base of equations (5.1), (5.2) and (5.3).

$$V_1 = -P_{LH} \cdot \cos(\theta_1 + \theta_2) - P_{LV} \cdot \sin(\theta_1 + \theta_2) \quad (5.1)$$

$$N_1 = P_{LH} \cdot \sin(\theta_1 + \theta_2) - P_{LV} \cdot \cos(\theta_1 + \theta_2) \quad (5.2)$$

$$M_1 = P_{LH} \cdot \cos(\theta_1 + \theta_2) \cdot x_1 + P_{LV} \cdot \sin(\theta_1 + \theta_2) \cdot x_1 \quad (5.3)$$

Section 2

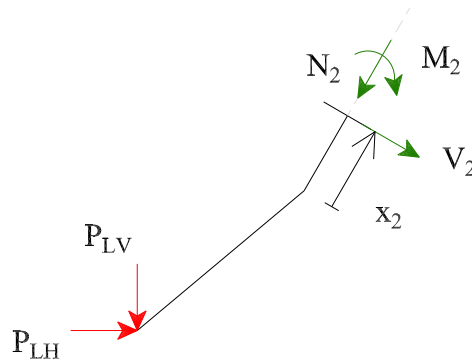


Figure 5.4: Section 2 of static system. The figure comprise the base of equations (5.4), (5.5) and (5.6).

$$V_2 = -P_{LH} \cdot \cos(\theta_1) - P_{LV} \cdot \sin(\theta_1) \quad (5.4)$$

$$N_2 = -P_{LH} \cdot \sin(\theta_1) + P_{LV} \cdot \cos(\theta_1) \quad (5.5)$$

$$M_2 = P_{LV} \cdot \sin(\theta_1) \cdot (\cos(\theta_2) \cdot L_{lower} + x_2) + P_{LH} \cdot \cos(\theta_1) \cdot (\cos(\theta_2) \cdot L_{lower} + x_2) \\ + P_{LV} \cdot \cos(\theta_1) \cdot L_{lower} \cdot \sin(\theta_2) - P_{LH} \cdot \sin(\theta_1) \cdot L_{lower} \cdot \cos(\theta_2) \quad (5.6)$$

5.1.5 Movements and Forces of Interest

The moment occurring in the elbow and the shoulder are extracted during different movements. The movements of interest are the ones that challenges the joint the most with respect to the moment around the z-axis (figure 3.4).

Two movements are conducted, and the moment experienced in both the shoulder and elbow are plotted as a function of the movement:

1. Arm going from completely vertical to completely horizontal. The first part of the movement includes only the elbow. The position of the elbow, θ_1 , is varied from 0° to 90° while the shoulder is held in 0° . When the elbow is flexed in 90° , the second part of the motion begins. In the second part of the motion, the elbow is extended again ($\theta_1: 90^\circ-0^\circ$) while the shoulder is lifting, changing θ_2 from 0° to 90° .
2. Arm going from completely vertical and to 60° above horizontal. The elbow is held extended ($\theta_1=0^\circ$) while the shoulder joint (θ_2) is going from 0° to 150° .

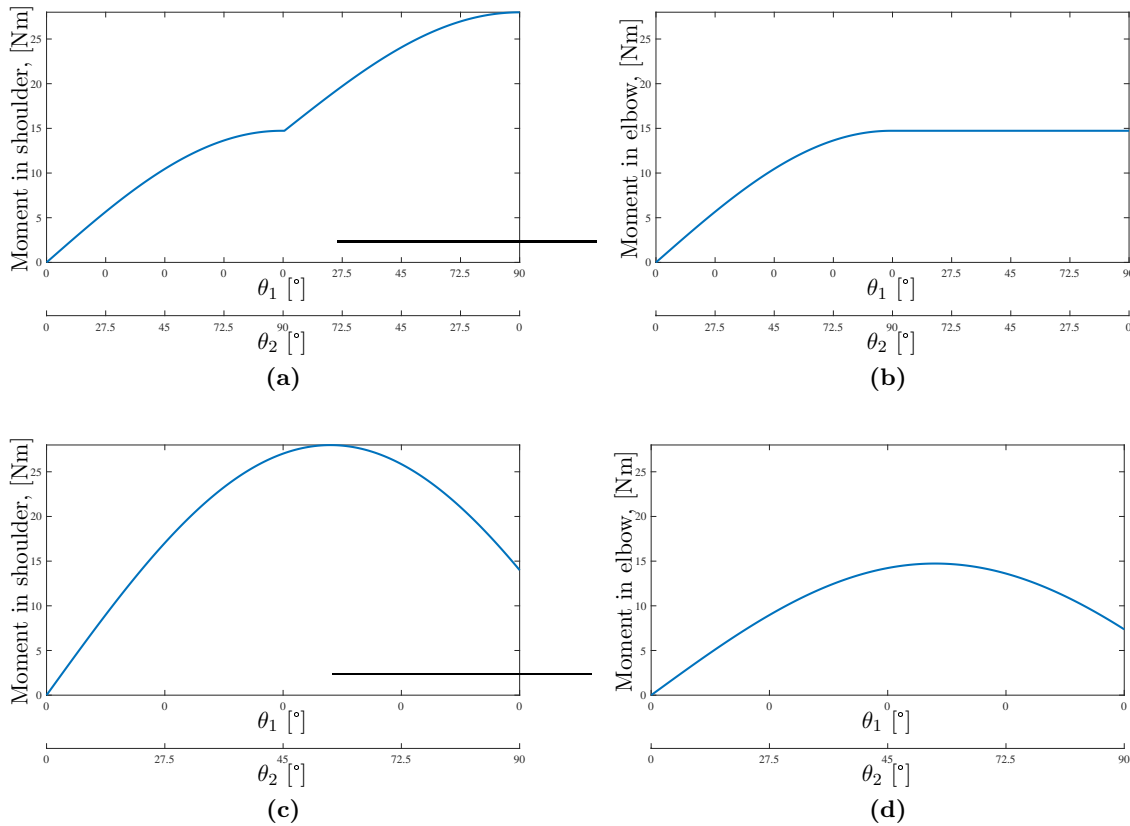


Figure 5.5: Moments occurring in the elbow and shoulder during movement. (a) and (c): moment in the shoulder, (b) and (d): moment the elbow. Upper and lower arm are estimated to be 300 mm each. In the hand (see figure 5.1 for position) is placed a vertical load (5kg)

The maximal moment occurring in the elbow joint of the test person with a payload of 5 kg is 14.7 Nm.

5.1.6 Load-Sharing Factor

The load-sharing factor is estimated from the highest occurring torque in the elbow joint and the torque from the motor.

$$LS_{factor} = \frac{M_{exoskeleton}}{M_{elbow}} \quad (5.7)$$

The maximal torque from the elbow is the moment occurring during the *backwards movement onto the wheelchair*, which is 85.17 Nm (chapter 4 on page 15). The motor works with a torque of 30.35 Nm (section 2.1 on page 3). Utilizing the entire power of the exoskeleton, and performing the most torque demanding movement, the loadsharing factor is estimated to:

$$LS_{factor} = \frac{30.35\text{Nm}}{85.17\text{Nm}} = 0.36 \quad (5.8)$$

Specifying the Load-Sharing Factor

The load-sharing factor is at any point defined by — meaning that a change in the LS-factor will change the needed torque and hence the current of the motor.

Its dependency can be illustrated by following relations: For different arm configurations, i.e. variations of θ_1 and θ_2 (figure 5.2 on page 30), different moments occur in the elbow. If the loadsharing factor is set at a fixed level, the needed torque provided by the exoskeleton varies with the arm configuration.

Notes about the Load-Sharing Factor

As the load-sharing factor is dependent on the moment occurring in the elbow, it will for the movements that include bodyweight be dependent on the weight of the person.

Materials & Manufacturing 6

This chapter introduces the materials used for the new exoskeleton design. The chapter explains the basic key concepts for the mechanical properties of composite materials as well as the manufacturing method.

6.1 Available Materials and Key Concepts

Aluminium alloys are typically used in structures in which there exists a need for a high specific strength, i.e. $\frac{\sigma}{\rho}$ in which σ is a typical strength material parameter such as the yield- or tensile strength, and ρ is the density. The alloy used in this application requires a high strength to decrease the amount of material needed and hereby reduce the weight of the structural elements in which the alloy is used. The University of Aalborg has several different alloys at their disposal, from which it is decided to use a 7075 T6 alloy, which offers the highest yield strength of 470 MPa and a tensile strength of 540 MPa. Unlike the composite materials described later on in this section, aluminium can be considered as an isotropic material, i.e. the material properties is the same in all directions. The assumption of isotropic material properties allows for the use of more general failure criteria. The failure criterion for the aluminium used in this thesis is selected to be the Von Mises failure criterion.

Composite materials, also referred to as orthotropic materials have directional dependant material parameters. They are two or more phased materials, that are bonded or combined on a macroscopic level. Typically they are a combination of a strong and stiff material, in this thesis thin and long fibres with a more less strong and more compliant matrix material, typically a thermosetting resin or thermoplastic polymer. The selection of fibre material greatly influence mechanical properties, whereas the matrix material often dictate the manufacturing method and process. Fibres and matrix materials are sold in various forms. This thesis limits itself to the use of unidirectional (UD) fibre mats, in which all of the fibres are oriented in the same direction. The mats are also referred to as lamina or ply, and stacking several of these lamina creates a laminate. The properties of the laminate depend on the orientation and stacking sequence of the lamina. In a laminate consisting of multiple lamina oriented in the same direction, the stiffness and strength is the greatest in the fibre direction, and lowest transverse to the fibre direction.

Currently the University of Aalborg have mechanical properties available for two different types of UD fibre mats - IM7K carbon and E-glass. The UD carbon mats contain pre-impregnated resin, whereas the UD glass mats needs to be impregnated with resin during the manufacturing process. The methods for manufacturing are explained in greater detail in section 6.2 on page 37. The mechanical properties of the lamina are defined in a local material coordinate system, and distinguish between tensile and compressional strength i.e. E_1 dictates the stiffness in the fibre direction and X_t and X_c the tensile and compressional strength in the fibre direction, whereas E_2 dictates the properties transverse the fibre direction. The mechanical properties are shown in table 6.1 on the next page and table 6.2 on the following page.

Material type	Density [kg/m^3]	Cured ply thickness [mm]	Young's Modulus [GPa]	Specific stiffness [MPa/ρ]	Tensile Strength [MPa]	Specific strength [MPa/ρ]
Unidirectional (IM7-12K)	1580	0.13	138/9.7	87.3	2200/66	1.39
Unidirectional (E-Glass)	2000	0.28	40/10	28.5	914/35	0.46
Aluminium (7075 T6)	2770	-	69	43.7	540	0.27

Table 6.1: Physical properties for the three available materials. Young's modulus and the tensile strength are displayed in the strongest and weakest directions for the composite materials.

Unidirectional (IM7-12K)				Unidirectional (E-Glass)			
	Symbol	Value	Unit		Symbol	Value	Unit
Fiber direction, 0°				Fiber direction, 0°			
Tensile modulus	E_1	138	GPa	Tensile modulus	E_1	40	GPa
Tensile strength	X_t	2200	MPa	Tensile strength	X_t	914	MPa
Compression strength	X_c	1800	MPa	Compression strength	X_c	525	MPa
Transverse direction, 90°				Transverse direction, 90°			
Transverse tensile modulus	E_2	9.7	GPa	Transverse tensile modulus	E_2	10	GPa
Transverse tensile strength	Y_t	66	MPa	Transverse tensile strength	Y_t	35	MPa
Compression strength	Y_c	248	MPa	Compression strength	Y_c	121	MPa
Properties in plane 1-2				Properties in plane 1-2			
Poissons ratio	ν_{12}	0.31	-	Poissons ratio	ν_{12}	0.29	-
Shear modulus	G_{12}	5.9	GPa	Shear modulus	G_{12}	5	GPa
Shear strength	S_{12}	139	MPa	Shear strength	S_{12}	35	MPa
Properties in plane 2-3				Properties in plane 2-3			
Poissons ratio	ν_{23}	0.04	-	Poissons ratio	ν_{23}	0.07	-
Shear modulus	G_{23}	3.1	GPa	Shear modulus	G_{23}	2.5	GPa
Shear strength	S_{23}	32	MPa	Shear strength	S_{23}	10	MPa

Table 6.2: Mechanical properties of the two available fibre materials.

Composite laminates do not have a well defined failure criteria such as the von Mises stress criteria for isotropic materials. Several failure criteria have been proposed at the World-Wide Failure Exercise. Simple or classical failure theories such as the max stress theory do not take combination of failure modes into account, whereas this is achievable with the Tsai-Wu failure criterion. However, Tsai-Wu needs experimental values that are difficult to determine, and in general overestimates the strength of laminates subjected to compressional loading. Furthermore, laminates can often transfer loads beyond what causes the first ply failure, which makes laminate failure difficult to predict. In this thesis, it is decided to use the max stress criterion to estimate the resistance against failure for the laminate design.

The maximum stress criterion is based on inequalities and distinguishes between five different failure modes i.e tensile and compression failure in the fibre direction, tensile and compression failure transverse to the fibre direction and shear failure. The failure assessment is based on a strength index denoted as the failure index (FI), which is the ratio between the maximum stress in each ply evaluated in the material coordinate system. Mathematically, the inequalities are

expressed as:

$$\begin{aligned}
 \text{For } \sigma_i > 0 : \quad & FI = \frac{\sigma_1}{X_t} \quad FI = \frac{\sigma_2}{Y_t} \quad FI = \frac{|\sigma_{12}|}{S} \\
 \text{For } \sigma_i \leq 0 : \quad & FI = \frac{\sigma_1}{X_c} \quad FI = \frac{\sigma_2}{Y_c} \quad FI = \frac{|\sigma_{12}|}{S} \\
 & \max(FI) \leq 1
 \end{aligned} \tag{6.1}$$

where the strength parameters measured the material directions in equation (6.1) are defined as:

X_t	Tensile strength in longitudinal fibre direction
X_c	Compressive strength in longitudinal fibre direction
Y_t	Tensile strength in transversal fibre direction
Y_c	Compressive strength in transversal fibre direction
S	In-plane shear strength

6.2 Manufacturing Method for Composites

The manufacturing of composite laminates is closely related to their end use [Jones, 1999]. It has been decided to manufacture the composite parts of the new structural design at the facilities available at the University of Aalborg to gain a deeper practical understanding of the design decisions made from simulation results and theoretical knowledge. The current manufacturing facilities are made for vacuum infused casting, and is explained in greater detail in the following.

Typically, manufacturing of composite laminates is manual and labour intensive process and involves several process steps. The manufacturing process is divided into four categories, i.e preparation of the fibre plies, a layup process onto a mould, curing, and lastly post treatment and/or post manufacturing. Initially, the fibre plies are cut out in the desired shape with the fibre directions oriented as specified by the designer. An illustration of this is shown in figure 6.1 on the next page.



Figure 6.1: An example of carbon fibre prepreg plies cut in in several sizes with fibres oriented in $0^\circ, \pm 20^\circ, \pm 45^\circ, \pm 70^\circ,$ and 90° .

After cutting out the plies, they are manually stacked at the specified location, typically in a mould, and in the stacking sequence prescribed. The mould is what gives the composite laminate its desired shape. Moulds are typically divided into two types, either female or male moulds, however they can be combined. The selection on mould type depends on the end use of the product. Typically, the surface pointing inwards towards the mould surfaces have the best surface quality e.g, surface geometry, surface appearance, surface roughness, etc. A male mould is selected in this project, to obtain the best control of the surface geometry. The mould is placed in a vacuum bag once the fibres are stacked correctly on the mould and How the resin is added depends on the type of fibre ply. The carbon fibre plies are already pre-impregnated with resin. The glass fibre plies however are dry and resin is applied to the plies through vacuum infusion instead. Lastly a layer of peel ply is added on top of the fibre plies and a layer of breath ply onto the peel ply. The peel ply is added to avoid adhesion between the composite laminate and the breath ply, whereas the breath ply is added to soak up excess resin. An example of the result of the layup process is shown in figure 6.2 on the facing page.



Figure 6.2: *Fill*

The mould is placed in an oven to consolidate the fibres with the resin, once the layup process is finished. The resin needs to be heated to cure and harden. How long, and for how high of a temperature is specified by the supplier. The supplier often provide a curing cycle or curing diagram. An illustration of the curing cycle for the carbon fibre material is shown in figure 6.3. Note that some composites require postcuring, however this is not specified by the suppliers for the materials used in this thesis.

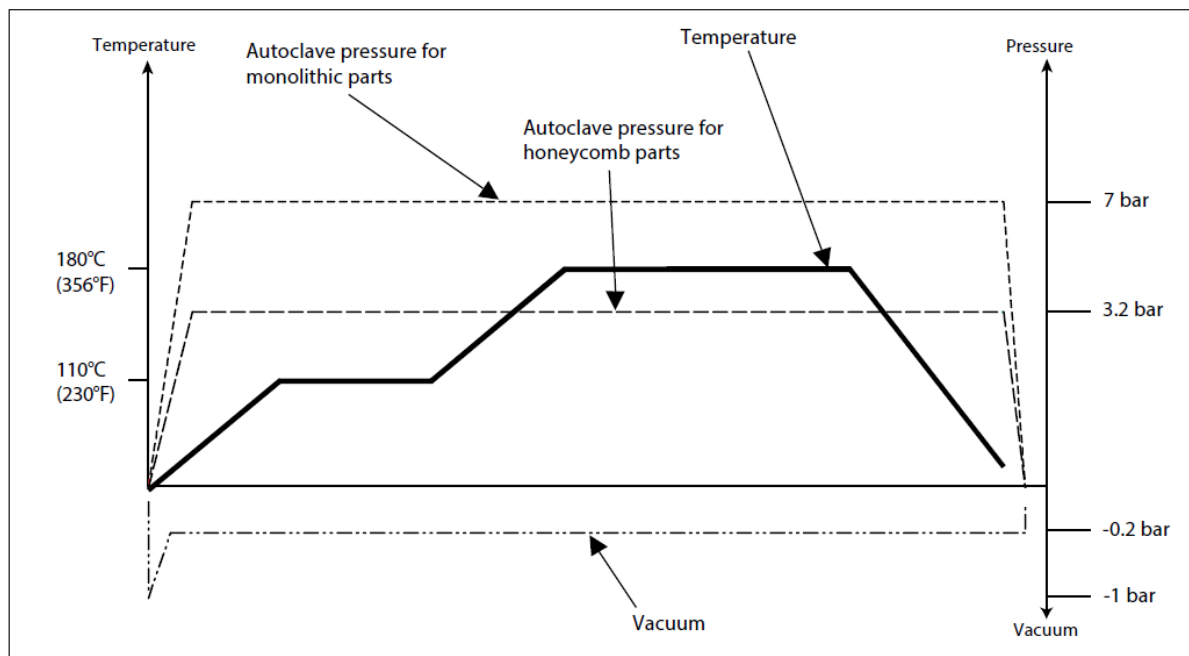


Figure 6.3: *Curing cycle, [Hexcel, 2016]*

Lastly, the vacuum bag is peeled of the moulded composite piece once the resin have cured. Excess material is then removed if it is required, e.g drilling holes, smoothing sharp edges, etc.

Evaluation of Comfort, Weight and Manufacturing 7

The overall purpose of this chapter is to gather information about the interaction between human and exoskeleton, and at the same time evaluate manufacturing and materials. The chapter will work as an initial evaluation of design choices with respect to manufacturing, materials selection, influence of structural compliance, and influence of a weight reduction in the new design. The design process for these specimen is explained in short. A more comprehensive explanation of the design approach for composite designs is described in section 10.2.

7.1 Design of Initial Prototypes

Three different composite supports are designed to investigate the influence of compliance and weight for a forearm support. The supports are made out of the carbon fibre material presented earlier in section 6.1. The compliance of the composite specimens are investigated through simulations. The simulations are created in ANSYS Workbench v18.2. The most compliant specimen is designed to carry a maximum weight of 3 kg. The specimens are designed such that they can be attached to the existing upper arm structure. Additional aluminium spacers are manufactured to ensure that they can be attached to the upper arm structure properly. The previous design generation requires a forearm structure with a thickness of 8.5 mm to connect the forearm structure to the gearwheel and upper arm structure. The specimen have a length of 210 mm and height of 35 mm with a varying thickness. The specimen has three layup sections as illustrated in figure 7.1.

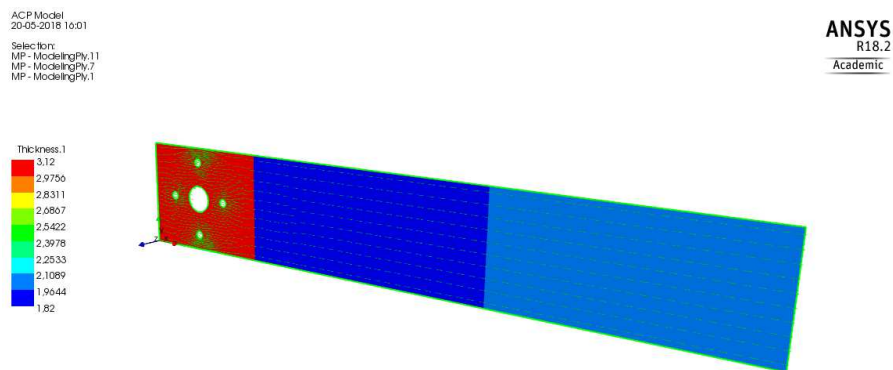


Figure 7.1: Illustration of the three individual layup sections for the test specimen - section 1 (red), section 2 (blue), section 3 (light blue).

Section 1 is defined with a quasi-isotropic layup, i.e fibres are oriented in 0° , 90° , -45° , and 45° . This layup is typically used in areas in which the force flow is poorly defined, e.g areas with bolted connections. Section 2 is defined with fibres that balance the load introduction. The loading is applied as a 3 kg load in the y-direction and 1 kg load in the negative z-direction. The loading will therefore result in a twisting of the specimen. Fibres should therefore be oriented to

accommodate this. However, orienting the fibres directly in direction of the loading stiffens the design too much. Compliance is sought and achieved by adding layers that are oriented slightly from the direction of the loading, e.g one layer oriented directly in the primary load path may give sufficient strength and stiffness, whereas two layers oriented with a slight offset angle will give sufficient strength, but more compliance. The fibres in section two are primarily oriented in 0° , $\pm 70^\circ$, $\pm 20^\circ$, and $\pm 45^\circ$ as this showed to give the best compliance without exceeding a FI of 0.7. Section 3 is also defined as quasi-isotropic as a thermoplastic cuff is bolted onto this section. The number of layers in the respective section is changed to increase the stiffness. The following simulation results are found for the three different specimen:

	Q1	Q2	Q3
δ [mm]	50.2	29	9.5
Weight [grams]	17	18.9	27.4

Table 7.1: *Simulation results for the three carbon fibre prototypes. Note that δ is the total deformation of the specimen.*

The layup used for the three prototypes are illustrated in figure 7.2, figure 7.3, and figure 7.4.

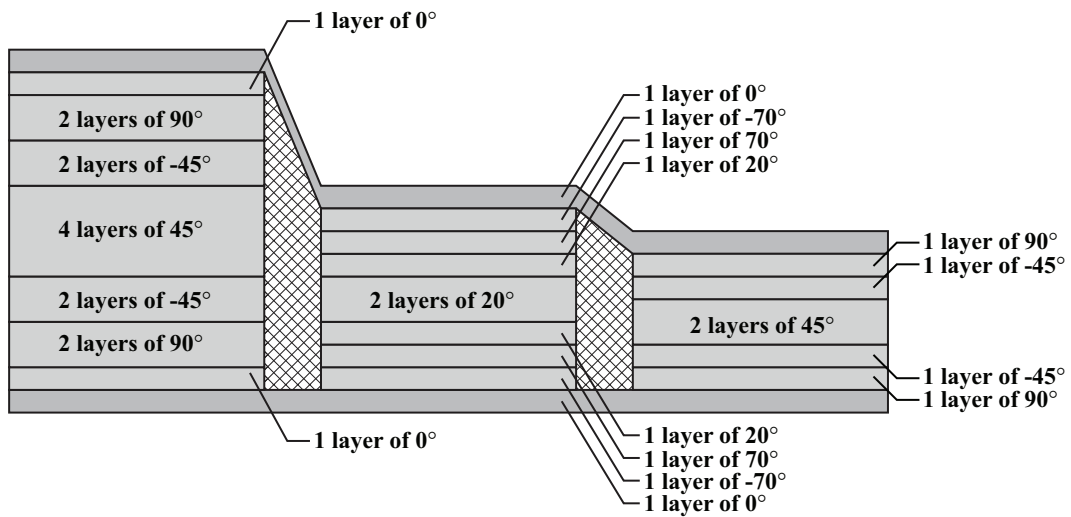


Figure 7.2: Illustration of the fibre layup used for Q1.

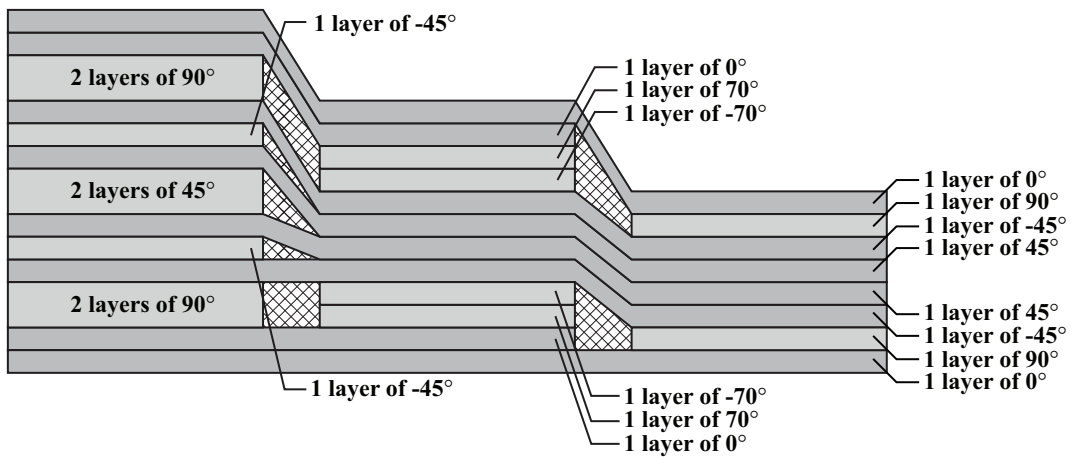


Figure 7.3: Illustration of the fibre layup used for Q2.

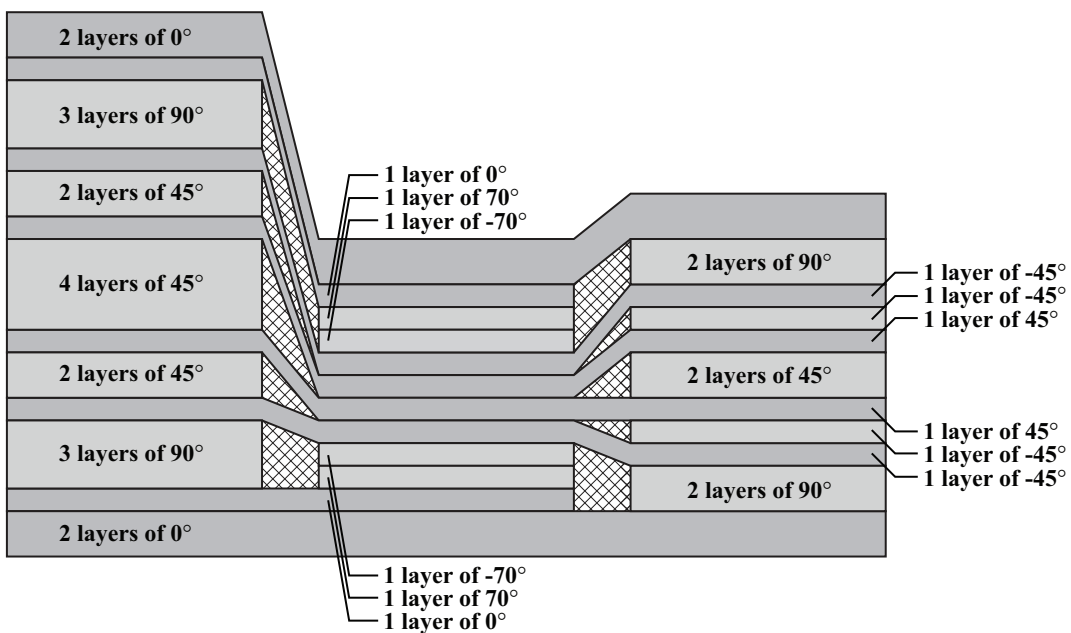


Figure 7.4: Illustration of the fibre layup used for Q3.

7.2 Manufacturing of Prototypes

Sections are cut according to the defined layout (section 7.1), and they are stacked on a planar surface. The preparation for the curing followed the guideline presented in section 6.2.

The curing process followed the guideline presented in section 6.2 on page 37.

The curing cycle prescribed by Hexcel [2016] is used, and it follows table 7.2.



Figure 7.5: Vacuum bag including samples prepared for curing.

7.3 Evaluation of Manufacturing

The plies are found easy to cut and handle, especially when they are kept at a temperature below 10°. Even though these first layouts are made on a planar surface, it is expected, that the plies will be easy to lay out in a mould, if that will be necessary.

During the curing it was experienced, that the oven was difficult to control in temperature, especially in the cooling process. An autoclave would have been preferable.

The tubes for application of vacuum melted at high temperatures, and it was assessed, that the tubes should not be subjected to temperatures above 140°C, which implies that the curing process should be adjusted.

Holes were drilled post curing such that the prototypes could be attached to the previous design generation of the exoskeleton. It was realised during this process that the fibres would break and tear as shown in figure 7.6. This issue could be solved by purchasing specific drills for composites, however these were not available at the current time. The issue could also be accommodated by

Phase	Temperature at start of phase, [°C]	Temperature at end of phase, [°C]	Time [min]
1	21	110±5	45±2
2	110±5	110±5	60±5
3	110±5	180±5	35±3
4	180±5	180±5	120±5
5	180±5	21	120+

Table 7.2: Curing cycle for Hexply 8552 [Hexcel, 2016]

using another fibre type, i.e a woven weave, however this was not available at the current time either.



Figure 7.6: *Surface of sample after drilling holes.*

7.4 Test of Prototypes

The term prototype is used, as the parts are made to test a concept, but it should be noted, that these are not suggested as replacements for the current aluminium forearm design. The overall geometry (i.e. attachment points) is similar to the Generation 2 forearm, and it is easily assembled with the exoskeleton presented in (section 2.1 on page 3). Test subjects were being asked to wear the exoskeleton in a fixed elbow position and perform limited movements. The purpose of the test was to test the ergonomics, which is one of the performance metrics suggested by Bostelman and Hong [2018].

The test population consists of healthy volunteers in the age 21-26, with a height between 170cm and 186cm. The test subjects have no limited muscle activity.

A requirement for the test subjects are that the length of their upper arm must not exceed 320 mm, from the elbow to the shoulder, and the length of their lower arm must not exceed 290 mm, from the elbow to the wrist.

The test uses a small sample size to be able to evaluate the results qualitatively. The sample size is 6 people.



Figure 7.7: *Original forearm part and prototypes.*

The test is divided in two parts:

- Test of exoskeleton Generation 2-forearm, G2
- Test of prototype-forearm (Three forearms, Q1, Q2 and Q3)

All test subjects are testing the Generation 2 in the first test. The prototypes are tested in order of varying compliance. The test subjects are not informed about the compliance of each test sample. Both parts of the test (G2 and Q1,2,3) are performed within one day. The test subject is asked to perform defined movements within both parts of the test. During the movements, the test subject will be wearing the exoskeleton in a fixed angle of 90 degrees.

Shoulder abduction Raising arm with the shoulder solely

Forearm rotation Rotating the upper arm around its own axis, causing the lower arm to move inwards and outwards - rotation around the y-axis

Flexion movement without weight Trying to rotate the lower arm to get a feel of how the exoskeleton restricts the natural movements.

Flexion movement with weight Carrying a weight to feel how the loading is shared between the user and the exoskeleton.

The evaluation of the tests are based on a questionnaire, which the subjects are asked to fill out after the tests. The answers from the test will be handled qualitatively to evaluate the prototype. The Questionnaire is situated in appendix A on page A79.

Scores from the Questionnaires

The level of comfort was scored at a level between 1 and 5 (with 5 as most comfortable), where the test subjects were to decide themselves how to define comfortable. Regardless of their definitions, 5 out of 6 evaluated the comfort level of the entire exoskeleton to be higher when Q1 were mounted in relation to when G2 were mounted.

The feeling of compliance was improved from 5 out of 6 test subjects when going from G2 to Q1. The variation of the parts (G2, Q1, Q2 and Q3) did not affect the score of the experienced weight of the entire exoskeleton significant.

Comments from the Testsubjects

During the tests, the test subject commented on their experience. Significant comments are included:

Generation 2:

"Too flexible in the supports"

"The compliance comes from the support"

Q1:

"The compliance of the studied part (Q1) increases, but it is difficult to appreciate due to the compliance of the support"

"The compliance is very comfortable"

"Good user experience thanks to the torsional compliance"

Q3:

"Same as aluminium"

"Less comfortable than Q1"

General:

"Lower support to close to elbow".

General Observations

One test subject experienced no significant difference in compliance when performing a supination/pronation. The reason for that could be, that the support was not capable of decreasing the circumference to a level that fitted the test subject. This indicates, that in order to gain improved from increased compliance, the support should be attached well to the arm, and stiff enough to transfer the load to the sections, where the compliance is desired.

7.5 Evaluation of Prototypes

From the tests it was discovered, that the compliance of the forearm was noticeable and that it improved the user experience. It is therefore decided to proceed with this which breaks with the initial concept of improving the stiffness. It is still the belief of the authors, that a reduction in weight would improve the experience of the user, and it should therefore be limited.

Additional Design Considerations 8

The load introduction onto the exoskeleton is discussed in chapter 4 and chapter 5. It is assessed from the results in these chapters that the loading can be simplified to two loading scenarios. The loading estimated in chapter 5 demonstrated that the loading introduced during everyday activities is lower than the maximum available torque from the motor. Based on these findings it is assessed that the highest loading will occur when the motor delivers maximum torque during wheelchair lifts. Furthermore, it is discovered in chapter 4 that an moment around the y-axis occurs during operation of the exoskeleton. This loading is introduced by the user at the same time as torque is delivered by the motor. The moment around the y-axis is seen to reach values as high as one third of the motor torque. It is therefore decided to use the maximum available motor torque, in combination with an secondary moment around the y-axis with a value of one third of the motor torque as the primary loading scenarios for the remainder of the thesis. The direction of the moment will be dictated by either biceps contraction (BC) or triceps contraction (TC), and is explained in greater detail later on in the thesis. This consideration initiated additional ideas with respect to the loading, which are explained in the following.

8.0.1 Dynamical Loading and Fatigue

A general rule of thumbs states that the dynamical response of the system can be neglected if the fundamental eigenfrequency is three times higher than the highest operational frequency [Overgaard, 2015,p. 140], i.e

$$\omega \leq \frac{1}{3}\omega_0 \quad (8.1)$$

in which

$$\begin{array}{l} \omega \quad \left| \text{Maximum operational frequency} \right. \\ \omega_0 \quad \left| \text{Fundamental eigenfrequency} \right. \end{array}$$

The maximum input RPM for the planetary gear is restricted to 12000 RPM. With a gear ratio of 1:270, the maximum RPM of the forearm is calculated to be 44.4 RPM or in Hz

$$\omega = \frac{44.4 \text{ RPM}}{60} = 0.75 \text{ Hz} \quad (8.2)$$

Therefore, the fundamental eigenfrequency should fulfil

$$\omega_0 > 2.25 \text{ Hz} \quad (8.3)$$

The need for fatigue analysis is dependent on the amount of load cycles experienced. Sandal et al. [2018] suggests that an average wheelchair user perform 20 wheelchair lifts per day. This is equivalent to roughly 7.300 lifts per year. This indicates that fatigue could be

considered. However, it is chosen not to investigate the consequence of fatigue loading at the current stage of the thesis. The primary investigation of this thesis is not to create a new exoskeleton design for commercial use, but rather to create a new prototype that investigates other means to improve the user comfort. Furthermore, composites do not experience fatigue in the same manner as isotropic materials. It would require comprehensive testing to investigate if and how fatigue would affect the composite structure.

8.0.2 Safety Factors

It is decided to apply safety factors on the loads and material characteristics, to ensure the structural integrity of the design. The selection of safety factors is based on the method of partial coefficients, in which two different design guidelines are used for alloys and composites. The selected standards used as guidelines are [DS/EN:1999-1-1, 2008] and [Veritas, 2010] for the aluminium alloy and composite material, respectively.

The approach of partial coefficient applies correction factors to both the load and material design parameters. It is decided to apply the same load coefficient for the aluminium and composite piece, as their respective loading is based on the same assumptions. The reduction in material parameters is different for the two materials as the partial coefficients are dependant on different partial factors and assumptions. Note that the reduction in material characteristics are used to incorporate a safety margin in the design and are not used as strict requirements, as the standards are used for load carrying structures such as buildings and wind turbine blades, and not directly applicable to the exoskeleton elbow joint. Available standards attempt to standardize how the exoskeletons should be tested, but does not specify the need for safety factors [Bai et al., 2017]. The reason being, that standards for medical equipment require a comprehensive risk assessment that reduces the need for safety factors.

In general, the following equation should be fulfilled for both materials:

$$S_d(\gamma_f F_k) \leq \frac{R_k}{\gamma_n \gamma_m} \quad (8.4)$$

where

F_k	Characteristic load
R_k	Characteristic material parameter
S_d	Maximum design load parameter
γ_f	Load partial coefficient
γ_n	Consequence of failure partial coefficient
γ_m	Material partial coefficient

Note that γ_f and γ_n remains the same for both materials. The selection of γ_f is found from [Veritas, 2010] to be $\gamma_f = 1.35$. This value is to be chosen for maximum loads that may occur during usage, which is assessed to be true. It is also assessed that the consequence of failure is small. The maximum available torque from the motor is 30.35 Nm, which with the assumption of an forearm length of 300 mm, results in a maximum payload of roughly 10.3 kg. It is assessed that dropping such a weight during common everyday activities involves no life threatening hazards should the structure fail. Furthermore [Veritas, 2010] suggests to use a value of $\gamma_n = 1$ when designing against a static failure, which is what is designed against for the new elbow design. Therefore it is decided that $\gamma_n = 1$.

Aluminium Alloy

It is suggested from [DS/EN:1999-1-1, 2008] that the partial coefficient γ_m should be either 1.1 or 1.25 depending on what type of failure that is to be investigated. For designs in which cross-sections are in tension it is suggested to use a value of $\gamma_m = 1.25$ which is assessed to be the case for the design of the sliding mechanism as it resembles a beam like structure subjected to bending moments. For the aluminium structure, the characteristic material parameter is selected to be the yield strength of the aluminium. The yield strength of the aluminium used for the design of the sliding mechanism is 470 MPa. The stress evaluation criteria used for the aluminium piece is selected to be the von Mises stress criterion, which means that the maximum allowable von Mises stress in the sliding mechanism is

$$\sigma_{max} = \frac{470 \text{ MPa}}{1.25} = 376 \text{ MPa}$$

Composite Materials

For composite materials the material partial coefficient is determined as

$$\gamma_m = \gamma_{m1}\gamma_{m2}\gamma_{m3}\gamma_{m4}\gamma_{m5}\gamma_{m6} \quad (8.5)$$

where

γ_{m1}	Base material factor
γ_{m2}	Correction factor for strength data referring to 97.5% reliability and not 95%
γ_{m3}	Strength reduction factor due to repeated loading/low cycle fatigue
γ_{m4}	Strength reduction factor due to size effects, temperature, humidity and ageing
γ_{m5}	Strength reduction factor due to e.g. ply-drops, sandwich structure and bonded joints
γ_{m6}	Strength reduction factor due to post curing

The first three partial coefficients differ depending on the type of limit state which is designed against. The base material factor γ_{m1} can be set as either 1.3 or 1.2 depending on whether the design is dimensioned against a ultimate limit state (ULS) or fatigue limit state (FLS), respectively. From this $\gamma_{m1} = 1.3$ Since the design is dimensioned against a maximum static load state. The correction factor γ_{m2} for the strength data is $\gamma_{m2} = 0.95$ for both limit states. The strength reduction factor γ_{m3} for repeated loading is $\gamma_{m3} = 1.1$ when designing against a ULS. The strength reduction factor γ_{m4} depends on what type of resin system which is used and for epoxy based resin systems $\gamma_{m4} = 1.1$. The strength reduction factor γ_{m5} is dependant on several categories and subcategories that consider different type of locally induced strength reductions. The described category that suits this design best is that the design will be a prepreg or resin infused structure, containing mainly UD-fibres and may include ply drops. For this category $\gamma_{m5} = 1.1$ The last partial coefficient γ_{m6} is a strength reduction factor related to the post curing process. The only available post curing process, due to the manufacturing equipment available at the University of Aalborg, is exothermic curing for which the partial coefficient $\gamma_{m6} = 1.1$. From the selection of partial coefficients above, the material partial coefficient is from (8.5) calculated to be

$$\gamma_m = 1.81$$

As mentioned earlier, composites use a FI (FI) ratio to determine whether or not the structure will fail as the characteristic material parameter. The composite structure should therefore be designed to to have a maximum FI of

$$FI = \frac{1}{1.8} = 0.55$$

Requirement Specification 9

9.1 Design Circumscription

Chapter 2 to chapter 8 presents a wide range of investigations related to definition of the problem. The study is not exhaustive, but does involve many topics and problems. Solving and designing solutions for all of these topics is not possible within the time span of this thesis. Therefore, a circumscription of the project must follow the initial inspections.

From the previous generation, initial objectives were defined, and they were mainly related to decreasing the weight and increasing stiffness, to obtain an exoskeleton, that is not metabolically exhausting, and still gives the user the feeling of assistance when transferring forces.

Aiming towards stiffness and low weight, load scenarios were analysed in chapter 4 to accommodate possible scenarios. By testing the forces occurring on the previous design during these scenarios, it was found that two conservative load scenarios could be defined. It was determined that this loading would be the most critical, hereby avoiding having to simulate the effect of other types of loadings in a variety of exoskeleton positions and functions. It was also found, that the initial concerns about ergonomics and limited comfort were confirmed chapter 7.

Some features to improve the comfort of the exoskeleton can be implemented with a weight increase. It must be evaluated, if this increase is acceptable compared to the comfort gain of the feature and in relation to the weight of the human upper limb. The investigation of interaction between human and exoskeleton is prioritized higher than a low weight, and the increase in weight is accepted for the purpose of testing features to improve the ergonomics of the prototypes.

Of the ergonomics considerations presented in section 3.3, it is estimated that the kinematic constraint, i.e. the extension of the lower arm during movements, is an important issue, that, when solved, would add a great improvement in ergonomics. The compliance is also chosen to be a topic, that should be granted further attention to test if it affects the comfort.

An important realization related to the comfort is that it is difficult to simulate the comfort of a design idea, and the use of prototypes for the purpose of testing design concepts is therefore chosen. This has the consequence, that qualitative objectives become just as important as quantitative objectives, which will be evident from table 9.1. Furthermore, due to the wish for prototypes, the manufacturability is prioritized. Using materials and facilities already available at Aalborg University, will make the design- and manufacturing process both faster and tolerant to design changes late in the process. It will also increase the practical understanding of application of more advanced materials such as composites. Furthermore it also develops a better understanding of the steps involved to bring an idea to a physical product.

It is chosen to limit this project to the development of a new forearm. This limitation hereby excludes development of the shoulder harness attachment, further development of the upper limb structure, cuff geometries, and lastly the drive train mechanism. The idea of introducing composite materials to create a light weight design is instead changed to adding compliance to the

new design. The use of composite materials introduces several design issues. Several challenges were discovered during- and after the manufacturing of the UD carbon fibre prototype specimen. The high curing temperatures and difficulties during drilling operations caused concerns with respect to how to assemble and shape the new exoskeleton design. A complete redesign of the upper limb structure and drive train mechanism would be required to avoid the large amount of post manufacturing required. This is assessed to be too comprehensive within the available time of this thesis. It is therefore decided to focus on testing whether the extra compliance and sliding mechanism adds more comfort to the exoskeleton. Showing in this thesis that the exoskeleton design benefits from the addition of these principles would mean that they could be incorporated in many other exoskeleton applications.

Thus it is decided to create a new forearm design, and reuse the existing upperlimb structure and drivetrain mechanism. The geometrical measurements shown in figure 9.1 needs to be fulfilled to ensure compatibility with the previous design.

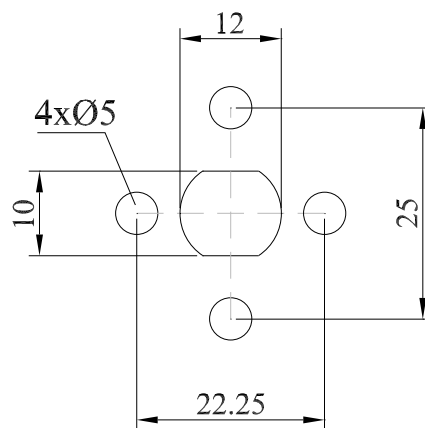


Figure 9.1: Geometrical limitations for the forearm piece/part.

This chapter functions as the end of the task clarification, and it specifies the necessities to generate design concepts.

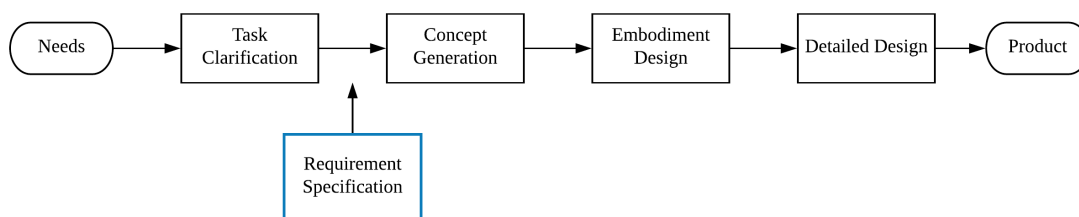


Figure 9.2: Design process with Requirement Specification input

9.2 Requirement Specification

No.	Requirements	Unit	Magnitude
1	The exoskeleton must be geometrical compatible with the previous design generation		
2	Payload	[kg]	5
3	The exoskeleton must be fitted to the geometrical dimensions of the test person		
4	The exoskeleton must be able to extend passively during motion	[mm]	30
5	Minimum eigenfrequency	[Hz]	2.25
6	Exoskeleton must withstand the following load cases:	Mz	My
		[Nm]	40.94 -13.65
		[Nm]	-40.94 -13.65
7	Torque input from motor	[Nm]	30.35
8	Minimum natural frequency	[Hz]	98
No. Wishes			
1	Compliance should be included in the forearm structure		
2	The weight of the exoskeleton should be as low as possible		
3	Manufacturing of the prototype at Aalborg University		
4	Materials: CFRP, GFRP or Aluminium available at Aalborg University		
5	Based on requirement no. 6, following is desired to be fulfilled:		
			$\sigma_{vM} < 376 \text{ MPa}$
			$FI < 0.55$
6	The forearm structure should be as compact as possible		

Table 9.1: *Requirements specification.*

Design of the Elbow Joint

Forearm

10

10.1 Conceptual Design

The following requirements are defined based on the requirement specification and practical experience gained from manufacturing of the initial prototypes.

- The new design must be able to extend/withdraw 30 mm
- It must be possible to be attached to the previous design generation
- It needs to be compliant around the area attached to the forearm
- Bolted connections with the composite parts should be avoided if possible
- Must be practically manageable to ease the manufacturing process
- It must fit the geometry of the forearm for the test person

The attachment to the upper limb structure of the previous design generation can be done in several ways. For now, it is decided to create a similar design as the one used in the previous design generation, and combine it with the sliding mechanism. This would require the attachment and sliding mechanism to be made of aluminium as the connection interface with the upper limb structure involves drilling four holes and one slot. Using aluminium for the sliding mechanism also enables better geometrical control of surfaces and the possibility of creating a rigid structuring on which a more compliant composite structure can be attached.

It is decided to integrate the cuff into the sliding mechanism. This reduces the surfaces that have to be bonded together, either chemically or with a bolted connection. The choice of composite material enables the possibility of customizing the shape of the cuff to a specific client, in this thesis the test person, as the composite has to be cast in a mould. This mould can be shaped to fit the test person exactly. The contact surface should fit the test person well, a male would therefore be preferable. It would be desirable to create a composite design in both carbon fibre reinforced polymer (CFRP) and glass fibre reinforced polymer (GFRP). The testing of the initial CFRP prototypes showed that the stiffness increased substantially when adding fibre layers a single layer. It is believed that a GFRP part could accommodate this better as its stiffness is approximately three times lower, with only half the strength.

It is quite clear that the design involves an aluminium part that can slide relatively to a composite part. Two different design proposals are made to allow this motion. The first involves bearings to allow for a smooth movement. The second uses a slot to support the composite structure instead. Polymer bearings are selected to reduce friction between the aluminium and the outer bearing surface and because of their low weight. The bearings are selected from the SKF bearing catalogue. The selected bearing is the 6000/HR11TN POM/stainless steel/PA66 polymer bearing. The dimensions of the bearing are shown in appendix B on page A84. An aluminium insert is used to connect the aluminium part to the composite part. The insert is glued together with the composite part and press fitted into the bearing. The dimensions of the aluminium housing, FRP support and aluminium insert are not shown for now as they will

be changed based on simulations results shown in section 10.3. Examples of the geometries will however be shown in the following as the design and simulation approach is explained.

10.2 Design and Simulation Approach

Evaluating design considerations through simulations presents several challenges related to the analysis approach. Firstly, understand that the simulations and models proposed in the following are intended to give indications or answers to whether or not ideas or design changes are viable. They are not created to simulate the actual response of the new design during operation, but merely created to ensure that the new design can withstand the loads introduced during operation. Emphasis in this thesis is put on creating prototypes, that can be used to test ideas and thoughts that necessarily cannot be verified through simulation results. ANSYS Workbench version 18.2 is used for the simulations throughout this thesis.

The challenge of ensuring structural integrity of the new parts for the exoskeleton arises as a consequence of different functional purposes of the respective parts. The support structure is designed to accommodate the shape of the human arm, and to add compliance to the exoskeleton to decrease discomfort. Many design changes have to be made to understand how the fibre direction and stacking sequence affect the strength and compliance of this structure. Simulations therefore have to be solved quickly with sufficient accuracy to enable the possibility for fast design changes.

The purpose of the aluminium housing is to integrate a sliding mechanism and attachment to the upper arm structure. It is desired that this structure deforms little around the contact surfaces with the support structure and SKF bearing to ensure relatively smooth elongations. Calculations are allowed to take a bit longer, as the number of design iterations is expected to be lower. However, the aluminium housing design is directly influenced by the results from the composite support simulations as the number of plies dictate the distance between the faces in contact with the support structure. Creating a model with both parts would increase the simulation time, and hereby also the time to obtain a suitable design result through this iterative design process. The following approach is proposed to accommodate these suppositions and is illustrated in figure 10.1 on the next page. Two simplified models will be created - one for the aluminium housing and one for the FRP support. The models will be created such that the boundary conditions of the respective models represent simplified assumptions to their interactions. As an example, a conservative model for the FRP support could be to include SKF bearings and assume these to be rigid, while applying suitable fixtures and loading. The results from the FRP models, i.e. thickness, can then be used in the housing model to define the distance between the SKF bearings. This allows FRP model simulations to run independently of the housing model. General model considerations such as the element selections, contact formulations etc. are explained in the following.

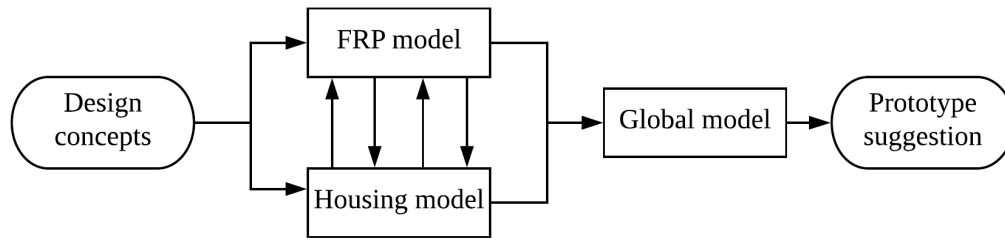


Figure 10.1: Flowchart of the iterative design approach between the simulation models of the new forearm design for the exoskeleton.

10.2.1 General Model Considerations

The main focus for the simulations is aimed towards fast computations with relatively accurate results. The model considerations are divided into three categories. The first category explains the geometric simplifications made to decrease the computational time of the simulations. The second category explains selections regarding model analysis settings.

In general, the geometries have been simplified by replacing convex fillets with sharp corners. The SKF bearing is simplified to a revolved polymer disk. These two simplifications are done to allow for a more coarse mesh.

The selection of appropriate element types, element properties, and model analysis settings are closely related to the solution time and accuracy of the simulation models. Two different element types are used in the simulation models - shell elements and solid elements. It is decided to use elements with quadratic shape function formulations. Elements with linear shape function formulations offer faster computations as they contain fewer element nodes, but require further investigations to ensure model accuracy. Two examples of typical investigations are locking effects and convergence studies, as linear elements are more prone to locking and in general converge slower. These investigations would have to be repeated whenever geometry changes are made. The element size is to be changed during the simulations when needed. The contact formulations available are either penalty methods, pure Lagrangian methods, or a combination of these two. The penalty method adds a large artificial stiffness between contact nodes to simulate contact forces. Small amounts of penetration between the contact faces can occur with this formulation. This can however be adjusted with a penalty scaling parameter of the contact stiffness, to reduce the amount of penetration. The pure Lagrangian method introduces extra variables to describe the kinematic conditions during contact. This formulation can cause solver instability as contact status can switch rapidly. The pure Lagrange formulation is either in full contact or separated, which can cause the aforementioned solver instability, opposed to the penalty method where the contact forces are gradually increased depending on the amount of penetration. However, the penalty method typically gives best results for contact problems involving contact surfaces consisting of the same material, as the unscaled contact stiffness is estimated from a weighted stiffness contribution from the materials in contact. The augmented Lagrange method is a combination of the two contact formulations described in the above. However, ANSYS [2017] does not specify exactly how this contact formulation works, but previous experience with this formulation has good results when analysing materials with very different stiffness, e.g. the SKF polymer bearing and the aluminium house. The contact types used in the models are bonded and frictionless. The bonded contact type enforces that the distance between the contact nodes remains the same during loading through penalty forces. The frictionless contact allows the two contact surfaces to move relatively to each other, but

can only transfer normal forces. The models are solved as geometric non-linear models as large rotations could be expected. Material is removed in the aluminium housing, and compliance is sought in the FRP support, both of which can cause large rotations and deflections.

10.2.2 FRP Composite Design Approach

The first model investigates the principle stress orientations and and strain energy density. A good rule of thumb when designing a FRP composite is to orient the fibres in the direction of the loading. An indication of the load path can be assessed by investigating the principle stress orientation (PSO). Furthermore, investigating the strain energy density (SED) yields information regarding how different areas contribute to the stiffness and strength of the the structure. The SED can be interpreted as a measurement of how much energy is stored at gives areas of the structure. Areas of high SED's contribute the most to the strength and stiffness of the structure. SED is used, in this thesis, to identify if there is a need for defining separate layup sections with local fibre reinforcement. The PSO and SED are investigated for a simplified support geometry as the one shown in figure 10.2. This support has a uniform thickness and is made of aluminium. It includes SKF bearings to mimic the contact between the aluminium housing and the support.

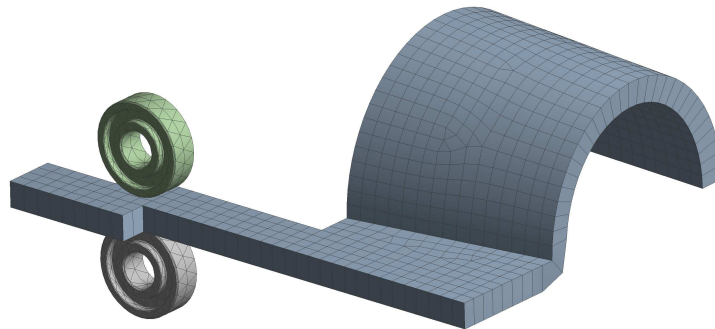


Figure 10.2: *The simplified model of the FRP support.*

The FRP support is modelled with shell elements, whereas the SKF bearings are modelled with solid elements. It is decided only to analyse the FRP design with the SKF bearing housing design. The selection of shell elements does not allow investigation of the out of plane stresses which most likely would be of interest around the contact area. Little difference can therefore be expected in the design results between the slot contact surface design and the SKF bearing design. Furthermore, it is decided only to simulate the FRP support in the extended sliding configuration. This configuration increases the distance between support cuff and the SKF bearings. This configure should therefore have the largest internal moment, and hereby also be the worst loading case. The contact type between the SKF bearings and FRP support is defined as frictionless. The center hole of the bearings are fixed such that it cannot move. The loading and boundary conditions are applied as shown in figure 10.3 on the next page. The boundary conditions lock translational movement in all directions and rotations around the y-axis and x-axis to mimic the connection to the aluminium housing. The loading is applied as a two component force across the entire surface of the support cuff. It is decided to simplify the force and apply is as a constant value across the cough surface. The force applied is calculated from the moments specified in the requirement specification. The force components are evaluated from the largest distance from the sliding mechanism attachment (213 mm), i.e

$$F_y = \pm \frac{40.972 \text{ Nm}}{0.213 \text{ m}} = \pm 192 \text{ N}$$

$$F_z = -\frac{13.657 \text{ Nm}}{0.213 \text{ m}} = -64 \text{ N}$$

The two load cases are defined for the FRP support model. These are shown in table 10.1 and represent the loading during biceps contractions (BC) and triceps contractions (TC).

	F_y [N]	F_z [N]
Extended - BC	-192	-64
Extended - TC	192	-64

Table 10.1: Load cases used for the FRP support model.

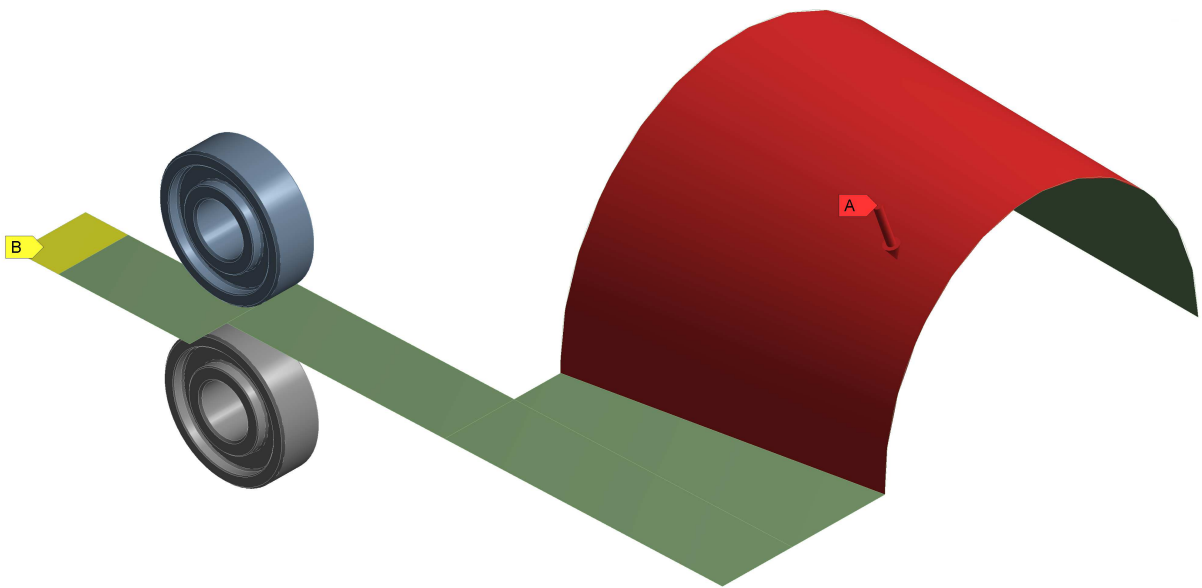


Figure 10.3: Illustration of where the boundary conditions (yellow) and loading (red) is applied on the FRP support.

The design approach used for the FRP support is illustrated in figure 10.4 on the next page. An initial ply layup is created with the information gained from the isotropic model. This model then runs through an iterative process in which layers are added and the fibre directions changed. Finally, the remaining load cases are then checked once the model shows satisfactory results.

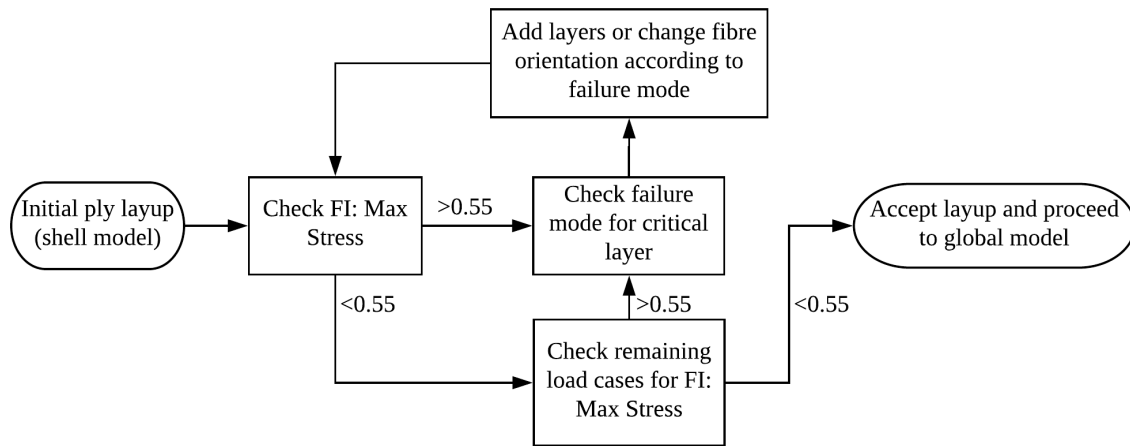


Figure 10.4: Flowchart illustrating the iterative process in defining a suitable layup for the FRP support.

10.2.3 Aluminium Design Approach

The aluminium housing designs are modelled with solid tetrahedral elements. The models include one simplified SKF bearing to mimic the contact of the FRP support. The contact type between the bearing and aluminium housings is defined as bonded as the bearing cannot move in its outer positions. The center hole of the bearing is fixed. The two initial models, boundary conditions, and loading are shown in figure 10.5. The contact face between FRP support and slot is fixed such that it cannot displace along the y-axis. Likewise for the SKF bearing design, the contact faces between the bearings fixed in the same manner. This is a rough approximation of the contact that would else wise occur between the aluminium housing and FRP support. The loading is applied as two moments, one around the z-axis representing the motor torque, and one around the y-axis which represents the user force discovered in chapter 4 on page 15. Both of the aluminium designs are subjected to four load cases shown in table 10.2 on the facing page.

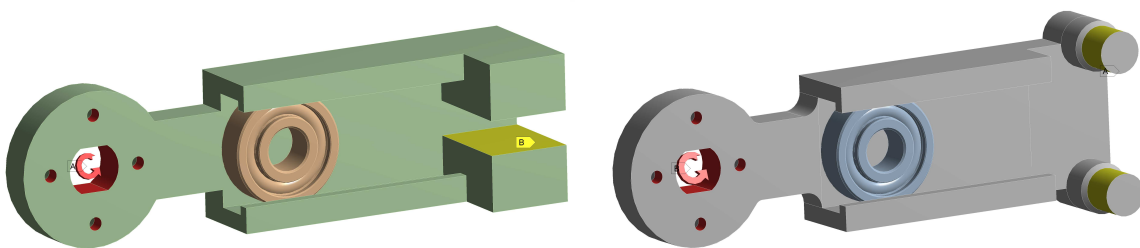


Figure 10.5: The boundary conditions (yellow) and the areas in which the loading is applied (red) on the slot design (left) and the SKF bearing design (right). This image illustrates the withdrawn loading configuration.

The design of the aluminium housings is changed based on the stress distribution, both normal stresses, shear stresses and von Mises stresses. Local stress concentrations are reduced by adding fillets and increasing their radius if needed. Material is removed in areas with low stresses and SED's. This iterative design approach is illustrated in figure 10.6 on the next page.

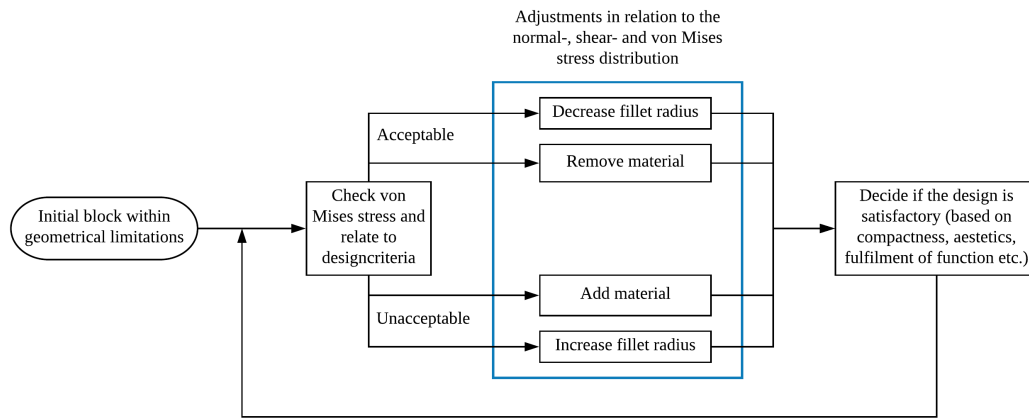


Figure 10.6: Flowchart illustrating the iterative design process of the aluminium housing.

The model is analysed in two configurations referred to as extended and withdrawn. These configurations will also be used in the FRP model and the global model. An illustration of the two configurations is shown in figure 10.7

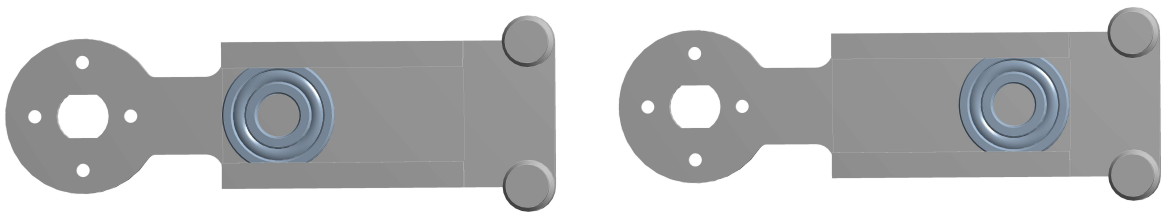


Figure 10.7: The two outer sliding configurations investigated - withdrawn(left), extended(right).

	M_z [Nm]	M_y [Nm]
Extended - BC	40.94	13.65
Extended - TC	-40.94	13.65
Withdrawn - BC	40.94	13.65
Withdrawn - TC	-40.94	13.65

Table 10.2: Load cases analysed in the two aluminium housing models.

10.2.4 Global Model

The global model consists of four components: an aluminium housing, an aluminium insert, a FRP support and either one or three SKF bearings depending on the housing design. Both solid and shell elements are used in this model. The model includes both bonded and frictionless contact types. The contact between the SKF bearings, aluminium housings, and aluminium insert is set as bonded. The contact definitions between the aluminium housing/SKF bearings and the FRP support is defined as frictionless contacts. The simplification of the SKF bearing does not allow for the bearing to perform rigid body rotation as it is intended to when functioning in real life operations. It is possible to add a bearing contact definition instead to allow this. However it requires determination of additional simulation parameters and is neglected as it is expected that the rotations of the bearing in the end positions are very small. The model is solved as a geometric non-linear model as large rotations and deflections are expected. Four

load cases are applied to the model, identical to those presented in table 10.2 on page 63. The boundary conditions are applied such that the entire cuff of the FRP support is prevented from displacing and rotating, representing how the support is attached to the forearm.

10.3 Design Results

The design of the new structural components is based on simulation results, manufacturing considerations and practical experience gained from the carbon fibre prototypes.

10.3.1 FRP Support

It has been decided in chapter 9 on page 53 to design the support in both glass fibre reinforced polymer (GFRP) and carbon fibre reinforced polymer (CFRP). The simulation model uses a quadratic SHELL281 8-node element formulation. It was observed during the design iterations, that a an element size of 4 mm shows good results. This element allows for good geometry representation of curvatures, fast computations compared to solid elements, and it prohibits shear locking, which is desired to be able to perform changes to the fibre layup efficiently and accurately. The model has been geometrically simplified as described in section 10.2 on page 58. The contact type used between the two polymer wheels and FRP support is set as frictionless, allowing only normal forces to be transferred between contact interfaces. The contact formulation used is the Augmented Lagrange-formulation. The model is defined as a geometric non-linear model, because large deflections and rotations are expected as in the search of compliance. This analysis also uses a minimum substep size of 10 and a maximum substep size of 20. This substep size setting yielded good solver stability. The loading and boundary conditions is introduced as described in section 10.2 on page 58. The support is initially modelled as an uniform aluminium structure to investigate the orientation of the principle stresses and strain energy density to analyse how the loading affects the structure. The purpose of the model is to give initial indications on if separate layup sections should be defined and how to orient fibre directions. The results of these simulations are displayed in figure 10.8 on the next page.

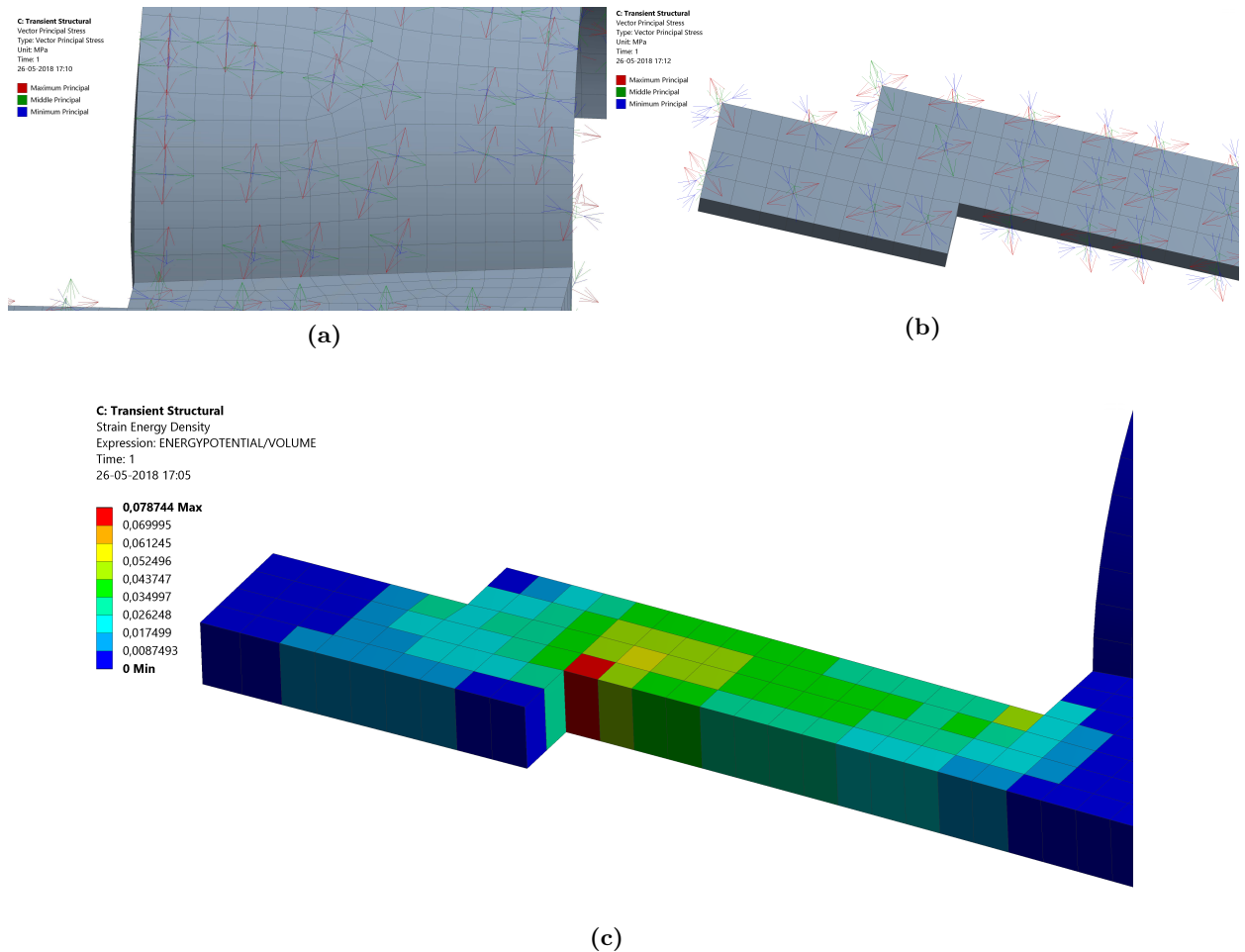


Figure 10.8: (a) Principle stress orientations at the forearm support, (b) Principle stress orientation at the sliding mechanism connection, (c) Strain energy density.

The simulation results show that the principle stress orientation for the largest absolute principle stresses (tensile) in the part of the support which is in contact with the forearm, are oriented along the z-axis, whereas the principle stresses nearest the sliding mechanism are aligned closer to the x-axis. Furthermore, the results also show that the largest amount of energy is stored in near the SKF bearings. It is decided from these results to create two independent layup sections as shown in figure 10.9.

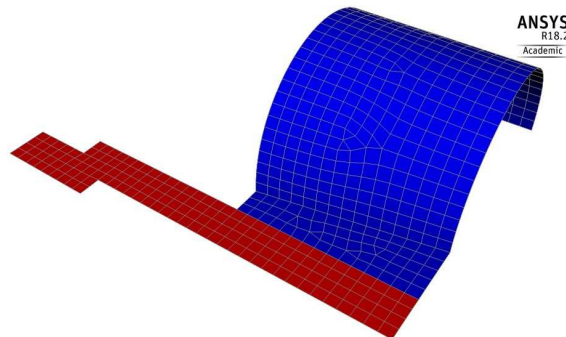


Figure 10.9: Illustration of the two independent layup sections. The red area is defined as section 1 and blue area as section 2.

The fibre layup is defined in Ansys Composite PrepPost (ACP). The fibre angle is defined such that the 0° fibre angle is aligned with the x-axis and the 90° fibre angle is aligned with the z-axis

as illustrated in figure 10.10.

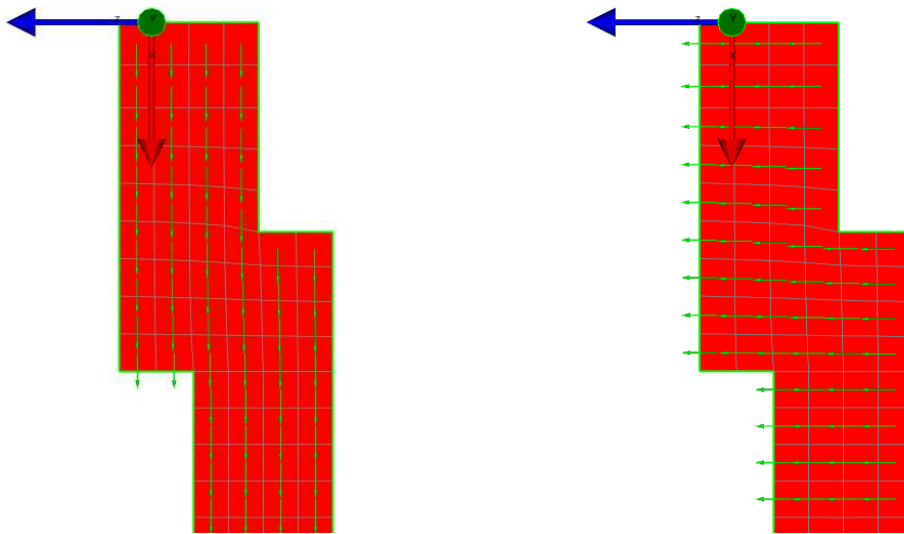


Figure 10.10: Fibre orientation - 0° (left), 90° (right). The coordinate system is defined such that the blue arrow is aligned with the z-axis and the red arrow with the x-axis.

The fibre stacking sequence, number of plies, and fibre orientation are changed according to the approach described in section 10.2 on page 58. The initial layups had fibres oriented primarily in 0° and $\pm 20^\circ$ in section 1 and in 90° in section 2. It was realised during the design process that the GF mats are unsuitable for this design application as the lamina thickness is too thick to vary the fibre angles to gain sufficient compliance. Structural thickness, and hereby the moment of inertia, increases rapidly with the number of GF mats, as they are approximately three times thicker than the CF mats. A final design is therefore only presented for a CFRP support. The final layup for the CFRP design is shown in figure 10.11 on the next page, and the simulation results with this layup are shown in table 10.3. The layup consists of a total of 70 plies, of which 20 are global and 50 are local. It is concluded from the results presented in table 10.3 that the CFRP support fulfils the requirements set for the maximum allowable FI. Furthermore, it is concluded that the selection of two layup sections is appropriate, as it allowed the fibre orientation and number of plies to vary considerably, which is thought to have increased the compliance substantially as opposed to a single uniform section. It is also observed during the design iterations that orienting the $\pm 60^\circ$ fibres in $\pm 55^\circ$ in section 1 and the 90° fibres in -85° in section 2 increases the stiffness of the support without much decrease in the FI. This may be an indication that other fibre angles can result in greater compliance without too large of an increase in FI.

	δ_z [mm]	δ_y [mm]	FI
Extended - BC	4.9	13.5	0.55
Extended - TC	-3.4	-10.2	0.44

Table 10.3: Simulation results from the CFRP support design.

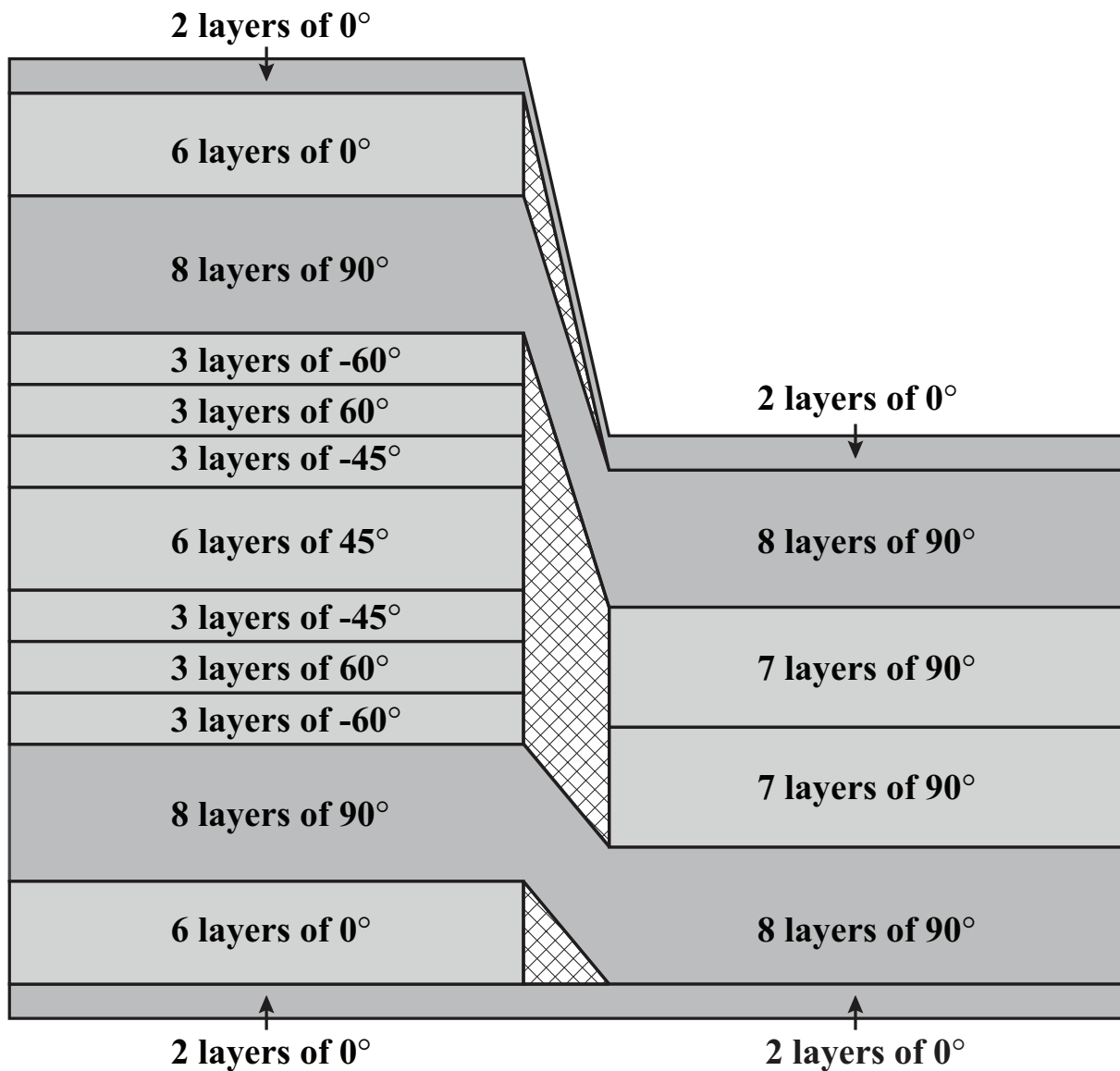


Figure 10.11: *Front view illustration of the final layup for the CFRP support.*

10.3.2 Aluminium Housing

Two design proposals have been made for the aluminium slider mechanism, both of which have been analysed. The composite structure is directly in contact with and supported by the aluminium housing in the first design proposal. The second design proposal includes SKF bearing supports to reduce friction between the composite structure and the aluminium housing. Both design proposals include several geometric simplifications to reduce computational time. Convex fillets are simplified to sharp corners to allow a more coarse discretization. The SKF bearings have been simplified to revolved polymer disks, with a Young's modulus of 3.1 GPa and Poisson's ratio of 0.44 - values typically used for POM [Osswald and Mendes, 2012]. The element choice for the two designs is the quadratic SOLID187 tetrahedral element. Local mesh refinement and fillets are added during the design iterations. The final design iterations have a local element size of 1 mm in stress concentrated areas, with fillet radii ranging between 2mm and 4mm depending on the local von Mises stress levels. The contact type between the SKF bearing and aluminium housing is set as bonded, with the Augmented Lagrange contact formulation. The bonded contact assumes that the element nodes remain relative to each other during loading which is assumed to be valid as the slider will be constrained at its two elongation endpoints. The model is defined as a geometric non-linear model because large rotations are expected

during design iterations as material is removed. The analysis uses a minimum substep size of 10 and a maximum substep size of 20. This substep size setting yielded fast results and good solver stability. The loading and boundary conditions are applied as described in section 10.2 on page 58. An example of the von Mises stress distribution for the final design iteration is shown in figure 10.12. The maximum von Mises stress for all loading scenarios is shown in table 10.4. From these results it is concluded that the SKF bearing design fulfils the requirements specified for the maximum allowable von Mises stress. It is also concluded that the slot design exceeds the maximum allowable von Mises stress in three out of four load cases. However, the loads, model set-up, and selection of safety factors are considered conservative. Furthermore, the location of the high stress value is very local and is caused by a stress concentration. It should therefore not jeopardize the safety of the entire structure, and it is still well below the actual yield strength of 470 MPa. The total height of the SKF bearing design is 64 mm, whereas the the slot design has a height of 40 mm. Compactness is desired and for this reasons, it is decided to continue with the slot design regardless of the design not fulfilling the requirements entirely.

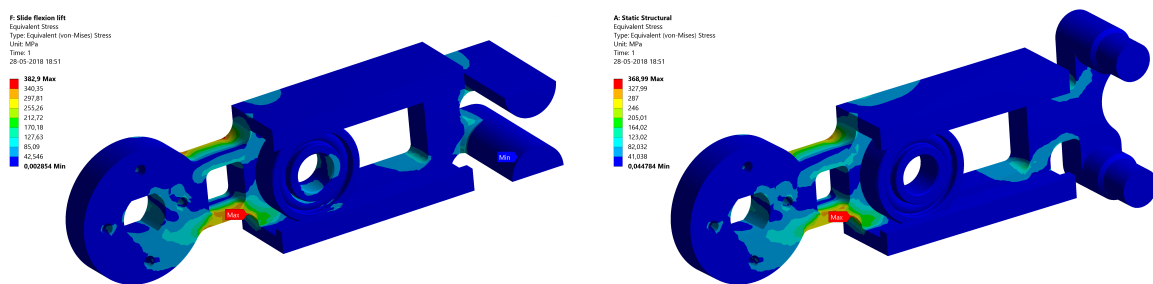


Figure 10.12: Von Mises stress distribution of the aluminium housing without bearing supports (left), von Mises stress distribution of the aluminium housing with bearing supports (right).

	σ_{max} [MPa]	
	Slot design	SKF bearing design
Extended - BC	386.4	365.1
Extended - TC	378.5	345.8
Withdrawn - BC	382.9	369.0
Withdrawn - TC	375.3	340.9

Table 10.4: Maximum von Mises stress

10.3.3 Global Model

The global model includes the aluminium slot housing design, an aluminium insert, one SKF bearing, and the CFRP support. The selection of element type and element size remains as for the two simplified models. An additional three contact pairs are added to this model - two bonded pairs and one frictionless pair. Bonded contact types are added between the aluminium insert and SKF bearing and also between the insert and CFRP support. Frictionless contact is added between the aluminium slots and CFRP support to allow sliding between faces. Frictional contact can be implemented, but shows no significant difference in initial simulation results for the withdrawn BC loading case, whereas solver stability issues are noticeable. A test simulation is run in which the Maximum von Mises stress is found to be 380.5 MPa, FI 0.5, and the total deflection 6.1 mm. A coefficient of friction of 0.23 [Schön, 2003] is used for this test model.

The model is once again defined as a geometric non-linear model as large rotations are expected. The minimum substep size is set to 50 and the maximum substep size is set to 100. The substep

size increases for the global model as the frictionless contact pair would miss initial contact and instead penetrate with a lower substep size. The loading and boundary conditions are defined as described in section 10.2 on page 58. Some results from the extended BC loadcase are illustrated in figure 10.13, whereas relevant results from all loadcases are shown in table 10.5 on the next page. It is concluded from the results that the CFRP support for new design forearm design fulfils the design requirements with respect to resistance failure. It is also concluded that the lowest eigenfrequency mode is sufficiently high to validate the assumption of static loading. However, the initial expectation that the global model should have lower levels of von Mises stresses, than the simplified model, is disproved. The largest von Mises stresses exceeds the maximum allowable von Mises stress levels, and also the maximum stresses found in the simplified model of the aluminium housing. However, the location of the maximum von Mises stress is once again found in a stress concentrated area. The stress levels could most like be reduced below the maximum allowable von Mises stress by increasing the fillet size from 4 mm to 5 mm. Lastly, it is observed that the global stiffness is considerably higher than what is observed in the two simplified models. It could be considered removing some layers in the CFRP support to increase the compliance as the FI are all below the maximum allowable of 0.55. This would require design changes to the aluminium housings to accommodate the geometrical changes to the CFRP support. This should be considered if simulations of the aluminium housings are to be redone with a larger fillet radii. However, this is not done due to limited time resources. Lastly, it is decided not to create a global model with the SKF bearing design, as it assessed that it is too bulky with the polymer bearings selected.

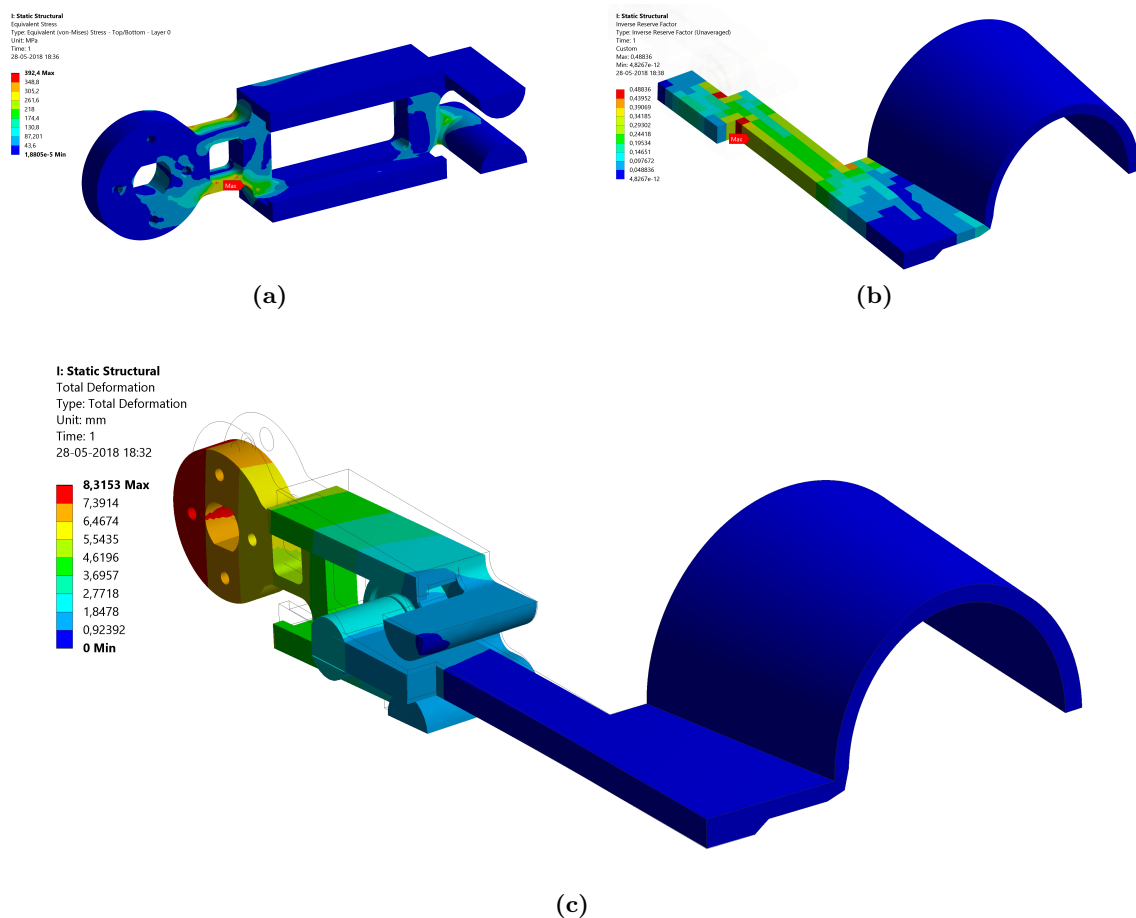


Figure 10.13: (a) Von Mises stress distribution, (b) FI distribution of the CFRP support, (c) Total deformation with an undeformed wireframe.

	δ_z [mm]	δ_y [mm]	σ_{max} [MPa]	FI	ω_0 [Hz]
Extended - BC	4.9	-6.7	392.4	0.49	196.6
Extended - TC	5.0	7.1	391.1	0.46	
Withdrawn - BC	3.6	-5.2	379.2	0.49	274.3
Withdrawn - TC	3.7	5.4	377.7	0.43	

Table 10.5: *Simulation results from the global model including all structural parts for the new forearm support structure.*

The final weight of the new components are shown in table 10.6. Note that the new design has a support cuff integrated in its design. The volume that represents the cuff results in a weight for the cuff alone of 54 grams out of the 79 grams. Lastly, it should be noted that a polymer is 3D printed to prevent users of getting their fingers pinched during use. The weight of the cover adds another 31.2 grams. However it is not considered as a structural component of the new forearm design. An overview of the structural components are shown in appendix C on page A94

Component	Weight [grams]
Aluminium housing	76.4
CFRP Support	79.0
SKF bearing	6.2
Aluminium insert	6.4
Total	168

Table 10.6: *Weight of the structural components for the new forearm design.*

Discussion and Conclusion

11

11.1 Discussion

The objective of this thesis of how to design an elbow exoskeleton joint has changed throughout the investigation. The initial objective was to create a lighter and stiffer exoskeleton, as it was initially thought that this would improve the ergonomics compared to the previous exoskeleton design generation. It was discovered during the analysis of requirements for the new exoskeleton design, that the comfort could be increased by improving the human-exoskeleton interaction instead. It was thought that the comfort could be increased not only by decreasing the weight, but rather to allow the exoskeleton to accommodate the natural movements of the human arm. Previous design generations limited the supination and pronation. Resolving this issue was not entirely achieved, but an attempt to reduce the discomfort caused by this limitation was made by implementing compliance in the new design. It was attempted to add the compliance with the use of carbon fibre reinforced polymer (CFRP) and glass fibre reinforced polymer (GFRP). However, conservative loading cases and conservative selection of safety factors most likely reduced the full potential of compliance that could be achieved with the use of an orthotropic materials. A consequence of this was also that the GFRP became unsuitable for the support application. It could be considered to determine appropriate safety factors based on a comprehensive risk assessments instead of design standards used for load carrying structures. Furthermore, it was realised that the user comfort could be greatly increased by allowing the new forearm design to extend during flexion and extension movements.

The new design does however possess some design flaws. The initial selection of aluminium and CFRP can lead to issues with galvanic corrosion. The selection of polymer bearings from SKF led to a rather bulky design, that could be created more compact with the use of steel bearings instead, as these can carry higher loads, when comparing the prescribed load with their outer diameter.

It was also discovered that the new design proposal exceeded the desired maximum von Mises stress. However, this is not considered a major issue, due to the conservative application of loading and selection of safe factors.

With respect to the manufacturing, it was realised that the curing temperatures for the CFRP were too high for the materials and facilities available at the University of Aalborg. It should be considered to cure the CFRP at lower temperatures, i.e 120°, but for a longer curing time than the two hours suggested by HexPly, i.e six or eight hours and to see what results could be achieved at this curing temperature.

Lastly, the model accuracy for the FRP model may have decreased due the initial choice of shell elements. The final suggested plies became rather thick (7.28 mm), which may have violated the assumptions of the shell elements.

11.2 Conclusion

Two design concepts have been proposed. Both of them fulfil the geometrical requirements specified in the requirement specification. The design concepts can elongate a total of 30 mm along the x-axis and are both geometrically compatible with the previous design generation. Furthermore, a CFRP support cuff has been integrated into the two new design concepts. This support cuff also fulfils the geometrical requirements dictated by the geometry of the test persons forearm. It is therefore concluded that the two new design proposals fulfil the geometrical specifications specified by the requirement specifications. Lastly it is also concluded that the best suitable design for now is the slot design as it was found to be more compact than the SKF bearing housing design - same width but 24 mm less in height.

It is concluded that the two new design concepts fulfil the requirement of being able to carry a payload of 5 kg, with a load sharing factor of 1, as it is shown that torque provided by the motor, used to define the load cases applied, is able to carry a maximum payload of 10.3 kg.

The lowest found eigenfrequency in the global model is found to be 196.6 Hz. This is well above the the requirement that the minimum eigenfrequency should be above 2.25 Hz. Therefore it is concluded that the assumption of static loading is considered valid.

The loading defined in the requirement specification is used to create four different load cases. These load cases have been applied to various simulation models to investigate the structural integrity of the new designs. The conservative selection of safety factors did however cause the maximum von Mises stresses to exceed the desired maximum von Mises stress of 376. It is assessed that the design proposals are suitable for prototype use. The FI for the CFRP is below the maximum allowable FI.

It has been discovered through experiments, that the implementation of compliance improves the user comfortability. The compliance helped to accommodate the natural supination and pronation rotation of the wrist during lifting operations. Compliance has been implemented with the use of a CFRP support structure. The human-exoskeleton interaction is been improved even further with the addition of a sliding mechanism.

It has been possible to manufacture carbon fibre prototypes with the manufacturing facilities and materials available at Aalborg University. The manufacturing of the carbon fibre required high curing temperatures. The high processing temperature imposes manufacturing challenges, as the vacuum bag peel plies and vacuum tubes melted. It could be considered to cure the CFRP at lower temperatures for a longer time period. Alternatively, other types of composite with lower curing temperatures could be considered.

The increase in weight in relation to the previous generation does not worsen the human-exoskeleton interaction. In fact, the new design is assessed to improve the human-exoskeleton interaction as it accommodates the upper limb kinematics to a larger extend than the previous design generation. The previous exoskeleton forearm weighs approximately 69.8 grams. The new slot design weights a total of 113.7 grams when neglecting the weight of the integrated CFRP cuff. This is an increase of 44 grams, which is considered of no importance when considering, that a typical human arm contributes to approximately 4.3% of the human body weight.

11.3 Future work

It has been attempted to follow the design process illustrated in figure 11.2 throughout this thesis. The current stage of the thesis has reached the embodiment design. The next step would be to create prototypes to test the thoughts and design solutions presented in this thesis.

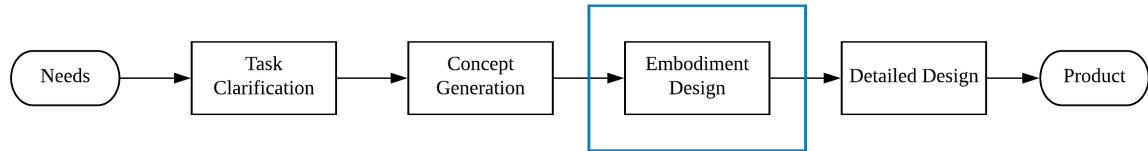


Figure 11.1: Replication of design proces from Shefelbine et al. [2002].

A prototype of the aluminium housing, aluminium insert, SKF bearing, and polymer cover has been 3D printed to verify if the new design proposal improves the human-exoskeleton interaction to the extend it is expected. An image of the 3D printed prototypes are shown in

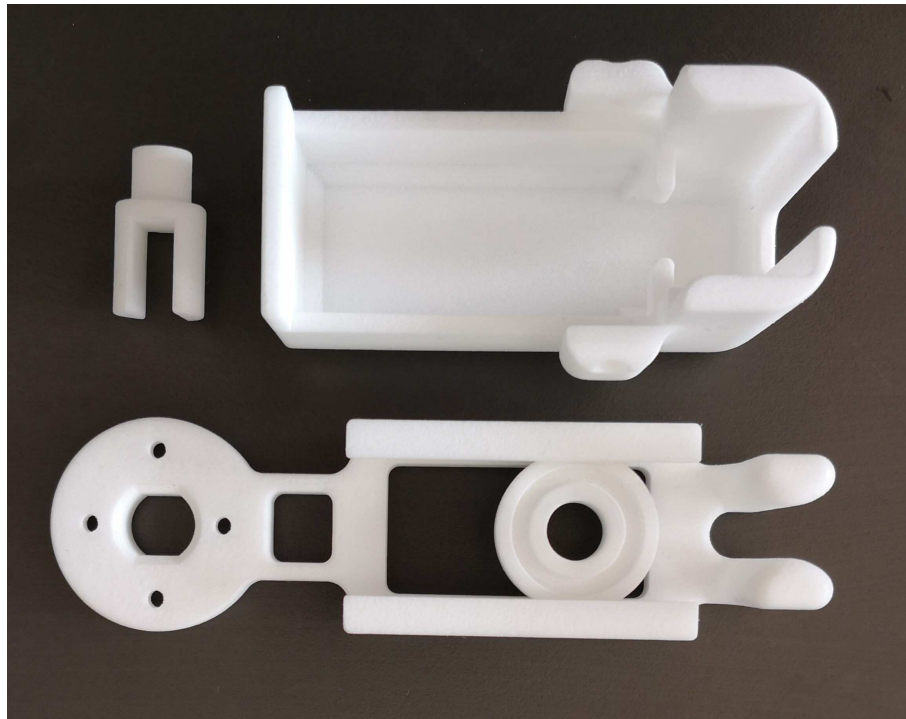


Figure 11.2: 3D printed slot housing, SKF bearing, insert, and cover.

The prototype does however still need a support piece. It should be attempted to manufacture the CFRP support. A template needs to be created in order to cut out the necessary plies needed to manufacture the support. The same must be done for a mould in order to shape the plies. Such a template and mould has been proposed in appendix D on page A96. Note that the template is a 1:1 true scale.

The compliance of the support piece has been achieved by manually changing the layup according the failure type indicated by the max stress criterion. Another approach could be to combine the solution model with an optimization algorithm to investigate alternative fibre layups. Likewise, it could be considered to apply topological optimization on the aluminium housing to see how the algorithm would remove material. This could bring additional ideas to the tables to how material could be removed to save weight.

Bibliography

Amis, 2002. A. A. Amis. *Biomechanics of the elbow*. 2002.

ANSYS, 2017. ANSYS. *Ansys Documentation*. SAS IP, Inc., 18.2.0 edition, 2017.

Bai, Virk, and Sugar, 2017. Shaoping Bai, Gurvinder s. Virk, and Thomas G. Sugar. *Wearable Exoskeleton Systems - Design, control and application*. The Institution of Engineering and Technology, 1 edition, 2017.

Bastide, Vignais, Geffard, and Berret, 2017. S. Bastide, N. Vignais, F. Geffard, and B. Berret. *Analysis of human-exoskeleton interactions: an elbow flexion/extension case study*. 2017. *Computer Methods in Biomechanics and Biomedical Engineering*, 20:sup1, 9-10, DOI: 10.1080/10255842.2017.1382835.

Best Performance Group. Best Performance Group. *Elbow Complex - Anatomical Considerations*. http://bestperformancegroup.com/?page_id=2386. Localised 01-06-2018.

Bostelman and Hong, 2018. Roger Bostelman and Tsai Hong. *Test methods for exoskeletons - lessons learned from industrial and responsive robotics*. 2018.

DS/EN:1999-1-1, 2008. DS/EN:1999-1-1. *Eurocode 9: Design of Aluminum Structures*. 2008.

Erhan, Gündüz, Bardak, Ozcan, Çarli, Er, Tekin, and Lüzçakar, 2013. B Erhan, B Gündüz, AN Bardak, S Ozcan, A Çarli, H Er, L Tekin, and Lüzçakar. *Elbow problems in paraplegic spinal cord injured patients: frequency and related risk factors-a preliminary controlled study*. *Spinal Cord*, 51(5), pp. 406–408, 2013.

Felstead and Ricketts, 2017. Alisdair J. Felstead and David Ricketts. *Biomechanics of the shoulder and elbow*. 2017.

Hale, Dorman, and Gonzalez, 2010. Rena Hale, Daniel Dorman, and Roger V. Gonzalez. *Individual Muscle Force Parameters and Fiber Operating Ranges for Elbow Flexion-Extension and Forearm Pronation-Supination*. *Journal of Biomechanics*, 2010.

Hexcel, 2016. Hexcel. *Product Data Sheet, Hexply[®] 8552*. Hexcel Corporation, 2016.

Hoffman. Michael Hoffman. *Member Spotlight: Super-Releaser Applies Soft Robotics to Exoskeletons, Prosthetics*.

<http://www.tandemnsi.com/2016/03/super-releaser-applies-soft-robotics-to-exoskeletons-p>

Localised 01-06-2018.

Hoffmann, 1989. Karl Hoffmann. *An Introduction to Measurements using Strain Gages*. Hottinger Baldwin Messtechnik GmbH, Darmstadt, 4 edition, 1989.

Wan, Qin, Wang, Sun, and Liu, 2017. Jing jing Wan, Zhen Qin, Peng yaun Wang, Yang Sun, and Xia Liu. *Muscle fatigue: general understanding and treatment*. *Experimental & Molecular Medicine*, 2017.

Jones, 1999. Robert M. Jones. *Mechanics of Composite Materials*. Taylor and Francis, 2. edition, 1999.

Kankipati, 2012. Padmaja Kankipati. *Investigation of transfer technique biomechanics among persons with Tetraplegia and Paraplegia*. 2012.

Masia, Hussain, Xiloyannis, Pacchierotti, Capello, Malvezzi, Spagnoletti, Antuvan, Khanh, Pozzi, and Prattichizzo, 2017. Lorenzo Masia, Irfan Hussain, Mechele Xiloyannis, Claudio Pacchierotti, Leonardo Capello, Monica Malvezzi, Giovanni Spagnoletti, Chris Wilson Antuvan, Dihn Binh Khanh, Maria Pozzi, and Domenico Prattichizzo. *Soft Wearable Assitive Robotics: Exosuits and Supernumerary Limbs*. 2017.

Maxon Motor, 2018. Maxon Motor. *EC-4pole 22 ø22 mm, brushless, 90 Watt*.

https://www.maxonmotor.com/maxon/view/category/motor?etcc_cu=onsite&etcc_med_onsite=Product&
2018. Localised 22-03-2018.

Mulroy, Hatchett, Eberly, Haubert, Conners, and Requejo, 2015. Sara J. Mulroy, Patricia Hatchett, Valerie J. Eberly, Lisa Lighthall Haubert, Sandy Conners, and Philip S. Requejo. *Shoulder strength and physical activity predictors of shoulder pain in people with paraplegia from spinal injury: prospective cohort study*. *Physical therapy*, 95(7), pp 406–408, 2015.

National Instruments, 2016. National Instruments. *Measuring strains with strain gages*. <http://www.ni.com/white-paper/3642/en/>, 2016. Localised 22-05-2018.

Osswald and Mendes, 2012. Tim A. Osswald and Georg Mendes. *Materials Science of Polymers for Engineers*. Hanser, 3. edition, 2012.

O’Sullivan, Power, Virk, Masud, Haider, Christensen, Bai, Cuypers, D’Havé, and Vonck, 2015. Leonard O’Sullivan, Valerie Power, Gurvinder Virk, Nauman Masud, Usman Haider, Simon Christensen, Shaoping Bai, Ludo Cuypers, Michel D’Havé, and Kristl Vonck. *End user needs elicitation for a full-body exoskeleton to assist the elderly*. 2015.

Overgaard, 2015. Lars Terndrup Overgaard. *Maskinelementer, analyse og dimensionering - Elementmetoden Lecture notes 6-10*. Department of Mechanical and Manufacturing Engineering, Aalborg University, 2015.

Pigeon, Yahia, and Feldman, 1996. Pascale Pigeon, L’Hocine Yahia, and Anatol G. Feldman. *Moment Arms and Lengths of Human Upper Limb Muscles as Functions of Joint Angles*. 1996.

ROC, 2016. ROC. *Elbow and Forearm*.

<https://www.rocmd.com/conditions-treated/elbow-and-forearm-anatomy/>, 2016.
Localised 01-06-2018.

Sandal, Battistella, and Katsianis, 2018. R. Sandal, F. Battistella, and A. Katsianis. *Determination of Mechanical Loading on Elbow Joint during everyday movements of Paraplegics: a preliminary study*. 2018.

Schön, 2003. Joakim Schön. *Coefficient of friction for aluminum in contact with a carbon fiber epoxy composite*. *Tribology International* 37 (2004) 395–404, 2003.

Shefelbine, Clarkson, and Farmer, 2002. Sandra Shefelbine, John Clarkson, and Roy Farmer. *Good design practice for medical devices and equipment - requirements capture*. University of Cambridge Engineering Design Centre, 1. edition, 2002.

- Simona, Andrea, Emilio, Andrea, Marco, Matteo, Matteo, Mario, Francesco, Chiara, and Nicola, 2017.** Crea Simona, Parri Andrea, Trigli Emilio, Baldoni Andrea, Muscolo Marco, Fantozzi Matteo, Moisé Matteo, Cortese Mario, Giovacchini Francesco, Carozza Maria Chiara, and Vitiello Nicola. *Control and Performance of Upper- and Lower Extremity SEA-based Exoskeletons*. 2017.
- Steinfeld, Fong, Kaber, Lewis, Scholtz, Schultz, and Goodrich, 2006.** Aaron Steinfeld, Terrance Fong, David Kaber, Michael Lewis, Jean Scholtz, Alan Schultz, and Mochael Goodrich. *Common Metrics for Human-Robot Interaction*. Proceedings of the 1st ACM SIGCHI/SIGART conference on Human-robot interaction, Pages 33-40, 2006.
- Sugar, Armstrong, Najafi, Redkar, and Ward, 2017.** Thomas G. Sugar, David Armstrong, Bijan Najafi, Sangram Redkar, and Jeffrey A. Ward. *Lower-limb Wearable Robotics*. 2017.
- TED.** TED. *Exoskeletons - for war and health*.
<https://pi.tedcdn.com/r/pe.tedcdn.com/images/ted/3f40cd656640838f4e6e49d55db0d9404c96cd>
Localised 01-06-2018.
- Tözeren, 2000.** Aydin Tözeren. *Human Body Dynamics*. Springer, 1 edition, 2000.
- Veritas, 2010.** Veritas. *DESIGN AND MANUFACTURE OF WIND TURBINE BLADES, OFFSHORE AND ONSHORE WIND TURBINES*. 2010.
- Wilfredofitness, 2018.** Wilfredofitness. *Bicep and Forearm Exercise*.
<http://www.wilfredofitness.com/exercises/a-super-secret-forearm-exercise>,
2018. Localised 16-05-2018.
- Xie, 2016.** Shane (S.G.) Xie. *Advanced Robotics for Medical Rehabilitation*. Springer, 2016.

Questionnaire for Concept Test

A

Test of prototypes

Questionnaire

May 24, 2018

Evaluation of exoskeleton component

Test subject no.:

Height [m]:

Upper arm [mm]:

Lower arm [mm]:

Experience, test 1

Comfortlevel	Low				High
General experience	1	2	3	4	5

Feeling of compliance	Not existing			Prominent	
When trying to move	1	2	3	4	5
When carrying weight	1	2	3	4	5

Weight	Heavy			Light	
During all tests	1	2	3	4	5

Comments on the overall experience:

In relation to expectations, feeling, look, attachment, etc.

Experience, test 2

Test subject no.:

Comfortlevel	Low				High
General experience	1	2	3	4	5

Feeling of compliance	Not existing			Prominent	
When trying to move	1	2	3	4	5
When carrying weight	1	2	3	4	5

Weight	Heavy			Light	
During all tests	1	2	3	4	5

Comments on the overall experience:

In relation to expectations, feeling, look, attachment, etc.

--

Experience, test 3

Test subject no.:

Comfortlevel	Low				High
General experience	1	2	3	4	5

Feeling of compliance	Not existing				Prominent
When trying to move	1	2	3	4	5
When carrying weight	1	2	3	4	5

Weight	Heavy				Light
During all tests	1	2	3	4	5

Comments on the overall experience:

In relation to expectations, feeling, look, attachment, etc.

Experience, test 4

Test subject no.:

Comfortlevel	Low				High
General experience	1	2	3	4	5

Feeling of compliance	Not existing			Prominent	
When trying to move	1	2	3	4	5
When carrying weight	1	2	3	4	5

Weight	Heavy			Light	
During all tests	1	2	3	4	5

Comments on the overall experience:

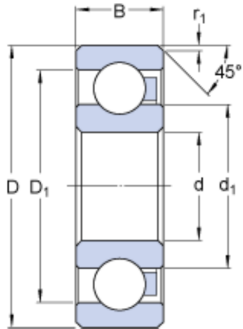
In relation to expectations, feeling, look, attachment, etc.

--

Datasheets **B**

6000/HR11TN

Dimensions



d	10	mm
D	26	mm
B	8	mm
d ₁	15.1	mm
D ₁	21.4	mm
r ₁	min. 0.4	mm

Calculation data

Basic dynamic load rating ¹⁾	C	0.13	kN
Basic static load rating ¹⁾	C ₀	0.09	kN
Speed rating ²⁾		1900	r/min

Mass

Mass bearing		6.2	g
--------------	--	-----	---

Prepreg fibre types	Resin content	Curing [°C]	Max service temperature [°C]	Fibre density [g/cm ³]	Laminate density [g/cm ³]	Mass [g/m ²]	Cured thickness
Unidirectional (IM7-12K)	38% 32%	177-204	-59 to 204 (232 Short-term)	1.78 Mangler	1.58 1.25	145/228 Mangler FIBRE WEIGHT	0.13 mm Mangler 0.21 mm
Woven (AGP193-PW-3K)	40%	175-185	121	1.77	1.57	193 (FIBRE WEIGHT)	0.19 mm
Woven (IM7-6K-5HS)	38%	177-204	-59 to 204 (232 Short-term)	1.78 Mangler	1.56 1.25	203 Mangler FIBRE WEIGHT	0.21 mm Mangler

LEA

Unidirectional (IM7-12K) Symbol Value Unit

Fiber direction, 0°

Tensile modulus	E ₁	162·10 ³	MPa	69 GPa 138 GPa
Tensile strength	X _t	2000	MPa	~2200
Compression strength	X _c	158	MPa	~1800

Transverse direction, 90°

Transverse tensile modulus	E ₂	9.7·10 ³	MPa
Transverse tensile strength	Y _t	66	MPa
Compression strength	Y _c	248	MPa

Properties in plane 1-2

Poissons ratio	ν ₁₂	0.31 Mangler	-
Shear modulus	G ₁₂	5.9·10 ³	MPa
Shear strength	S	139	MPa

Properties in plane 2-3

Poissons ratio	ν ₂₃	0.45 Ambient Mangler	-
Shear modulus	G ₂₃	5.9 Mangler	MPa

RELEVANT MOD
EGENSLABER OMKLÄRUNG
BOLTHÜLLER

Woven (IM7-6K-5HS) Symbol, Value Unit

Fiber direction, 0°

Tensile modulus	E ₁	69 87·10 ³	MPa
Tensile strength	X _t	862 723	MPa
Compression strength	X _c	689 Mangler	MPa

Transverse direction, 90°

Transverse tensile modulus	E ₂	75·10 ³	MPa
Transverse tensile strength	Y _t	862	MPa
Compression strength	Y _c	Mangler	MPa

Properties in plane 1-2

Poissons ratio	ν ₁₂	0.04 Ambient Mangler	-
Shear modulus	G ₁₂	4.9 Mangler	MPa
Shear strength	S	114 Mangler	MPa

Properties in plane 2-3

Poissons ratio	ν ₂₃	0.076 Ambient Mangler	-
Shear modulus	G ₂₃	3.3 Mangler	MPa

Woven (AGP193-PW) Symbol, Value Unit

Fiber direction, 0°

Tensile modulus	E ₁	68·10 ³	MPa
Tensile strength	X _t	828 728	MPa
Compression strength	X _c	883 721	MPa

Transverse direction, 90°

Transverse tensile modulus	E ₂	66·10 ³	MPa
Transverse tensile strength	Y _t	793	MPa
Compression strength	Y _c	Mangler	MPa

Properties in plane 1-2

Poissons ratio	ν ₁₂	0.049 Mangler	-
Shear modulus	G ₁₂	4.4 Mangler	MPa
Shear strength	S	83	MPa

Properties in plane 2-3

Poissons ratio	ν ₂₃	0.076 Mangler	-
Shear modulus	G ₂₃	3.3 Mangler	MPa



HexPly[®] 8552

Epoxy matrix (180°C/356°F curing matrix)



Product Data Sheet

Description

HexPly[®] 8552 is a high performance tough epoxy matrix for use in primary aerospace structures. It exhibits good impact resistance and damage tolerance for a wide range of applications.

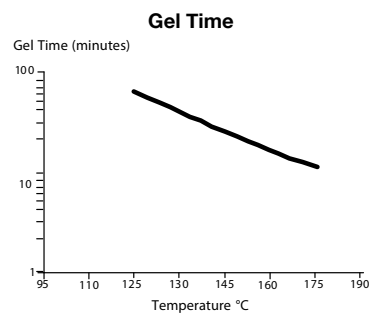
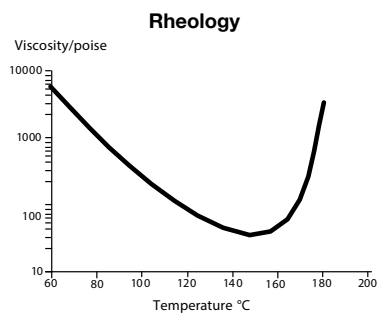
HexPly[®] 8552 is an amine cured, toughened epoxy resin system supplied with unidirectional or woven carbon or glass fibres.

HexPly[®] 8552 was developed as a controlled flow system to operate in environments up to 121°C (250°F).

Benefits and Features

- Toughened epoxy matrix with excellent mechanical properties
- Elevated temperature performance
- Good translation of fibre properties
- Controlled matrix flow in processing
- Available on various reinforcements
- Excellent drape and tack

Resin Matrix Properties





Prepreg Properties - HexPly® 8552 UD Carbon Prepregs

Physical Properties

	Units	AS4	IM7
Fibre Density	g/cm ³ (lb/in ³)	1.79 (0.065)	1.77 (0.064)
Filament count/tow		12K	12K
Resin density	g/cm ³ (lb/in ³)	1.30 (0.047)	1.30 (0.047)
Nominal Cured Ply Thickness 8552 /35% /134	mm (inch)	0.130 (0.0051)	0.131 (0.0052)
Nominal Fibre Volume	%	57.42	57.70
Nominal Laminate Density	g/cm ³ (lb/in ³)	1.58 (0.057)	1.57 (0.057)

Mechanical Properties

Test	Units	Temp °C (°F)	Condition	AS4	IM7
0°Tensile Strength	MPa (ksi)	-55 (-67)	Dry	1903 (267)	2572 (373)
		25 (77)	Dry	2207 (320)	2724 (395)
		91 (195)	Dry	-	2538 (368)*
90°Tensile Strength	MPa (ksi)	-55 (-67)	Dry	-	174 (25.3)
		25 (77)	Dry	81 (11.7)	64 (9.3)
		93 (200)	Dry	75 (10.9)	92 (13.3)*
0°Tensile Modulus	GPa (msi)	-55 (-67)	Dry	134 (19.4)	163 (23.7)
		25 (77)	Dry	141 (20.5)	164 (23.8)
		91 (195)	Dry	-	163 (23.7)*
90°Tensile Modulus	GPa (msi)	-	-	-	-
		25 (77)	Dry	10 (1.39)	12 (1.7)
		93 (200)	Dry	8 (1.22)	10 (1.5)*
0°Compression Strength	MPa (ksi)	-55 (-67)	Dry	1586 (230)	-
		25 (77)	Dry	1531 (222)	1690 (245)
		91 (195)	Dry	1296 (184)	1483 (215)
0°Compression Modulus	GPa (msi)	-55 (-67)	Dry	124 (18)	-
		25 (77)	Dry	128 (18.6)	150 (21.7)
		91 (195)	Dry	122 (17.7)	162 (23.5)
0° ILSS (Shortbeam shear)	MPa (ksi)	-55 (-67)	Dry	164 (23.8)	-
		25 (77)	Dry	128 (18.5)	137(19.9)
		91 (195)	Dry	122 (14.7)	94 (13.6)*
		25 (77)	Wet	117 (16.9)	115 (16.7)
		71 (160)	Wet	84 (12.2)	80 (11.6)**
In-plane Shear Strength	MPa (ksi)	25 (77)	Dry	114 (16.6)	120 (17.4)
		93 (200)	Dry	105 (15.2)	106 (15.4)*

Bold 93°C (200°F) Bold* 104°C (220°F) Bold 82°C (180°F)**



Prepreg Properties - HexPly® 8552 Woven Carbon Prepregs (AS4 Fibre)

Physical Properties

	Units	AGP193-PW	AGP 280-5H
Fibre Type	–	AS4 3K	AS4 3K
Fibre density	g/cm ³ (lb/in ³)	1.77 (0.065)	1.77 (0.065)
Weave	–	Plain	5HS
Mass	g/m ² (oz/yd ²)	193 (5.69)	286 (8.44)
Weight Ratio, Warp : Fill		50 :50	50 :50
Nominal cured ply thickness @ 37% resin content	mm (inch)	0.195 (0.0076)	0.289 (0.0114)
Nominal Fibre Volume	%	55.29	55.29
Nominal Laminate Density	g/cm ³ (lb/in ³)	1.57 (0.057)	1.57 (0.057)

Mechanical Properties

Test	Units	Temp °C (°F)	Condition	AGP193-PW	AGP280- 5H
0°Tensile Strength	MPa (ksi)	-55 (-67)	Dry	766 (111)	828 (120)
		25 (77)	Dry	828 (120)	876 (127)
		91 (195)	Dry	–	903 (131)
90°Tensile Strength	MPa (ksi)	-55 (-67)	Dry	710 (103)	752 (109)
		25 (77)	Dry	793 (115)	800 (116)
		93 (200)	Dry	759 (110)	772 (112)
0°Tensile Modulus	GPa (msi)	-55 (-67)	Dry	66 (9.5)	70 (10.2)
		25 (77)	Dry	68 (9.8)	67 (9.7)
		91 (195)	Dry	–	69 (10)
90°Tensile Modulus	GPa (msi)	-55 (-67)	Dry	66 (9.6)	67 (9.7)
		25 (77)	Dry	66 (9.5)	66 (9.5)
		93 (200)	Dry	68 (9.8)	65 (9.4)
0°Compression Strength	MPa (ksi)	-55 (-67)	Dry	959 (139)	–
		25 (77)	Dry	883 (128)	924 (134)
		91 (195)	Dry	759 (110)	752 (109)
0°Compression Modulus	GPa (msi)	-55 (-67)	Dry	60 (8.7)	–
		25 (77)	Dry	60 (8.7)	64 (9.3)
		91 (195)	Dry	61 (8.8)	67(9.7)
0° ILSS (Shortbeam shear)	MPa (ksi)	-55 (-67)	Dry	101 (14.6)	–
		25 (77)	Dry	84 (12.2)	79 (11.4)
		91 (195)	Dry	70 (10.2)	–
		-55 (-67)	Wet	75 (10.9)	69 (10)
		25 (77)	Wet	72 (10.4)	–
		91 (195)	Wet	59 (8.5)	–

Bold 93°C (200°F) Bold* 104°C (220°F) Bold 82°C (180°F)**



Prepreg Properties - HexPly® 8552 Woven Carbon Prepregs (IM7 Fibre)

Physical Properties

	Units	SPG 196-P	SPG 370-8H
Fibre Type	-	IM7 6K	IM7 6K
Fibre density	g/cm ³ (lb/in ³)	1.77 (0.064)	1.77 (0.064)
Weave	-	Plain	8HS
Mass	g/m ² (oz/yd ²)	196 (5.78)	374 (11.03)
Weight Ratio, Warp : Fill		50 :50	49 :51
Nominal cured ply thickness @ 37% resin content	mm (inch)	0.199 (0.0078)	0.380 (0.0150)
Nominal Fibre Volume	%	55.57	55.57
Nominal Laminate Density	g/cm ³ (lb/in ³)	1.56 (0.056)	1.56 (0.056)

Mechanical Properties

Test	Units	Temp°C (°F)	Condition	SPG 196-PW	SPG 370-SH
0°Tensile Strength	MPa (ksi)	-55 (-67)	Dry	979 (142)	965 (140)
		25 (77)	Dry	1090 (158)	1014 (147)
		91 (195)	Dry	-	-
90°Tensile Strength	MPa (ksi)	-55 (-67)	Dry	862 (125)	903 (131)
		25 (77)	Dry	945 (137)	959 (139)
		93 (200)	Dry	979 (142)*	879 (130)*
0°Tensile Modulus	GPa (msi)	-55 (-67)	Dry	85 (12.3)	86 (12.5)
		25 (77)	Dry	85 (12.3)	86 (12.4)
		91 (195)	Dry	-	-
90°Tensile Modulus	GPa (msi)	-55 (-67)	Dry	80 (11.6)	81 (11.7)
		25 (77)	Dry	80 (11.6)	81 (11.7)
		93 (200)	Dry	79 (11.5)*	79 (11.5)*
0° ILSS (Shortbeam shear)	MPa (ksi)	-55 (-67)	Dry	-	-
		25 (77)	Dry	88 (12.7)	90 (13)
		91 (195)	Dry	69 (10)*	74 (10.8)*
		25 (77)	Wet	80 (11.6)	83(12.1)
		71 (160)	Wet	61 (8.8)**	63 (9.1)**
		91 (195)	Wet	-	-

Bold 93°C (200°F) Bold* 104°C (220°F) Bold 82°C (180°F)**

Typical Neat Resin Data

Colour	Yellow	
Density	1.301 g/cc	(0.0470 lb/in ³)
Glass Transition Temperature, T _g dry	200°C	(392°F)
Glass Transition Temperature, T _g wet	154°C	(309°F)
Tensile Strength	121 MPa	(17.5 ksi)
Tensile Modulus	4670 MPa	(0.677 msi)



Curing Conditions

Cure cycle for monolithic components

1. Apply full vacuum (1 bar).
2. Apply 7 bar gauge autoclave pressure.
3. Reduce the vacuum to a safety value of 0.2 bar when the autoclave pressure reaches approximately 1 bar gauge.
4. Heat at 1- 3°C/min (2-8°F/min) to 110°C ± 5°C (230°F ± 9°F)
5. Hold at 110°C ± 5°C (230°F ± 9°F) for 60 minutes ± 5 minutes.
6. Heat at 1-3°C/min (2-8°F/min) to 180°C ± 5°C (356°F ± 9°F)
7. Hold at 180°C ± 5°C (356°F ± 9°F) for 120 minutes ± 5 minutes.
8. Cool at 2 - 5°C (4-9°F) per minute
9. Vent autoclave pressure when the component reaches 60°C (140°F) or below.

Cure cycle for honeycomb sandwich components

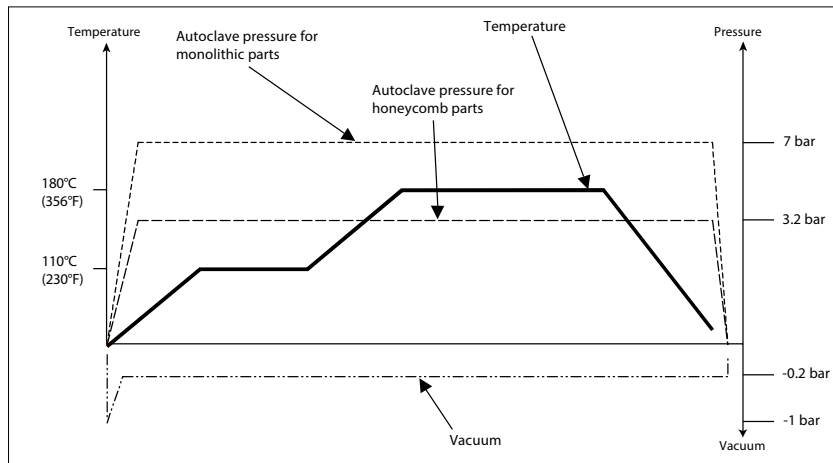
1. Apply full vacuum (1 bar).
2. Apply 3.2 bar gauge autoclave pressure.
3. Reduce the vacuum to a safety value of 0.2 bar when the autoclave pressure reaches approximately 1 bar gauge.
4. Heat at 1- 3°C/min (2-8°F/min) to 110°C ± 5°C (230°F ± 9°F)
5. Hold at 110°C ± 5°C (230°F ± 9°F) for 60 minutes ± 5 minutes.
6. Heat at 1-3°C/min (2-8°F/min) to 180°C ± 5°C (356°F ± 9°F)
7. Hold at 180°C ± 5°C (356°F ± 9°F) for 120 minutes ± 5 minutes.
8. Cool at 2 - 5°C (4-9°F) per minute
9. Vent autoclave pressure when the component reaches 60°C (140°F) or below.

Note: For both cure cycles – at each stage, use the temperature shown by the leading thermocouple.

Heat-up rates are dependent on component thickness, eg, slow heat-up rates should be used for thicker components and large tools. Accurate temperature measurements of the component should be made during the cure cycles by using thermocouples.

Performance testing should accompany alternative cure cycles to ensure suitability for the particular application.

Curing Cycle for Honeycomb and Monolithic Components



Copyright © 2016 – Hexcel Corporation – All Rights Reserved.



HexPly® 8552

Epoxy matrix (180°C/356°F curing matrix)



Product Data Sheet

Prepreg Storage Life

- Tack Life: 10 days at RT (23°C/73°F)
- Out Life: 30 days at RT (23°C/73°F)
- Shelf Life: 12 months at -18°C(0°F) (from date of manufacture)

Definitions:

- Shelf Life: The maximum storage life for HexPly® Prepreg, upon receipt by the customer, when stored continuously, in a sealed moisture-proof bag, at -18°C(0°F). To accurately establish the exact expiry date, consult the box label.
- Tack Life: The time, at room temperature, during which prepreg retains enough tack for easy component lay-up.
- Out Life: The maximum accumulated time allowed at room temperature between removal from the freezer and cure.

Precautions for Use

The usual precautions when handling uncured synthetic resins and fine fibrous materials should be observed, and a Safety Data Sheet is available for this product. The use of clean disposable inert gloves provides protection for the operator and avoids contamination of material and components.

For more information

Hexcel is a leading worldwide supplier of composite materials to aerospace and industrial markets. Our comprehensive range includes:

- HexTow® carbon fibers
- HexForce® reinforcements
- HexPly® prepregs
- HexMC® molding compounds
- HexFlow® RTM resins
- Redux® adhesives
- HexTool® tooling materials
- HexWeb® honeycombs
- Acousti-Cap® sound attenuating honeycomb
- Engineered core
- Engineered products

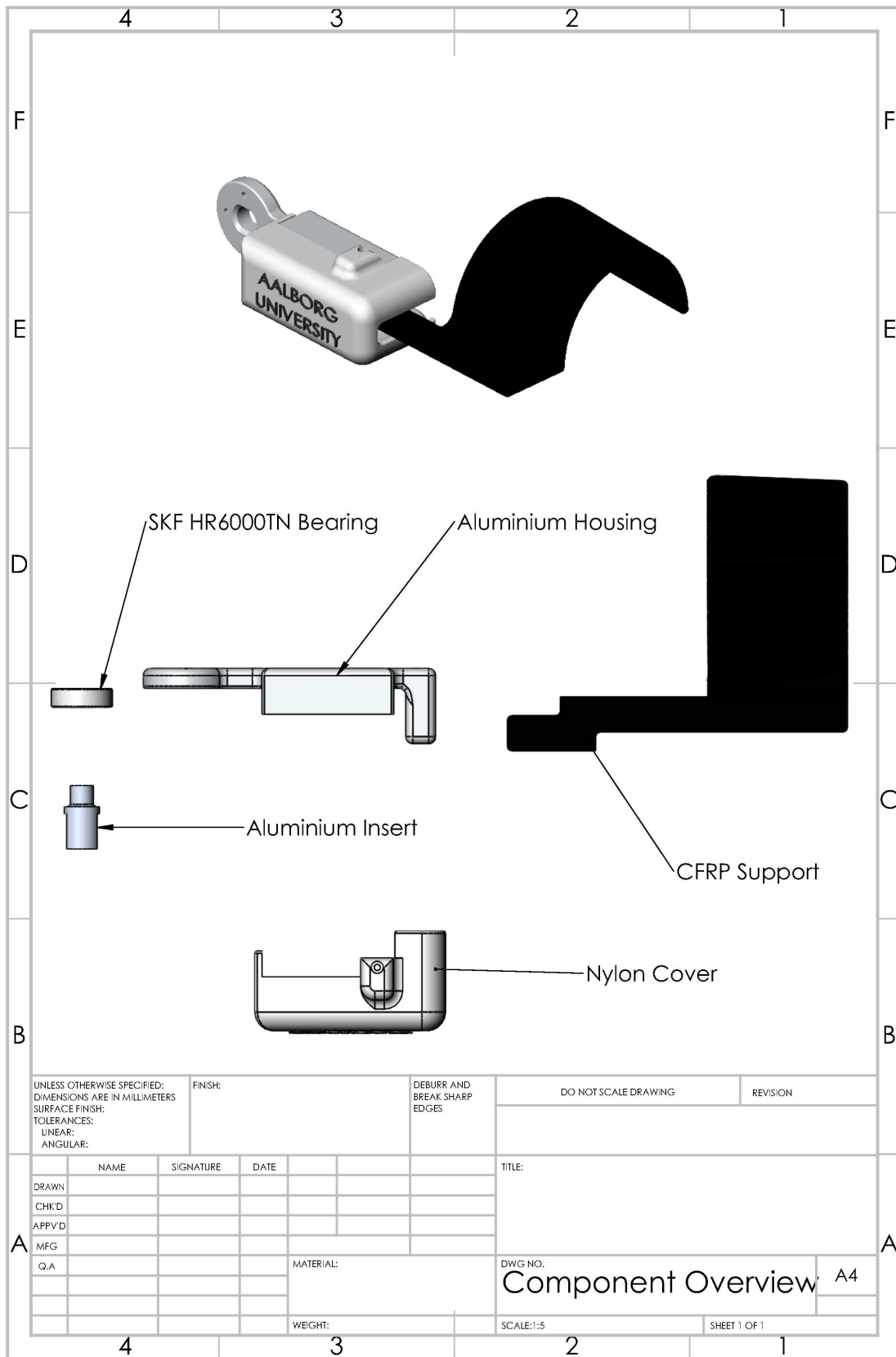
For US quotes, orders and product information call toll-free 1-800-688-7734. For other worldwide sales office telephone numbers and a full address list, please go to:

<http://www.hexcel.com/contact/salesoffice>

©2016 Hexcel Corporation – All rights reserved. Hexcel Corporation and its subsidiaries ("Hexcel") believe that the technical data and other information provided herein was materially accurate as of the date this document was issued. Hexcel reserves the right to update, revise or modify such technical data and information at any time. Any performance values provided are considered representative but do not and should not constitute a substitute for your own testing of the suitability of our products for your particular purpose. Hexcel makes no warranty or representation, express or implied, including but not limited to the implied warranties of merchantability and fitness for a particular purpose, and disclaims any liability arising out of or related to, the use of or reliance upon any of the technical data or information contained in this document.

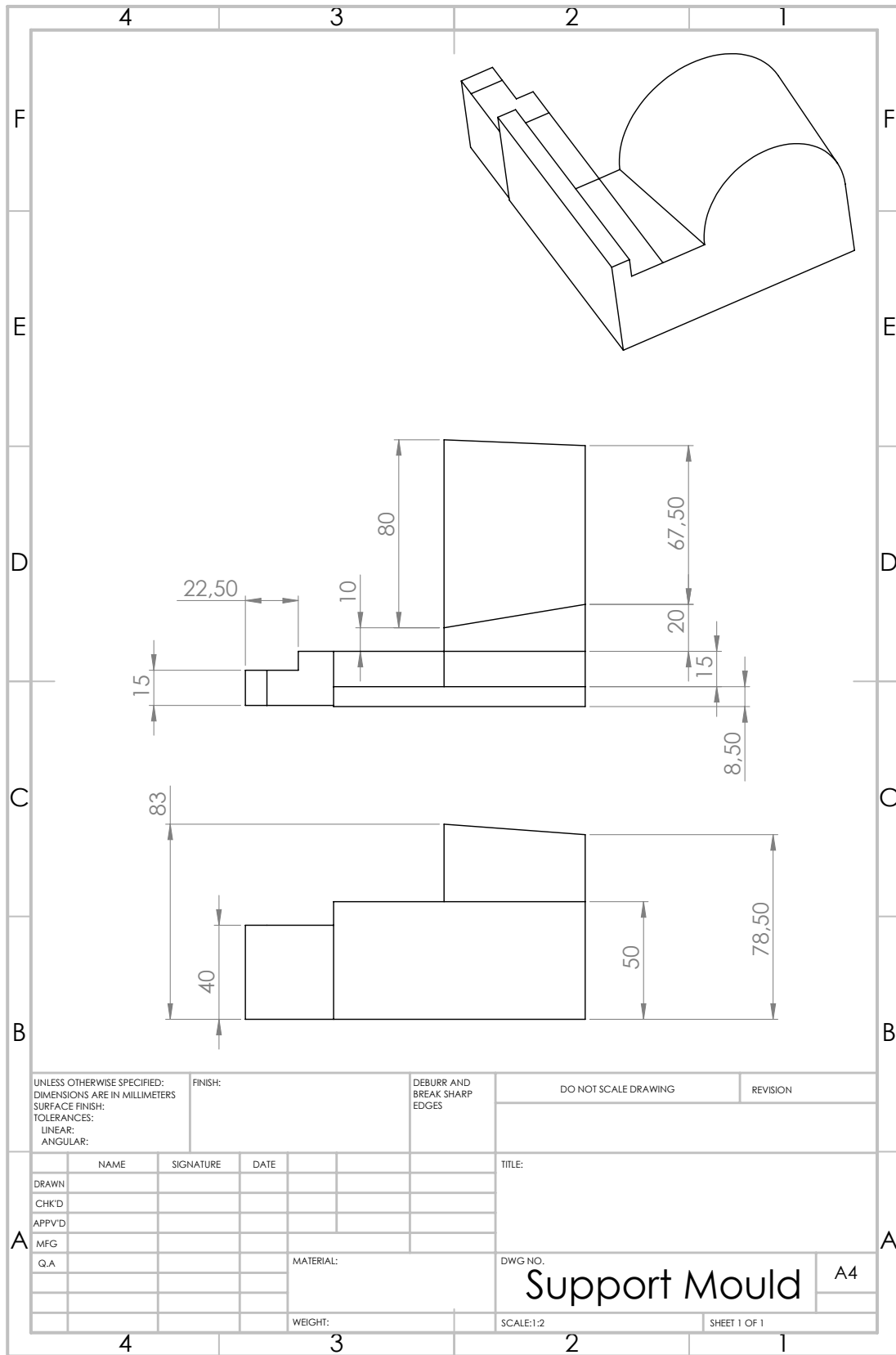
FFA-072-AG16

Component Overview



UNLESS OTHERWISE SPECIFIED: DIMENSIONS ARE IN MILLIMETERS SURFACE FINISH: TOLERANCES: LINEAR: ANGULAR:		FINISH:	DEBURR AND BREAK SHARP EDGES		DO NOT SCALE DRAWING	REVISION
DRAWN			NAME		TITLE:	
CHK'D			SIGNATURE		DWG. NO.	
APP'VD			DATE		Component Overview	
MFG					A4	
Q.A			MATERIAL:		SCALE: 1:5	
			WEIGHT:		SHEET 1 OF 1	

Mould & Template D



UNLESS OTHERWISE SPECIFIED: DIMENSIONS ARE IN MILLIMETERS SURFACE FINISH: TOLERANCES: LINEAR: ANGULAR:		FINISH:	DEBURR AND BREAK SHARP EDGES		DO NOT SCALE DRAWING	REVISION
DRAWN		SIGNATURE		DATE		TITLE:
CHK'D						
APPV'D						
MFG						
Q.A.				MATERIAL:		DWG. NO.
						Support Mould
		WEIGHT:		SCALE: 1:2		A4
				SHEET 1 OF 1		

4	3	2	1
F			F
E			E
D			D
C			C
B			B
UNLESS OTHERWISE SPECIFIED: DIMENSIONS ARE IN MILLIMETERS SURFACE FINISH: TOLERANCES: LINEAR: ANGULAR:		FINISH:	DEBURR AND BREAK SHARP EDGES
		DO NOT SCALE DRAWING	REVISION
DRAWN	NAME	SIGNATURE	DATE
CHK'D			
APP'VD			
MFG			
Q.A.			
		MATERIAL:	DWG NO.
		Support Template	
		SCALE:1:2	SHEET 1 OF 1
4	3	2	1